# Geochemical, biological and clumped isotopologue evidence for substantial microbial methane production under carbon limitation in serpentinites of the Samail Ophiolite, Oman

Daniel B. Nothaft[a,*], Alexis S. Templeton[a,*], Jeemin H. Rhim[b], David T. Wang[b,1], Jabrane Labidi[c], Hannah M. Miller[a,2], Eric S. Boyd[d], Juerg M. Matter[e], Shuhei Ono[b], Edward D. Young[c], Sebastian H. Kopf[a], Peter B. Kelemen[f], Mark E. Conrad[g], The Oman Drilling Project Science Team

[a] *Department of Geological Sciences, University of Colorado, Boulder, CO, USA*

[b] *Department of Earth, Atmospheric and Planetary Sciences, Massachusetts Institute of Technology, Cambridge, Massachusetts, USA*

[c] *Department of Earth, Planetary, and Space Sciences, University of California, Los Angeles, CA, USA*

[d] *Department of Microbiology & Immunology, Montana State University, Bozeman, MT*

[e] *National Oceanography Centre, University of Southampton, Southampton, UK*

[f] *Lamont-Doherty Earth Observatory, Columbia University, Palisades, NY, USA*

[g] *Lawrence Berkeley National Laboratory, Berkeley, CA, USA*

**Abstract**

In hyperalkaline (pH > 10) fluids that have participated in low-temperature (< 150 °C) serpentinization reactions, the dominant form of C is often methane ($CH_4$), but the origin of this $CH_4$ is uncertain. To assess $CH_4$ origin in serpentinite aquifers within the Samail Ophiolite, Oman, we determined fluid chemical compositions, analyzed taxonomic profiles of fluid-hosted microbial communities, and measured isotopic compositions of hydrocarbon gases. We found that 16S rRNA gene sequences affiliated with methanogens were widespread in the aquifer. We measured clumped isotopologue ($^{13}CH_3D$ and $^{12}CH_2D_2$) relative abundances less than equilibrium, consistent with substantial microbial $CH_4$ production. Further, we observed an inverse relationship between dissolved inorganic C concentrations and $\delta^{13}C_{CH_4}$ across fluids bearing microbiological evidence of methanogenic activity, suggesting that the apparent C isotope effect of microbial methanogenesis is modulated by C availability. An additional source of $CH_4$ is evidenced by the presence of $CH_4$-bearing fluid inclusions in the Samail Ophiolite and our measurement of high $\delta^{13}C$ values of ethane and propane, which are similar to those reported in studies of $CH_4$-rich inclusions in rocks from the oceanic lithosphere. In addition, we observed 16S rRNA gene sequences affiliated with aerobic methanotrophs and, in lower abundance, anaerobic methanotrophs, indicating that microbial consumption of $CH_4$ in the ophiolite may further enrich $CH_4$ in $^{13}C$. We conclude that substantial microbial $CH_4$ is produced under varying degrees of C limitation and mixes with abiotic $CH_4$ released from fluid inclusions. This study lends insight into the functioning of microbial ecosystems supported by water/rock reactions.

*Keywords:* serpentinization, hydrogen, alkane, methanogenesis, methanotrophy, *Methanobacterium*

## Plain Language Summary

Mantle rocks from beneath Earth's crust can be thrust to the surface, where they are exposed to rain and air containing carbon dioxide ($CO_2$). The groundwaters that become stored in these rocks often contain methane ($CH_4$, a major component of "natural gas"), which can be formed from carbon dioxide in the subsurface. To investigate these methane-forming processes, we sampled water, gas, and suspended particles from groundwaters using wells previously drilled into the rocks. The particles contained microbes with the genetic ability to produce methane. We also precisely measured the amounts of combinations of C and H atoms of different masses (isotopes) in the natural gas to determine how it was formed. The results of these measurements suggest that microbes could actively produce a considerable amount of the methane, which mixes with methane from another source that was formed by non-biological processes, possibly long ago under different conditions than today's. Rocks like those studied here are widespread in the Solar System, so our finding that microbes live and produce methane in these rocks could help guide the search for life beyond Earth.

## Key Points

- 16S rRNA gene sequences affiliated with methanogens and $CH_4$ clumped isotopologue compositions suggest substantial microbial $CH_4$ production.
- A second $CH_4$ source, release of $CH_4$ from fluid inclusions, is indicated by $^{13}$C-enriched ethane and propane.
- Scarcity of C substrates ($CO_2$ and formate) may decrease the apparent C isotope effect of microbial methanogenesis.

## 1. Introduction

At temperatures and pressures near the Earth's surface ($< 400\,^{\circ}C$, $< 100\,MPa$), ultramafic rocks such as peridotite in contact with water are thermodynamically driven to hydrate and oxidize, forming variable amounts of serpentine, magnetite, brucite, hydrogen ($H_2$), and other phases (Evans, 1977; Frost, 1985; McCollom and Bach, 2009; Klein and Bach, 2009; Klein et al., 2009, 2019). This process, often called "serpentinization", can produce $H_2$ at temperatures at least as low as $55\,^{\circ}C$ (Miller et al., 2017b). The resultant $H_2$ can be thermodynamically favored to reduce carbon dioxide ($CO_2$) to methane ($CH_4$) (Shock,

*Corresponding authors
*Email addresses:* daniel.nothaft@colorado.edu (Daniel B. Nothaft), alexis.templeton@colorado.edu (Alexis S. Templeton )
[1]Current address: ExxonMobil Upstream Research Company, Spring, TX 77389, USA
[2]Current address: Itasca Denver, Inc., 143 Union Blvd. Suite 525 Lakewood, CO 80228, USA

1992). The reduction of $CO_2$ by $H_2$ to form $CH_4$ can be catalyzed on mineral surfaces as in the Sabatier reaction (Etiope and Ionescu, 2015; Klein et al., 2019), or enzymatically through microbial methanogenesis (Whiticar, 1999).

In continental settings undergoing serpentinization, where fluid-rock reactions typically occur at low temperatures ($< 150\,^{\circ}C$), there is disagreement regarding the origin of $CH_4$. Three key potential $CH_4$ sources have been identified in these environments. One potential source is the abiotic reduction of $CO_2$ to $CH_4$ at warmer-than-present temperatures in fluid inclusions within crystals that can store $CH_4$ and subsequently release it. Another potential source is the abiotic, mineral-catalyzed reduction of $CO_2$ to $CH_4$ at the low temperatures that prevail in the present-day weathering environment. A third potential source is microbial methanogenesis.

Storage of $CH_4$ produced at temperatures of $270\,^{\circ}C$ to $800\,^{\circ}C$ in fluid inclusions in minerals such as olivine and the release of this $CH_4$ through subsequent chemical/physical alteration are the dominant processes contributing to $CH_4$ fluxes from sediment-poor seafloor hydrothermal vents (Kelley, 1996; Kelley and Früh-Green, 1999; McDermott et al., 2015; Wang et al., 2018; Labidi et al., 2020). In continental, low-temperature serpentinizing settings, however, debate continues as to whether fluid inclusions can sustain observed $CH_4$ fluxes (Etiope and Whiticar, 2019; Grozeva et al., 2020).

Abiotic reduction of $CO_2$ to $CH_4$ can occur at temperatures at least as low as $20\,^{\circ}C$ when catalyzed by the transition metal ruthenium (Ru) (Etiope and Ionescu, 2015). Ru is present in considerable abundance in chromitite bodies in ultramafic rock accumulations (Etiope et al., 2018), but it has only been shown to catalyze $CO_2$ hydrogenation under conditions where free gas phases exist (Etiope and Ionescu, 2015). The prevalence of this process, particularly in aquifers whose fluid compositions appear to be dominantly influenced by aqueous reactions with harzburgite, is another matter of ongoing debate (Etiope, 2017; Miller et al., 2017a).

Low-temperature $CH_4$ production can also be mediated by microbes called "methanogens". Microbial $CH_4$ has traditionally been viewed as a minor/negligible source of $CH_4$ in serpentinizing settings. This is due in large part to the relatively $^{13}C$-enriched composition of $CH_4$ in serpentinizing settings ($\delta^{13}C$ commonly $-20\,‰$ VPDB to $5\,‰$ VPDB), which contrasts with the more $^{13}C$-depleted composition of $CH_4$ in sedimentary settings dominated by microbial methanogenesis ($\delta^{13}C$ commonly $-90\,‰$ VPDB to $-50\,‰$ VPDB) (Etiope, 2017; Milkov and Etiope, 2018; Etiope and Whiticar, 2019). However, cultures of methanogens can produce $CH_4$ with minimal C isotope fractionation in $H_2$-rich, $CO_2$-poor fluids simulating serpentinizing systems (Miller et al., 2018). In these cultures, it has been inferred that the net C isotope effect of methanogenesis was attenuated due to microbial conversion of a large proportion of available $CO_2$ to $CH_4$ when $CO_2$ was the limiting substrate. Such results illustrate that $^{13}C$-enriched $CH_4$ in natural serpentinizing settings does not necessarily derive from non-microbial sources. Still, the quantity and isotopic composition of microbial $CH_4$ in serpentinizing settings remains uncertain.

In this study, we assessed sources and sinks of $CH_4$ in the Samail Ophiolite of Oman, a site of active, low-temperature serpentinization and carbonation. Fluids and particulates in groundwaters accessed via wells in the Samail Ophiolite have been sampled for biogeochemical studies annually from 2014 through 2018 from January to March. Microbiological and geochemical data from sampling campaigns in 2014 through 2017 and a limited number of C and H bulk stable isotope analyses of $CH_4$ sampled in 2014 have been previously reported (Miller et al., 2016; Rempfert et al., 2017; Kraus et al., 2021; Fones et al., 2019, 2020) Here, we present new geochemical and 16S rRNA gene amplicon sequencing data from samples acquired in 2018. We also present new bulk stable isotope data on $CH_4$, ethane ($C_2H_6$), and propane ($C_3H_8$) from samples obtained from 2015 through 2018. Further, we report analyses of multiply-substituted "clumped" isotopologues of $CH_4$, $^{13}CH_3D$ and $^{12}CH_2D_2$, for the first time on samples from this ophiolite. Leveraging one of the largest longitudinal data sets on $CH_4$ biogeochemistry in an ophiolite, we have identified robust trends across years and hydrogeologic settings. We observed a wide range of C isotopic compositions of $CH_4$ and short-chain alkanes, intramolecular isotopologue disequilibrium in $CH_4$, and widespread occurrence of gene sequences affiliated with methanogens, which collectively indicate that substantial quantities of microbial $CH_4$ are produced and mix with abiotic $CH_4$ released from fluid inclusions in the Samail Ophiolite. Our finding that microbial methanogenesis proceeds even in hyperalkaline fluids lends insight into the functioning of microbial ecosystems that leverage reactions between water and ultramafic rocks to power metabolic processes on Earth and perhaps on other rocky bodies of the Solar System (Ménez, 2020; Glein and Zolotov, 2020).

## 2. Geologic Setting

The Samail Ophiolite (Figure 1) consists of pelagic sedimentary rocks ($< 0.1$ km), volcanic rocks (0.5 km to 2.0 km), sheeted dikes (1 km to 1.5 km), gabbro and igneous peridotite (0.5 km to 6.5 km), residual mantle peridotites, (8 km to 12 km), and a metamorphic sole of greenschist- to granulite-facies metamorphic rocks ($< 0.5$ km) (Glennie et al., 1973; Coleman and Hopson, 1981; Lippard et al., 1986; Nicolas, 1989; Nicolas et al., 2000). The ophiolite crust formed from 96.12 Ma to 95.50 Ma, and convergence began at about the same time (Rioux et al., 2016), or up to 10 Myr earlier (Guilmette et al., 2018; Soret et al., 2020). Ophiolite emplacement continued until 78 Ma to 71 Ma (Rabu et al., 1993). Part of the ophiolite was subaerially eroded in the Late Cretaceous, then became covered in parts by Maastrictian to Eocene limestones due to subsidence and transgression (Nolan et al., 1990; Skelton et al., 1990).

The mantle section of the ophiolite is mainly composed of highly depleted, residual mantle harzburgites, together with 5 % to 15 % dunite, which both contain a few percent chromian spinel (Godard et al., 2000; Hanghøj et al., 2010; Boudier and Coleman, 1981; Collier, 2012). The extent of serpentinization is typically 30 % to 60 %, reaching 100 % in some cases (Dewandel et al., 2003; Boudier et al., 2009; Miller et al., 2016; Kelemen et al., 2020). Chromitites are most often found in association with dunites near the crust-mantle

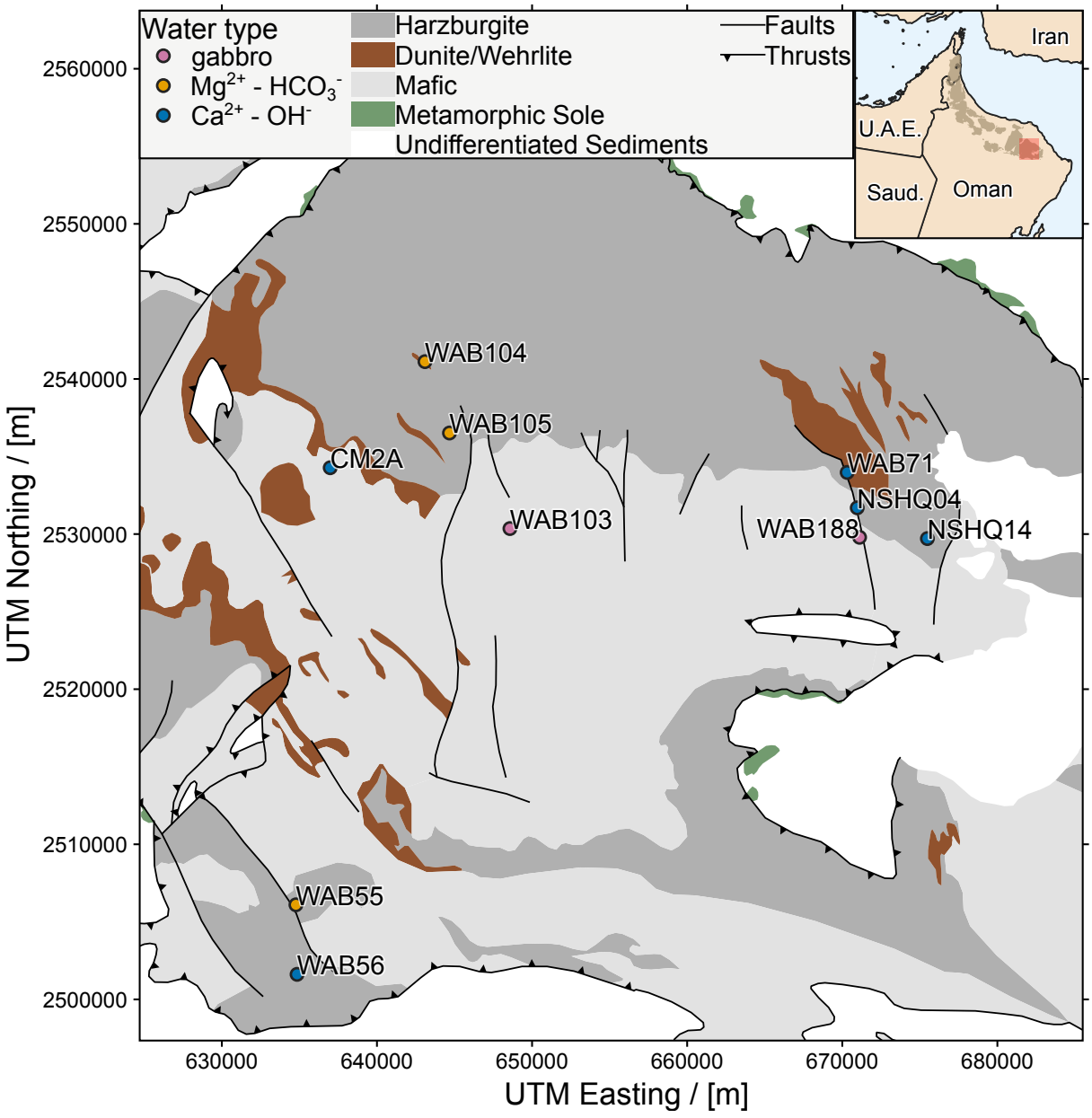


Figure 1: Study area in Samail Ophiolite, Sultanate of Oman. Geologic map data from Nicolas et al. (2000). Inset: overview of Samail Ophiolite (shaded in brown) with study area (larger map) indicated by the red shaded box. A topographic map of the study area is provided in Supporting Information Figure S1.

transition, possibly representing bases of cumulate piles, but are also found dispersed throughout the mantle section (Rollinson, 2005).

Geologic reservoirs of C underlying the ophiolite include Mid Permian to Late Cretaceous shallow marine carbonates, which host oil and gas fields in parts of northern Oman and the United Arab Emirates (Terken,

1999; Alsharhan, 1989; Etiope et al., 2015). Maastrictian to Eocene limestones that partially overly the ophiolite have been shown to transfer inorganic C to peridotites where they are in contact (de Obeso and Kelemen, 2018). C is also stored within the ophiolite, primarily in the form of carbonate minerals (Neal and Stanger, 1985; Kelemen and Matter, 2008; Kelemen et al., 2011; Noël et al., 2018). Hydration and carbonation of $> 20\,000\,\mathrm{km}^3$ of peridotite continue today in the Samail Ophiolite, largely at $< 60\,^\circ\mathrm{C}$ (Neal and Stanger, 1983, 1985; Kelemen and Matter, 2008; Kelemen et al., 2011; Streit et al., 2012; Paukert et al., 2012; Chavagnac et al., 2013a,b; Mervine et al., 2014; Falk et al., 2016; Miller et al., 2016; Paukert Vankeuren et al., 2019).

## 3. Methods

### *3.1. Fluid sampling and field measurements*

Wells were drilled into the Samail Ophiolite by the Ministry of Regional Municipalities and Water Resources of the Sultanate of Oman prior to 2006 ("WAB" and "NSHQ" wells in this study) and by the Oman Drilling Project in 2016 through 2018 ("CM") (Parsons International & Co., 2005; Kelemen et al., 2013). Information on well location, construction, and water level are given in Table 1. In sampling campaigns in 2014 and 2015, a 12 V submersible Typhoon ® pump (Proactive Env. Products, Bradenton, FL, USA) with typical flow rates of $5\,\mathrm{L{\cdot}min^{-1}}$ was used. This pump was used in all years of sampling at well NSHQ04 due to partial obstruction of this well. In all other sampling from 2016 onwards, a larger submersible pump (Grundfos SQ 2-85) with typical flow rates of $20\,\mathrm{L{\cdot}min^{-1}}$ was used. The pumping depths are reported in Tables 1 and 2. For fluids sampled in 2018, temperature, conductivity, and pH were measured using a ColeParmer PC100 Meter, while *Eh* was measured using a Mettler Toledo SG2 SevenGo meter. The analytical uncertainties for temperature, conductivity, pH, and *Eh* are $0.5\,^\circ\mathrm{C}$, 1.0 % of measured value, $0.01\,\mu\mathrm{S}\cdot\mathrm{cm}^{-1}$, and 1 mV, respectively. Each well was pumped for $\geq 20\,\mathrm{min}$ prior to sampling. Sampling commenced once fluid pH and conductivity measurements stabilized.

### *3.2. Chemical and isotopic analyses of fluids*

To analyze aqueous concentrations ($c$) of non-carbonaceous chemical species, samples were collected by passing groundwater through a $0.2\,\mu\mathrm{m}$ filter into polypropylene conical tubes. Aqueous concentrations of $\sum\mathrm{Na}$, $\sum\mathrm{Ca}$, $\sum\mathrm{Mg}$, $\sum\mathrm{Al}$, $\sum\mathrm{Fe}$, and $\sum\mathrm{Si}$ were measured by inductively coupled plasma (ICP) atomic emission spectroscopy on a PerkinElmer Optima 5300 (repeatability as median relative standard deviation of 3 %). Aqueous concentrations of $\mathrm{Cl}^-$, $\mathrm{Br}^-$, $\mathrm{F}^-$, and $\mathrm{SO}_4^{2-}$ were measured on a Dionex IC25 ion chromatograph with an AS9-HC IonPac column, with the exception of $\mathrm{NO}_3^-$, which was measured on a Dionex 4500I ion chromatograph with an IonPac AS14 column using EPA method 300.0 (analytical uncertainty of 2 %).

The concentration and $\delta^{13}C$ of dissolved inorganic C ($\sum CO_2$) were measured by acidification of water samples and transfer of resultant $CO_2$ (g) via a Thermo Fisher GasBench II to a Thermo Delta V Plus isotope ratio mass spectrometer. We optimized the methods of Assayag et al. (2006) for the wide range of $c_{\sum CO_2}$ observed in ophiolite groundwaters. Complete methodological details are available at `http://dx.doi.org/10.17504/protocols.io.zduf26w`. Sample $\delta^{13}C$ values were converted to the VPDB reference frame using measured $\delta^{13}C$ values of international reference materials (Harding Iceland Spar and LSVEC). Isotopic reference frame calculations were performed using the Isoverse suite of packages (Kopf et al., 2021) for the statistical programming language, R (R Core Team, 2019) (Section 6).

Water $\delta^{18}O$ and $\delta D$ were measured on a Picarro L2120-i cavity ring down spectrometer. The instrument analyzed each sample six times, excluding the first three analyses to avoid memory effects. Reported precision is the standard deviation of the last three measurements. Reported accuracy is the mean difference between accepted values and measured values of standards. Mean precision in the run was 0.06 ‰ for $\delta^{18}O$ and 0.23 ‰ for $\delta D$; mean accuracy was 0.04 ‰ for $\delta^{18}O$ and 0.47 ‰ for $\delta D$.

Gases dissolved in pumped groundwaters were sampled by injecting water into $N_2$ purged vials for headspace gas analysis using methods described by Miller et al. (2016) in field campaigns occurring from 2014 to 2017. In addition, the bubble strip method (modified from Kampbell et al., 1998) was used from 2016 to 2018. Details on bubble strip gas sampling are available at `http://dx.doi.org/10.17504/protocols.io.2x5gfq6`. The gas concentrations reported in this study were determined from bubble strip samples. These concentrations were measured on an SRI 8610C gas chromatograph (GC) with $N_2$ as the carrier gas. $H_2$, CO, $CH_4$, and $CO_2$ were separated with a 2 mm by 1 mm ID micropacked ShinCarbon ST column, whereas alkanes of 2 to 6 C atoms ("$C_2 - C_6$ short-chain alkanes") were separated with a PORAPAK Q 6 ft by 0.085 in ID column. Peak intensities were measured concurrently using a thermal conductivity detector (TCD) and a flame ionization detector (FID) and calibrated with standard gas mixes (Supelco Analytical, Bellefonte, PA, USA; accuracy of ±2 % of reported concentration). Measurement repeatability expressed as relative standard deviation was 5 % over most of the calibrated range. The limit of quantitation was defined as the signal at which the relative standard deviation increased to 20 %. In 2018, $H_2$ and CO were analyzed on a Peak Performer 1 gas chromatograph equipped with a reducing compound photometer (RCP). Due to the high sensitivity of the RCP, the signal at limit of quantitation ($S_{LQ}$) for these analyses was defined as $S_{LQ} = S_b + 10 \cdot \sigma_b$, where $S_{mb}$ is the mean signal of blanks prepared in field and $\sigma_b$ is the population standard deviation of these blanks, in accordance with American Chemical Society guidelines (MacDougall et al., 1980). Gaseous concentrations were converted to aqueous concentrations using gas solubilities (Sander, 2015) and corrected for temperature and volume changes between sampling and analysis.

Prior to 2017, bulk stable isotope analyses of $CH_4$ were conducted at the Center for Isotope Geochemistry at the Lawrence Berkeley National Laboratory (LBNL) by gas chromatography/combustion/pyrolysis isotope-ratio mass spectrometry (GC/C/Pyr/IRMS) using methods described by Miller et al. (2016). The

measurement repeatability expressed as 1 sample standard deviation ($s$) for these analyses is $\pm 0.2$ ‰ for $\delta^{13}$C and $\pm 5$ ‰ for $\delta$D.

From 2017 onwards, bulk stable isotope analyses of $CH_4$ and co-occurring alkane gases were conducted at the University of Colorado - Boulder (CUB) by GC/C/Pyr/IRMS using a Trace 1310 GC equipped with an Agilent J & W GS-CarbonPLOT column (30 m length, 0.32 mm ID, 3.0 $\mu$m film) coupled to a Thermo Scientific MAT253 IRMS. $CH_4$ isotope standards purchased from Airgas (uncertainties of $\pm 0.3$ ‰ for $\delta^{13}$C and $\pm 5$ ‰ for $\delta$D) were used for calibration. Over the range of peak amplitudes of analyses reported here, the repeatability expressed as 1 $s$ on analyses of standards is $\pm 0.6$ ‰ for $\delta^{13}$C and $\pm 7$ ‰ for $\delta$D. The analytical uncertainty (accuracy) expressed as 1 standard error on a 3-point calibration was $< 0.3$ ‰ for $\delta^{13}$C and $< 9$ ‰ for $\delta$D (Supporting Information Section S1).

The relative abundances of $CH_4$ isotopologues, including the doubly-substituted isotopologue, $^{13}CH_3D$, were measured at the Massachusetts Institute of Technology (MIT) by tunable infrared laser direct absorption spectroscopy following the methods described by Ono et al. (2014). Abundances of $CH_4$ isotopologues, including both $^{13}CH_3D$ and $^{12}CH_2D_2$, were measured at the University of California, Los Angeles (UCLA) by high-mass-resolution gas-source isotope ratio mass spectrometry following the procedure of Young et al. (2016). The abundance of $^{13}CH_3D$ relative to a random (stochastic) distribution of isotopes among the isotopologues in a $CH_4$ sample is described by its $\Delta^{13}CH_3D$ value, which is defined as: $\Delta^{13}CH_3D = \ln Q$, where $Q$ is the reaction quotient of the isotope exchange reaction:

$$^{13}CH_4 + {}^{12}CH_3D \rightleftharpoons {}^{12}CH_4 + {}^{13}CH_3D. \quad (1)$$

Analogous expressions can be written for doubly-deuterated $CH_4$, $^{12}CH_2D_2$.

### *3.3. 16S rRNA gene sequencing and analysis*

Biomass for DNA extraction was concentrated by pumping 5 L to 20 L of groundwater through Millipore polycarbonate inline filters (0.45 $\mu$m pore diameter, 47 mm filter diameter). At well NSHQ04, a 0.22 $\mu$m pore diameter polyethersulfone Millipore Sterivex filter was used instead due to the lower-flow pump used at this well (Section 3.1). Filters were placed in cryovials, transported frozen in liquid $N_2$, and stored in a $-70$ °C freezer until extraction. DNA was extracted from one quarter subsamples of each filter using a Qiagen PowerSoil DNA extraction kit. The V4 hypervariable region of the 16S rRNA gene was amplified by PCR in duplicate reactions using the 515 (Parada) - 806R (Apprill) primer pair modified to include Illumina adapters and the appropriate error-correcting barcodes. Each 25-$\mu$L reaction mixture included 12.5 $\mu$L of Promega HotStart Mastermix, 10.5 $\mu$L of PCR-grade water, 1 $\mu$L of PCR primers (combined at 10 M), and 1 $\mu$L of purified genomic DNA. PCR consisted of an initial step at 94 °C for 3 min followed by 35 cycles of 94 °C for 45 s, 50 °C for 1 min, and 72 °C for 1.5 min. PCR concluded with a final elongation step at 72 °C for 10 min. No-template controls and DNA extraction controls were subjected to PCR to

check for potential contamination in our PCR and DNA extraction reagents, respectively. Amplification was evaluated via electrophoresis in a 2 % agar gel. Amplicons from duplicate reactions were pooled, cleaned, and their concentrations normalized using a Thermo Fisher SequalPrep normalization plate kit. Amplicons were sequenced on an Illumina MiSeq at the CUB Next-Generation Sequencing Facility with 2-by-150 bp paired-end chemistry.

Sequences were demultiplexed with idemp (`https://github.com/yhwu/idemp`). The resultant fastq files were quality filtered using Figaro v1.1.1 (`https://github.com/Zymo-Research/figaro`) and the DADA2 v1.16 R package (Callahan et al., 2016). Amplicon sequence variants were assigned taxonomy to the genus level using the RDP classifier (Wang et al., 2007) trained on the Silva SSU 138 reference database (Quast et al., 2012) using the DADA2 assignTaxonomy function. Species level assignments were based on exact matching between amplicon sequence variants and sequenced reference strains using the DADA2 addSpecies function. Sequences assigned to mitochondria, chloroplast, and Eukaryota, or not assigned at the domain level (collectively $< 1\,\%$ of sequences), were removed. After all of the above filtering, 24 000 to 40 000 reads per sample remained for the samples presented here obtained in 2018. In addition, 16S rRNA gene sequencing data from previous Oman sampling campaigns (2014 through 2017; Miller et al., 2016; Rempfert et al., 2017; Kraus et al., 2021) were reprocessed in accordance with the methods outlined here to facilitate comparisons across the data sets. The complete data processing pipeline for samples across all years, from raw data provided by the sequencing facility through to taxonomic assignment, are available at `https://github.com/danote/Samail_16S_compilation`. Additional analyses and plotting can be found in the Github supplement for this paper (Section 6). For samples presented in this study, demultiplexed fastq files (without additional processing) are also accessible on the NCBI Short Read Archive under accession PRJNA655565.

### *3.4. Thermodynamic calculations*

Oxidation-reduction potential, pH, and concentrations of major ions and $\sum CO_2$ were used as inputs for the modeling software PHREEQC (Charlton and Parkhurst, 2011; Parkhurst and Appelo, 2013), with which fluids were speciated using the LLNL database. Activities of formate and acetate were separately calculated according to the Debye-Hückel equation. Activities of the aqueous gases were assumed equivalent to their concentrations, which is reasonable for neutral species in low ionic strength solutions. Standard Gibbs free energies ($\Delta G_r^\circ$) of the $CH_4$-forming reactions were calculated using the program SUPCRTBL (Johnson et al., 1992; Zimmer et al., 2016) using conditions of 1 bar and 35 °C to approximate *in situ* conditions. Gibbs free energies were then calculated as $\Delta G_r = \Delta G_r^\circ + RT \ln Q_r$, where $R$ is the universal gas constant, $T$ is temperature, and $Q_r$ is the reaction quotient. All of the above calculations and software inputs and outputs can be found in the Github supplement (Section 6).

## 4. Results and discussion

### *4.1. Controls on groundwater chemistry*

To assess the source and reaction histories of Samail Ophiolite groundwaters, we measured their stable isotopic compositions and solute concentrations. Groundwater $\delta$D and $\delta^{18}$O plotted near local and global meteoric water lines (Weyhenmeyer et al., 2002; Terzer et al., 2013), indicating that the groundwaters derive from rain (Table 3; Supporting Information Figure S2; Matter et al., 2006; Miller et al., 2016; Paukert Vankeuren et al., 2019). The sampled groundwaters included oxidized and moderately alkaline $Mg^{2+} - HCO_3^-$ waters, typical of reaction with peridotite in communication with the atmosphere, and reduced and hyperalkaline $Ca^{2+} - OH^-$ waters, typical of extensive hydration and oxidation of peridotite in closed-system conditions with respect to the atmosphere (Table 3; Barnes et al., 1967; Barnes and O'Neil, 1969; Neal and Stanger, 1985; Bruni et al., 2002; Cipolli et al., 2004; Kelemen et al., 2011; Paukert et al., 2012). $Ca^{2+} - OH^-$ waters had higher conductivities ($930.\,\mu S \cdot cm^{-1}$ to $3350\,\mu S \cdot cm^{-1}$) than $Mg^{2+} - HCO_3^-$ waters ($498\,\mu S \cdot cm^{-1}$ to $1183\,\mu S \cdot cm^{-1}$) (Table 1). The increase in conductivity from $Mg^{2+} - HCO_3^-$ waters to $Ca^{2+} - OH^-$ waters is driven by enrichments in $Ca^{2+}$ derived from dissolution of primary silicate minerals in addition to $Na^+$ and $Cl^-$ derived from mineral dissolution, sea spray, and/or leaching of sea salts introduced during subseafloor alteration and/or ophiolite emplacement (Neal and Stanger, 1985; Stanger, 1986; Murad and Krishnamurthy, 2004; Paukert et al., 2012; Rempfert et al., 2017). The increase in pH from $Mg^{2+} - HCO_3^-$ waters (pH 8.66 to 9.62) to $Ca^{2+} - OH^-$ waters (10.51 to 11.39) was accompanied by a shift to lower $f_{O_2}$ and $Eh$ ($\sim 10^{-51}$ bar and $-174$ mV to $-253$ mV, respectively, in most $Ca^{2+} - OH^-$ waters) (Table 1), indicating reduced conditions in $Ca^{2+} - OH^-$ waters.

Concentrations of $\sum CO_2$ were relatively high in $Mg^{2+} - HCO_3^-$ waters and gabbro waters (up to $3490\,\mu mol \cdot L^{-1}$), but below the limit of quantitation ($< 12\,\mu mol \cdot L^{-1}$) in most $Ca^{2+} - OH^-$ waters (Table 3). This is consistent with water-harzburgite reaction path modeling that terminates at chrysotile-brucite-diopside-calcite equilibrium, corresponding to a $c_{\sum CO_2}$ of $8\,\mu mol \cdot L^{-1}$ at 25 °C and 1 bar (Leong and Shock, 2020). Literature values for $c_{\sum CO_2}$ in ophiolitic $Ca^{2+} - OH^-$ waters are often higher than those predicted by reaction path modeling, but the lower range of reported values approaches $1\,\mu mol \cdot L^{-1}$ (Barnes et al., 1967; Barnes and O'Neil, 1969; Barnes et al., 1978; Neal and Stanger, 1985; Bruni et al., 2002; Cipolli et al., 2004; Paukert et al., 2012; Falk et al., 2016; Brazelton et al., 2017; Canovas III et al., 2017; Crespo-Medina et al., 2017; Rempfert et al., 2017; Fones et al., 2019; Paukert Vankeuren et al., 2019). This spread in the data could reflect groundwater mixing, atmospheric contamination during sampling, differences in reaction temperature and progress, and/or kinetic inhibitions to carbonate mineral precipitation. In $Mg^{2+} - HCO_3^-$ waters and waters from gabbroic aquifers, $\delta^{13}C_{\sum CO_2}$ ranged from $-13.54$ ‰ VPDB to $-10.88$ ‰ VPDB (Table 3), which is comparable to $\delta^{13}C_{\sum CO_2}$ of $Mg^{2+} - HCO_3^-$ waters elsewhere in the ophiolite ($-15.56$ ‰ VPDB to $-13.60$ ‰ VPDB; Matter et al., 2006; Nothaft et al., 2021).

Variable concentrations of $H_2$ and $CH_4$ across wells suggest spatial heterogeneities in sources and sinks of these gases in the ophiolite. In some $Ca^{2+} - OH^-$ waters, $c_{H_2}$ was high (up to $253\,\mu mol \cdot L^{-1}$), but $c_{H_2}$ was below limits of quantitation in other $Ca^{2+} - OH^-$ waters (Figure 2; Table 4). In $Mg^{2+} - HCO_3^-$ waters and waters from gabbroic aquifers, $c_{H_2}$ was generally below limits of quantitation. However, up to $0.992\,\mu mol \cdot L^{-1}$ $H_2$ was measured in well WAB188, which is in gabbro near a faulted contact with peridotites that contain $Ca^{2+} - OH^-$ waters (Figure 1; Table 1). This suggests production of $H_2$ within the gabbro host rock or migration of $H_2$ from peridotites into gabbros surrounding WAB188. In most $Ca^{2+} - OH^-$ waters, $c_{CH_4}$ was high (up to $483\,\mu mol \cdot L^{-1}$; Figure 2, Table 4). However, wells with high $c_{CH_4}$ did not always have high $c_{H_2}$ (Figure 2; Table 4). In $Mg^{2+} - HCO_3^-$ waters and gabbro waters, $c_{CH_4}$ was typically lower ($\leq 0.1\,\mu mol \cdot L^{-1}$), although $c_{CH_4}$ reached $1.83\,\mu mol \cdot L^{-1}$ in well WAB188, where $c_{H_2}$ was also quantitatable.

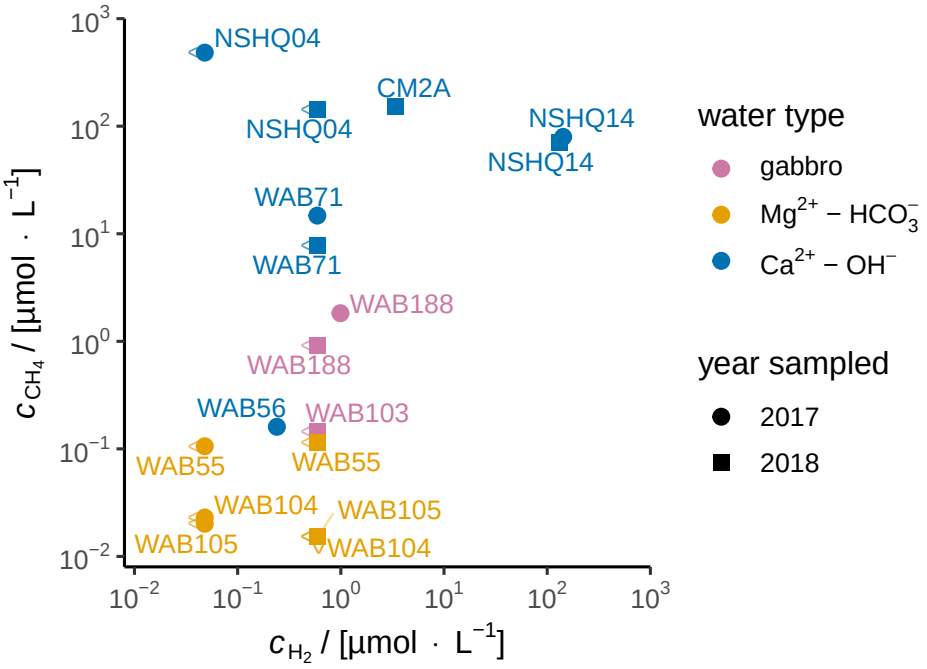


Figure 2: Aqueous concentrations of $CH_4$ and $H_2$ in Oman groundwater samples from 2017 and 2018. Left and down carrots denote "below limit of quantitation" for $CH_4$ and $H_2$, respectively, with the adjacent point plotted at the limit of quantitation for that gas and year of analysis.

### *4.2. Origin of $CH_4$ and co-occurring short-chain alkanes in the Samail Ophiolite*

We begin our examination of $CH_4$ origin in the Samail Ophiolite by calculating Gibbs free energies ($\Delta G_r$) of potential $CH_4$-forming reactions under relevant environmental conditions and discussing these results in light of recent microbiological studies on methanogenesis in the study area. Subsequent discussion focuses on fluid and particulate samples from a subset of wells (NSHQ14, NSHQ04, and WAB188) that yielded

particularly rich data sets from which we infer key $CH_4$ cycle processes. Discussion of three additional wells (WAB71, WAB56, and CM2A) in Supporting Information Text S1 illustrates that the processes outlined below occur throughout the broader study area with some variation due to local hydrogeologic factors.

*4.2.1. Assessing which $CH_4$-forming reactions might occur using thermodynamic and microbiological data*

To assess which $CH_4$-forming aqueous reactions might occur within the Samail Ophiolite, $\Delta G_r$'s were calculated for the following reactions:

$$CO_2(aq) + 4H_2(aq) = CH_4(aq) + 2H_2O(l) \text{ (hydrogenotrophic methanogenesis)} \quad (2)$$

$$CH_3COO^-(aq) + H^+(aq) = CH_4(aq) + CO_2(aq) \text{ (acetoclastic methanogenesis)} \quad (3)$$

$$4HCOO^-(aq) + 4H^+(aq) = CH_4(aq) + 3CO_2(aq) + 2H_2O(l) \text{ (formate disproportionation).} \quad (4)$$

Gas-phase, abiotic reactions are also possible (Etiope and Ionescu, 2015; Etiope et al., 2018), but measurements of partial pressures of relevant gases in unsaturated zones of the subsurface in the study area are absent. Thus, $\Delta G_r$'s of gas-phase reactions were not calculated. In addition to the common hydrogenotrophic and acetoclastic modes of methanogenesis, formate disproportionation (Equation 4) was considered because formate can be produced abiotically in serpentinizing settings (McCollom and Seewald, 2003; McDermott et al., 2015; Miller et al., 2017b) and has been suggested as an important substrate for microbial metabolism in these settings (Lang et al., 2018), including for methanogenesis (Fones et al., 2020).

Rather than calculate $\Delta G_r$'s of the above reactions for each individual groundwater chemical analysis, we investigate a range of generalized cases to highlight the most important factors controlling $\Delta G_r$'s and to assess energetic states of the system that lay beyond our analytical limits. For instance, $\sum CO_2$ was below the limit of quantitation for the majority of the $Ca^{2+} - OH^-$ groundwaters sampled in 2018 ($< 12\,\mu mol \cdot L^{-1}$; Table 3). $H_2$ was also below the limit of quantitation for several $Ca^{2+} - OH^-$ and $Mg^{2+} - HCO_3^-$ groundwaters ($< 0.048\,nmol \cdot L^{-1}$ in 2017 and $< 0.598\,nmol \cdot L^{-1}$ in 2018; Table 4). Further, formate and acetate were not measured explicitly for this study, but were measured on groundwaters from the studied wells sampled in 2015 (Rempfert et al., 2017). Thus, while robust constraints on the above parameters are available for the study area, complete sets of these parameters were generally not directly or simultaneously measured.

In light of this, we considered a representative $Mg^{2+} - HCO_3^-$ groundwater and a representative $Ca^{2+} - OH^-$ groundwater, made informed assumptions when direct concentration measurements were lacking, and evaluated $\Delta G_r$'s for a range of $H_2$ concentrations. Measurements of major inorganic dissolved constituents, pH, and *Eh* from wells WAB105 and NSHQ14 were used for the model $Mg^{2+} - HCO_3^-$ and $Ca^{2+} - OH^-$ fluids, respectively (Tables 1 and 3). Since measured $c_{\sum CO_2}$ was below the limit of quantitation in the

water sample from NSHQ14, $8\,\mu\text{mol}\cdot\text{kg}^{-1}$ was taken as the $c_{\sum \text{CO}_2}$ of the representative $\text{Ca}^{2+} - \text{OH}^-$ water, corresponding to the value at chrysotile-brucite-diopside-calcite equilibrium at 25 °C and 1 bar obtained from water-harzburgite reaction path modeling (Leong and Shock, 2020). Concentrations of formate and acetate were both assumed to be $1\,\mu\text{mol}\cdot\text{kg}^{-1}$, which is consistent with their concentrations in earlier samples from wells in Samail Ophiolite (Rempfert et al., 2017). Concentrations of $CH_4$ were assumed to be $100\,\mu\text{mol}\cdot\text{kg}^{-1}$ and $0.1\,\mu\text{mol}\cdot\text{kg}^{-1}$ for the representative $\text{Ca}^{2+} - \text{OH}^-$ and $\text{Mg}^{2+} - \text{HCO}_3^-$ waters, respectively, reflecting typical concentrations for these fluids (Table 4, Figure 2). $H_2$ concentrations vary widely between and within fluid types (Table 4, Figure 2), so calculations were performed for multiple $H_2$ concentrations ($1\,\text{mmol}\cdot\text{kg}^{-1}$, $1\,\mu\text{mol}\cdot\text{kg}^{-1}$, and $1\,\text{nmol}\cdot\text{kg}^{-1}$) encompassing the range of concentrations observed in $\text{Ca}^{2+} - \text{OH}^-$ fluids. The $1\,\text{mmol}\cdot\text{kg}^{-1}$ $H_2$ case was omitted for the $\text{Mg}^{2+} - \text{HCO}_3^-$ fluid, where such high $H_2$ concentrations are not observed. The log activities ($a$) of all relevant species are tabulated in Table 5.

The calculated $\Delta G_r$'s (Table 5) indicate that all of the $CH_4$-forming reactions considered here can have sufficient chemical potential to sustain microbial life in certain states of the system. That is, $\Delta G_r > \Delta G_{\text{min}}$, where $\Delta G_{\text{min}}$ (also known as the Biological Energy Quantum) is the minimum free energy that must be available to sustain life in a given environment (thought to be around $-9\,\text{kJ}\cdot\text{mol}^{-1}$ to $-20\,\text{kJ}\cdot\text{mol}^{-1}$; Schink, 1997; Hoehler, 2004; Schink and Stams, 2006). Acetoclastic methanogenesis had the most negative $\Delta G_r$ in all conditions tested. Formate disproportionation had more negative $\Delta G_r$ than hydrogenotrophic methanogenesis in all $\text{Ca}^{2+} - \text{OH}^-$ conditions tested, but formate disproportionation had less negative $\Delta G_r$ than hydrogenotrophic methanogenesis in the $\text{Mg}^{2+} - \text{HCO}_3^-$ case at $1\,\mu\text{mol}\cdot\text{kg}^{-1}$ $H_2$. Hydrogenotrophic methanogenesis had sufficient chemical potential to sustain microbial life only when $a_{H_2}$ was high enough, with the threshold $a_{H_2}$ being higher in $\text{Ca}^{2+} - \text{OH}^-$ waters, where $a_{\text{CO}_2\text{(aq)}}$ is lower. These calculations are generally consistent with those of Canovas III et al. (2017), who found that hydrogenotrophic methanogenesis had modest potential energy yields in waters from surface seeps in the Samail Ophiolite at pH ranging from 8 to 12.

Several additional factors should be considered when interpreting the $\Delta G_r$ results. First, reactions proceeding in environmental systems are often drawn towards equilibrium, and thus a large negative $\Delta G_r$ of a given reaction may indicate that that reaction is not actively occuring, but only has the potential to occur. Second, substrate transport into the cell is not addressed in our calculations. A more complete model would account for rates of $CO_2$ diffusion across the cell membrane and/or energy expended to transport charged species such as formate and acetate into the cell (Hoehler, 2004). Third, mixing is not explicitly accounted for in our calculations. Mixing has been suggested as a key factor controlling energetic favorability of various reactions in the Samail Ophiolite. This is especially pertinent to hydrogenotrophic methanogenesis because $c_{\text{CO}_2}$ is so much lower in endmember hyperalkaline fluids than in near-surface, atmosphere-influenced fluids (Canovas III et al., 2017; Leong and Shock, 2020). The $c_{\text{CO}_2}$ used for the example $\text{Ca}^{2+} - \text{OH}^-$ fluid in our calculations is representative of a minimum value for the system (Leong and Shock, 2020). Mixing would

tend to inject $CO_2$ into the fluids and increase the energetic favorability of hydrogenotrophic methanogenesis.

In addition to energetic considerations, microbiological approaches can help elucidate which $CH_4$-forming reactions occur. Kraus et al. (2021) found higher transcript abundances of carbonic anhydrase and formate dehydrogenase relative to acetate kinase and phosphate acetyltransferase in hyperalkaline groundwaters from wells in the Samail Ophiolite, suggesting that $CO_2/HCO_3^-$ and formate are more actively used substrates for methanogenesis than acetate in these conditions. Further, Fones et al. (2020) identified two lineages of *Methanobacterium* in Samail Ophiolite groundwaters that were shown by genomic and microcosm-based radiotracer approaches to use different methanogenic pathways. *Methanobacterium* Type I lineage predominated in circumneutral waters and is capable of using either $CO_2$ or formate for methanogenesis. *Methanobacterium* Type II lineage, which was more abundant in hyperalkaline waters and which branched from the Type I lineage, was exclusively capable of formatotrophic methanogenesis. It was postulated that gene loss and acquisition in Type II lineage allowed it to be specially suited to the high-pH and low-$\sum CO_2$ conditions resulting from extensive serpentinization. Thus, microbiological data suggest that hydrogenotrophic or formatotrophic methanogenesis are the most likely pathways for methanogenesis in the Samail Ophiolite and that the relative contributions of each of these pathways to microbial $CH_4$ production at a given site may depend on local geochemical factors such as $a_{CO_{2(aq)}}$. This notion is generally supported by our calculations in that formate disproportionation had more negative $\Delta G_r$ than hydrogenotrophic methanogenesis in all $Ca^{2+} - OH^-$ conditions tested, whereas the reverse was true for the $Mg^{2+} - HCO_3^-$ case at $1\,\mu mol \cdot kg^{-1}$ $H_2$.

Remarkably, although acetoclastic methanogenesis had the most negative $\Delta G_r$ of the investigated $CH_4$-forming reactions (Table 5), it has the least microbiological evidence of being a major methanogenic pathway in the Samail Ophiolite. Conversion of isotopically labeled acetate ($^{13}CH_3OO^-$) to $^{13}CH_4$, has, however, been documented in cultures from serpentinite springs in the Voltri Massif, Italy (Brazelton et al., 2017), indicating that acetoclastic methanogenesis can operate in some serpentinizing settings. In the aquifers sampled via wells in the Samail Ophiolite, methanogens may be out-competed for acquisition of acetate by other groups of microbes, such as sulfate reducers. Indeed, geochemical evidence of microbial acetate oxidation coupled to sulfate reduction has been reported in alkaline, $H_2$-rich, crystalline rock aquifers inhabited by microbial communities dominated by sulfate reducing bacteria and methanogens (Moser et al., 2005).

#### *4.2.2. Abiotic, $^{13}C$-enriched $CH_4$, $C_2H_6$, and $C_3H_8$ mixed with microbial $CH_4$ produced under C-limited conditions in the $Ca^{2+} - OH^-$ waters of well NSHQ14*

Well NSHQ14 is situated in a catchment dominated by partially serpentinized harzburgite with meter-scale partially serpentinized dunite bands (Figure 1; Supporting Information Figure S1; Table 1). The well is cased to 5.8 meters below ground level (mbgl) and drilled to 304 mbgl (Table 1). Groundwaters accessed via NSHQ14 had the highest pH (11.39), and lowest *Eh* (−253 mV) and $f_{O_2}$ ($1.19 \cdot 10^{-51}$ bar) among the

wells investigated (Table 1), indicating that fluids sampled from NSHQ14 have extensively participated in serpentinization. This is also reflected in the $c_{H_2}$ of groundwaters sampled at NSHQ14, which was the highest among the studied wells ($253\,\mu mol \cdot L^{-1}$ and $131\,\mu mol \cdot L^{-1}$ in 2017 and 2018, respectively; Table 4; Figure 2). NSHQ14 waters also had high $c_{CH_4}$ ($106\,\mu mol \cdot L^{-1}$ and $71.2\,\mu mol \cdot L^{-1}$ in 2017 and 2018, respectively).

$CH_4$ has ranged in $\delta^{13}C$ from $-6.89\,‰$ VPDB to $+3.7\,‰$ VPDB in fluid samples from NSHQ14, with a mean weighted by sample year of $-0.8\,‰$ VPDB (Figure 3a; Table 2). These $\delta^{13}C$ values are generally higher than those of $CH_4$ emanating from sediment-poor seafloor hydrothermal vents, where a dominantly abiotic origin has been proposed ((Welhan and Craig, 1983; Merlivat et al., 1987; Charlou et al., 1996, 2000, 2002; Proskurowski et al., 2008; Kumagai et al., 2008; McDermott et al., 2015; Wang et al., 2018); represented by Mid-Cayman Rise, Lost City, and Ashadze II in Figure 3a), higher than typical mantle values (Deines, 2002), and similar to marine carbonate (Schidlowski, 2001). $CH_4$ $\delta^{13}C$ at NSHQ14 is generally higher than $\delta^{13}C$ of carbonate veins in NSHQ14 ($-7.05\,‰$ VPDB to $-4.69\,‰$ VPDB; Miller et al., 2016), which is opposite to that which would be expected at equilibrium (Bottinga, 1969), indicating that $CH_4$ is not in isotopic equilibrium with co-existing carbonate minerals.

$CH_4$ is accompanied by $C_2-C_6$ alkanes in fluids from NSHQ14 (Table 4). These alkanes had $C_1/(C_2+C_3)$ ratios of 1240 in 2017 and 881 in 2018, which are similar to fluid samples and rock crushings from other ophiolites and sediment-poor seafloor hydrothermal vents (Abrajano et al., 1990; Charlou et al., 2010; McDermott et al., 2015; Grozeva et al., 2020), but $10^2$ times higher than those of Kidd Creek mine, Canada, for which a low-temperature, abiotic origin of alkanes has been proposed (Sherwood Lollar et al., 2002, 2008; Young et al., 2017) (Figure 3c). Thus, $C_1/(C_2+C_3)$ ratios could reflect differences in alkane formation mechanisms or extents of reaction in Precambrian shield sites like Kidd Creek versus ophiolites and sediment-poor seafloor hydrothermal vents.

$C_2H_6$ and $C_3H_8$ at NSHQ14 are strongly $^{13}C$-enriched ($\delta^{13}C$ of $-6.0\,‰$ VPDB and $+3.3\,‰$ VPDB, respectively; Table 2; Figure 4). The observed $\delta^{13}C$ values are $\sim 15\,‰$ higher than those in the most mature (and therefore most $^{13}C$-enriched) thermogenic $C_2H_6$ and $C_3H_8$ samples from confined systems (Milkov and Etiope, 2018; Fiebig et al., 2019). Increases in $\delta^{13}C_{C_3}$ of $\sim 15\,‰$ have been attributed to microbial oxidation of short-chain alkanes, which enriches the residual in $^{13}C$ (Martini et al., 2003). However, short-chain alkane oxidizing microbial species (Shennan, 2006; Singh et al., 2017; Laso-Pérez et al., 2019) were not detected in 16S rRNA gene sequences of DNA obtained from NSHQ14. Thus, there is not strong evidence to suggest that $\delta^{13}C_{C_2}$ and $\delta^{13}C_{C_3}$ at NSHQ14 result from post-genetic microbial alteration. Rather, $\delta^{13}C_{C_2}$ and $\delta^{13}C_{C_3}$ should reflect formation conditions and C source(s).

$C_2H_6$ and $C_3H_8$ at NSHQ14 are not likely to derive from nearby organic matter. Hydrocarbon-rich sedimentary formations in northern Oman not only lack a clear structural connection to the ophiolite aquifer, but also yield oils with $\delta^{13}C$ values (Terken, 1999) at least $20\,‰$ lower than those of $C_2H_6$ and

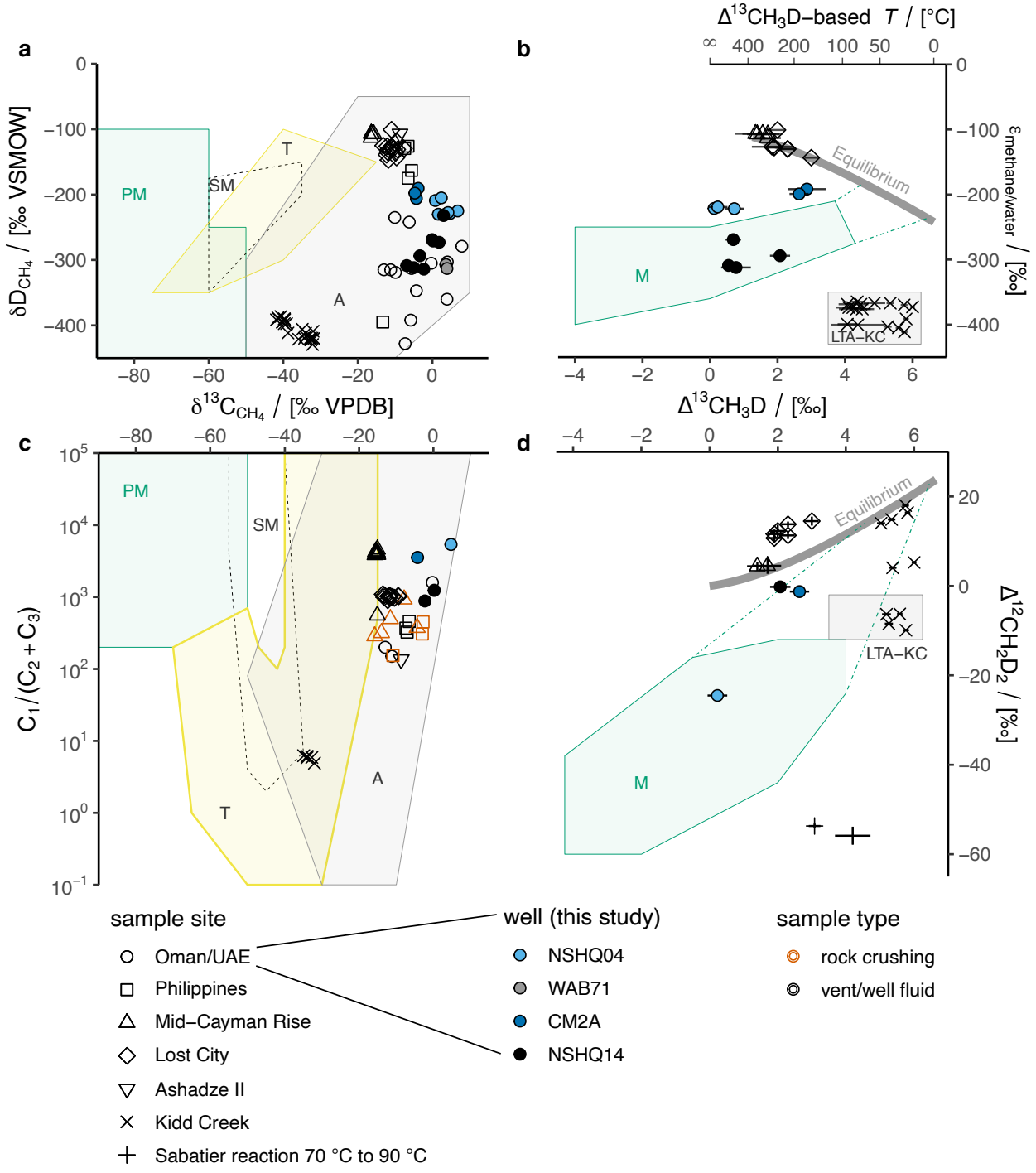


$C_3H_8$ at NSHQ14. Furthermore, total organic C in peridotites exposed to alteration at the seafloor, a proxy for organic C endogenous to the Samail Ophiolite, is also relatively $^{13}$C-depleted (approximately $-25 \pm 5$ ‰ VPDB; Alt et al., 2013, 2012a,b; Delacour et al., 2008). Closed-system thermal cracking of these organic matter sources is unlikely to have produced the comparatively $^{13}$C-enriched $C_2H_6$ and $C_3H_8$ at

Figure 3: Molecular and isotopic compositions of natural gases. (a) Plot of $\delta D_{CH_4}$ vs. $\delta^{13}C_{CH_4}$. Shaded fields of typical gas origin after Milkov and Etiope (2018). *Abbreviations:* PM, primary microbial; SM, secondary microbial; T, thermogenic; A, abiotic. (c) Plot of ratio of methane ($C_1$) to the sum of ethane ($C_2$) and propane ($C_3$) vs. $\delta^{13}C_{CH_4}$. Only analyses for which $C_2$ was above limit of quantitation are plotted. If $C_3$ was below limit of quantitation, its contribution to $C_1/(C_2 + C_3)$ was assumed to be negligible, and therefore $C_1/C_2$ is plotted. Fields and abbreviations same as in (a). In (a) and (c), uncertainties are smaller than plotted symbols. (b) Plot of $\varepsilon_{methane/water}$ vs. $\Delta^{13}CH_3D$. X and Y axes are swapped with respect to original publication of this type of plot (Wang et al., 2015) so that (b) is comparable against (d). The data from (b) are plotted in the Wang et al. (2015) orientation in Supporting Information Figure S4. Equilibrium line from Horibe and Craig (1995) and Young et al. (2017). *Abbreviations:* LTA-KC, low-temperature abiotic (Kidd Creek-type); M, microbial. Green dot-dashed lines in (b) and (d) indicate a range of $CH_4$ isotopic compositions that have been attributed to either low cell-specific rates of methanogenesis or anaerobic oxidation of methane; that is, they start at isotopic compositions produced by methanogen cultures and end at isotopic equilibrium between 5 °C and 70 °C, which is the range of temperatures over which anaerobic oxidation of methane has been documented (Wang et al., 2015; Stolper et al., 2015; Young et al., 2017; Ash and Egger, 2019; Giunta et al., 2019). (d) Plot of $\Delta^{13}CH_3D$ vs. $\Delta^{12}CH_2D_2$, after Young et al. (2017). Fields, abbreviations, and temperature axis same as in (b). In (b) and (d), error bars represent 95 % confidence interval for analyses performed at MIT, and 1 standard error for analyses performed at UCLA. Contextual data from ophiolites: Oman/UAE (Fritz et al., 1992; Etiope et al., 2015; Boulart et al., 2013; Miller et al., 2016; Vacquand et al., 2018), the Philippines (Abrajano et al., 1990; Grozeva et al., 2020); sediment-poor seafloor hydrothermal vents: Mid-Cayman Rise (McDermott et al., 2015; Wang et al., 2018; Grozeva et al., 2020), Lost City (Proskurowski et al., 2008; Wang et al., 2018; Labidi et al., 2020), Ashadze II (Charlou et al., 2010); Precambrian Shield: Kidd Creek, Canada (Sherwood Lollar et al., 2008; Young et al., 2017); and laboratory Sabatier reaction catalyzed by Ru (Young et al., 2017).

NSHQ14 and previously reported elsewhere in the ophiolite (Figure 4; Fritz et al., 1992).

Thermal cracking of organic matter and open-system degassing can enrich late-produced short-chain alkanes in $^{13}C$ due to kinetic isotope effects associated with the cleavage of precursor sites in the parent organic matter and the resultant Rayleigh distillation of these sites (Rooney et al., 1995; Fiebig et al., 2019). Thermogenic gas production can proceed slowly at temperatures as low as 60 °C, but substantial thermogenic gas production typically occurs at reservoir temperatures above 120 °C (Burnham, 1989; Hunt, 1996; Stolper et al., 2018; Cumming et al., 2019; Fiebig et al., 2019). These temperatures are higher than temperatures along groundwater flow paths intersecting the wells in this study. Measured groundwater temperatures in the study area are $\sim$ 35 °C (Table 1), and $H_2 - H_2O$ isotope thermometry and $C - O$ clumped isotope thermometry on carbonate veins with significant $^{14}C$ contents in Samail Ophiolite peridotites both indicate equilibrium $\leq$ 60 °C (Kelemen and Matter, 2008; Kelemen et al., 2011; Mervine et al., 2014; Miller et al., 2016). Geothermal gradients derived from geophysical logs of NSHQ14 are 25 °C $\cdot$ km$^{-1}$ (Paukert, 2014; Matter et al., 2017), which is typical of near-surface, continental settings (Lowell et al., 2014). At the low temperatures and ordinary geothermal gradients within the active alteration zone of the Samail Ophiolite, thermal cracking of organic matter is unlikely to proceed at sufficient rates to attain the high extents of reaction progress necessary to explain the observed $^{13}C$ enrichments in short-chain alkanes at NSHQ14 over relevant timescales.

Alternatively, short-chain alkanes in NSHQ14 fluids may have an abiotic source. Several studies have demonstrated storage of large quantities of $CH_4$ and associated short-chain alkanes in fluid inclusions in ophiolites (Sachan et al., 2007; Klein et al., 2019; Grozeva et al., 2020). However, the findings of these studies disagree with those of Etiope et al. (2018), who measured relatively low concentrations of $CH_4$ stored in serpentinized peridotites from Greek ophiolites. Since the rocks analyzed by Etiope et al. (2018) were sampled from outcrops, it is possible that chemical or physical processes associated with surface exposure resulted in loss of $CH_4$ once stored in peridotite-hosted fluid inclusions prior to analysis. Although further study of the quantity and spatial distribution of $CH_4$ storage in ophiolitic rocks is warranted, the presence of $CH_4$ + $H_2$ inclusions in olivine and $CH_4$ ± graphite inclusions in orthopyroxene in Samail Ophiolite harzburgites (Miura et al., 2011) requires that fluid inclusions be considered as a potential source for abiotic $CH_4$ and associated short-chain alkanes at NSHQ14 and elsewhere in the ophiolite.

A fluid inclusion source of $CH_4$ and short-chain alkanes is compatible with C stable isotopic compositions of these compounds in groundwaters pumped from NSHQ14. $CH_4$, $C_2H_6$, and $C_3H_8$ $\delta^{13}C$ values at NSHQ14 (−6.89 ‰ VPDB to +3.7 ‰ VPDB; Table 2) overlap with $CH_4$ and $C_2H_6$ $\delta^{13}C$ values measured by Grozeva et al. (2020) in rock crushing experiments on $CH_4$-rich fluid inclusion-bearing peridotites and dunites sampled from the Zambales ophiolite in the Philippines (−12.4 ‰ VPDB to −0.9 ‰ VPDB; Figure 4), which, in turn, overlap with $\delta^{13}C$ values of $CH_4$ from nearby gas seeps at Los Fuegos Eternos and Nagsasa in the Philippines (−7.4 ‰ VPDB to −5.6 ‰ VPDB; Figure 3a; Abrajano et al., 1990; Vacquand et al., 2018). Grozeva et al. (2020) also crushed $CH_4$-rich fluid inclusion-bearing rocks from the Mid-Cayman Rise. Of the Mid-Cayman Rise samples that yielded sufficient $CH_4$ and $C_2H_6$ for precise C isotopic analysis, which were all mafic intrusive rocks, $\delta^{13}C$ values ranged from −14.0 ‰ VPDB to +0.7 ‰ VPDB. The lower end of Mid-Cayman Rise rock crushing short-chain alkane $\delta^{13}C$ values are similar to those measured in Mid-Cayman Rise hydrothermal vent fluids (−15.8 ‰ VPDB to −9.7 ‰ VPDB; McDermott et al., 2015), whereas the higher end are similar to those of NSHQ14 (Figure 4). Furthermore, $C_2H_6$ and $C_3H_8$ $\delta^{13}C$ values of NSHQ14 fluids resemble those of fluids discharging from the sediment-poor hydrothermal vents at Ashadze II, Mid-Atlantic Ridge (Figure 4; Charlou et al. 2010). The similarities in short-chain alkane $\delta^{13}C$ values between circulating fluids and rock-hosted fluid inclusions in ophiolites and present-day oceanic lithospheric sites suggest that circulating fluids in both environments derive much of their $CH_4$ and short-chain alkanes from fluid inclusions.

Sources of $CH_4$ can also be assessed by measuring H isotopic compositions and clumped isotopologue relative abundances of $CH_4$ and comparing these isotopic compositions to temperature-dependent equilibria. These isotopic equilibria are represented by thick gray lines in Figure 3b and d. Intra-$CH_4$ equilibrium is governed by the increasing relative stability of bonds between two heavy isotopes (more "clumping") at lower temperatures, which is reflected in higher $\Delta^{13}CH_3D$ and $\Delta^{12}CH_2D_2$ values. However, isotopic equilibrium will only be expressed if kinetics allow it. In the first study to publish clumped isotopologue ($\Delta^{13}CH_3D$)

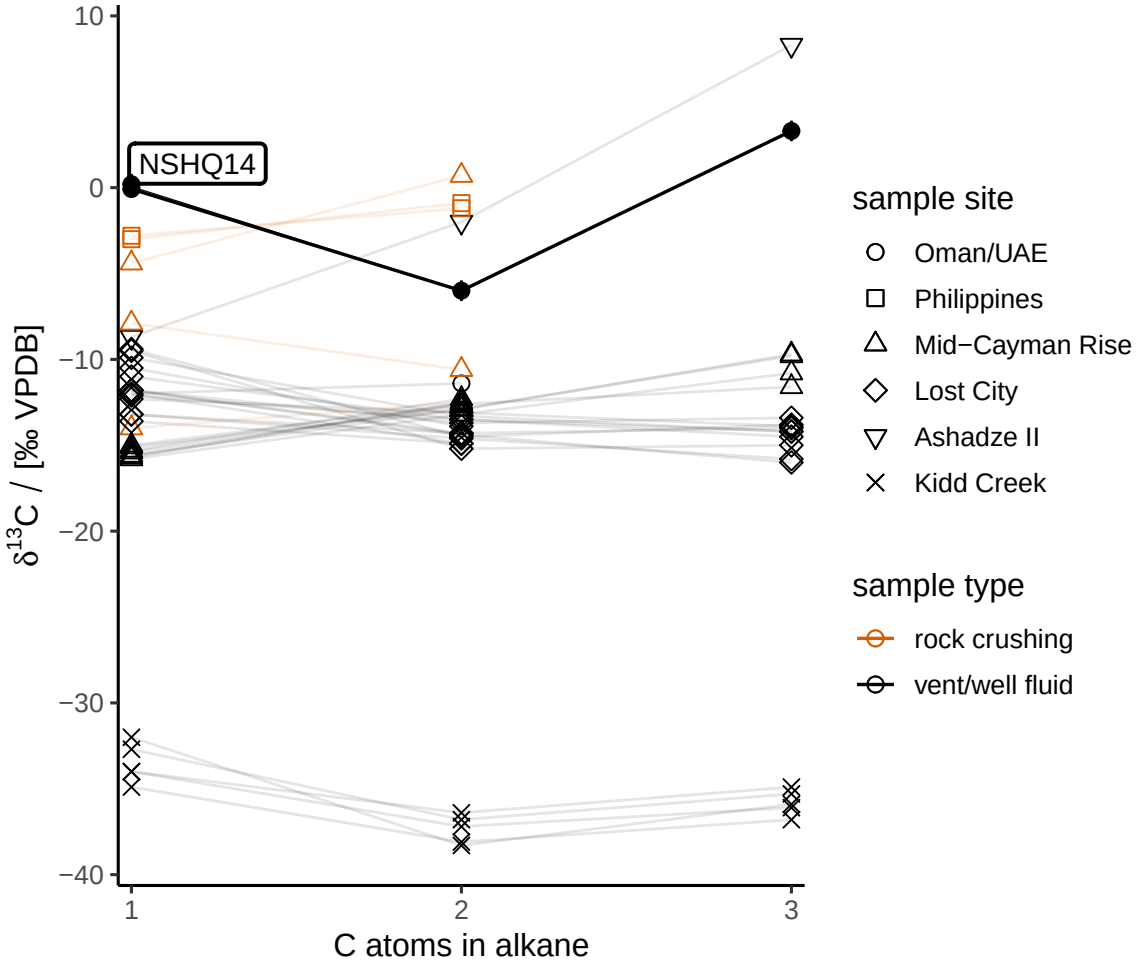


Figure 4: Plot of $\delta^{13}C$ of $CH_4$ and co-occurring $n$-alkanes vs. the number of C atoms per molecule. Error bars represent uncertainties on $\delta^{13}C$ analyses performed at CUB. Only samples for which $\delta^{13}C_{C_2}$ was determined are plotted. Contextual data from ophiolites: Oman/UAE (Fritz et al., 1992), the Philippines (Grozeva et al., 2020); sediment-poor seafloor hydrothermal vents: Mid-Cayman Rise (McDermott et al., 2015; Grozeva et al., 2020), Lost City (Proskurowski et al., 2008), Ashadze II (Charlou et al., 2010); and Precambrian Shield: Kidd Creek, Canada (Sherwood Lollar et al., 2008).

data on $CH_4$- and $H_2$- rich gases from sediment-poor seafloor hydrothermal vents, Wang et al. (2018) found that these gases yielded apparent $CH_4 - H_2O$ H isotopic and $\Delta^{13}CH_3D$ equilibrium temperatures of 270 °C to 360 °C, despite having a range of effluent fluid temperatures from 96 °C to 370 °C. This was interpreted as evidence for a closure temperature of 270 °C for H isotope exchange in the $CH_4 - H_2O$ and $CH_4 - H_2$ systems in seafloor hydrothermal settings (e.g. Mid-Cayman Rise in Figure 3b and d). However, in a subsequent study that re-analyzed some of the same samples, plus a greater number of samples from low-temperature vents at Lost City (96 °C to 64 °C), and contributed the first $\Delta^{12}CH_2D_2$ values from these settings, Labidi et al. (2020) found evidence for re-equilibration of clumped isotopologue and $CH_4 - H_2O$ H isotopic systems at lower temperatures. Of these isotopic systems, that of $^{12}CH_2D_2$ had the fastest apparent

re-equilibration kinetics (approximately twice as fast as $^{13}CH_3D$), which was explained by differences in symmetry numbers among the isotopologues. The $^{12}CH_2D_2$-based temperatures of the Lost City samples, which were as low as $69^{+4}_{-4}$ °C, closely matched their end member vent fluid temperatures. As a result of the apparent faster re-equilibration of $^{12}CH_2D_2$, the Lost City data plot above the $^{13}CH_3D - {}^{12}CH_2D_2$ equilibrium line (towards higher $\Delta^{12}CH_2D_2$) in Figure 3d. Therefore, isotopic compositions of $CH_4$ formed in fluid inclusions in the oceanic lithosphere and stored for millions of years at low temperatures may be expected to fall somewhere along a continuum from $\Delta^{13}CH_3D$, $\Delta^{12}CH_2D_2$, and $CH_4 - H_2O$ isotopic equilibrium at $\sim 330\,°C$ to compositions approaching lower temperature ($\sim 70\,°C$ or perhaps even lower) equilibrium, with $^{12}CH_3D$, $^{13}CH_3D$, $CH_4 - H_2O$ isotopic re-equilibration proceeding at varying rates. This is not the case for Samail Ophiolite samples, as detailed below.

Across five years of samples from NSHQ14, $\delta D_{CH_4}$ has ranged from $-232$ ‰ VSMOW to $-311.73$ ‰ VSMOW, with a mean weighted by sample year of $-275$ ‰ VSMOW (Figure 3a; Table 2). This $CH_4$ is D-enriched with respect to coexisting $H_2$ ($\delta D_{H_2} = -685$ ‰ VSMOW; Miller et al., 2016) and D-depleted with respect to coexisting water ($\delta D_{H_2O} = +0.2$ ‰ VSMOW in 2018; Table 3). Although $H_2$ and water reflect H isotopic equilibrium at $\sim 50\,°C$ (Miller et al., 2016), both $H_2$ and water are in H isotopic disequilibrium with $CH_4$ (Figure 3b). Moreover, NSHQ14 fluids exhibit intra-$CH_4$ disequilibrium, as indicated by $\Delta^{13}CH_3D$ and $\Delta^{12}CH_2D_2$ values (Table 2) plotting below the equilibrium line in Figure 3d. These non-equilibrium isotopic compositions indicate that post-genetic alteration of $CH_4$ must have occurred or that fluid inclusions are not the only source of $CH_4$ at NSHQ14.

One potential post-genetic alteration mechanism is diffusion. However, $CH_4$ at NSHQ14 cannot be the diffusion residual of $CH_4$ that was originally at intramolecular equilibrium (or with $\Delta^{12}CH_2D_2$ above the apparent $\Delta^{13}CH_3D$ equilibrium temperature) because the diffusion slope (change in $\Delta^{12}CH_2D_2$ over change in $\Delta^{13}CH_3D$) is shallower than the equilibrium line slope over the relevant temperature range (Young et al., 2017). Another potential alteration mechanism is microbial $CH_4$ oxidation. Two types of microbial $CH_4$ oxidation have been studied for their effects on $CH_4$ clumped isotopologue relative abundances: anaerobic methane oxidation of the ANME type and aerobic $CH_4$ oxidation. ANME-type anaerobic methane oxidation is suggested to be a highly reversible metabolic pathway (Knittel and Boetius, 2009; Timmers et al., 2017). This reversibility has been proposed to bring $\Delta^{13}CH_3D$ and $\Delta^{12}CH_2D_2$ towards equilibrium at low temperatures (70 °C to 30 °C) through continuous breaking and reforming of bonds in the $CH_4$ molecule (Young et al., 2017; Ash and Egger, 2019; Giunta et al., 2019). Thus, the comparatively low $\Delta^{13}CH_3D$ and $\Delta^{12}CH_2D_2$ values observed in samples from NSHQ14 and other wells in this study (Figure 3b and d) do not support a major role for anaerobic methane oxidation in the study area. Aerobic $CH_4$ oxidation is less reversible than ANME-type anaerobic methane oxidation due to differences in the enzymes and electron acceptors used for those respective processes. For this reason, aerobic $CH_4$ oxidation does not bring $CH_4$ into isotopic equilibrium, but rather imparts a normal, classical kinetic isotope effect during $CH_4$ consump-

tion. In a study of the effect of aerobic $CH_4$ oxidation on $\Delta^{13}CH_3D$, Wang et al. (2016) found that the fractionation factor for $^{13}CH_3D$ was closely approximated by the product of the fractionation factors for $^{13}CH_4$ and $^{12}CH_3D$. Although it has not yet been demonstrated experimentally, it is hypothesized that the fractionation factor for $^{12}CH_2D_2$ during aerobic $CH_4$ oxidation may likewise be approximated by the square of the fractionation factor for $^{12}CH_3D$ (Young, 2020). This "product rule" for isotopic fractionation during aerobic $CH_4$ oxidation results in decreases in $\Delta^{13}CH_3D$ and $\Delta^{12}CH_2D_2$ with concomitant increases in $\delta^{13}C$ and $\delta D$ in residual $CH_4$ (Wang et al., 2016; Young, 2020). Thus, aerobic $CH_4$ oxidation could draw $\Delta^{13}CH_3D$ and $\Delta^{12}CH_2D_2$ values originally near equilibrium down below the equilibrium line in Figure 3d. However, if $CH_4$ samples from NSHQ14 were originally near H isotope equilibrium with water of SMOW-like isotopic composition, aerobic methane oxidation would push the residual $CH_4$ towards higher $\delta D$ (and $\varepsilon_{\mathrm{methane/water}}$) values (above the equilibrium line in Figure 3b), which is inconsistent with the comparatively low $\delta D_{CH_4}$ observed at NSHQ14.

For the reasons outlined above, post-genetic alteration of $CH_4$ near $CH_4 - H_2O$ and intramolecular isotopic equilibrium does not explain the observed isotopic compositions of $CH_4$ sampled from NSHQ14. Therefore, the release of $CH_4$ stored in fluid inclusions cannot account for all of the $CH_4$ at NSHQ14. Alternative processes that do produce $CH_4$ with $\Delta^{13}CH_3D$ and $\Delta^{12}CH_2D_2$ values lower than equilibrium include microbial methanogenesis and low-temperature ($\leq 90\,^{\circ}C$) abiotic reduction of $CO_2$ or CO through Sabatier or Fischer-Tropsch-type reactions. In Figure 3b and d, microbial methanogenesis is represented by samples from cultures (green shaded areas; Wang et al., 2015; Stolper et al., 2015; Young et al., 2017; Gruen et al., 2018; Young, 2020), and low-temperature Sabatier or Fischer-Tropsch-type reactions are represented by field samples from Kidd Creek (gray shaded areas; Young et al., 2017; Sherwood Lollar et al., 2002, 2008) and laboratory experiments with synthetic Ru catalysts (Young et al., 2017; Etiope and Ionescu, 2015).

To independently assess the potential influences of microbial processes on $CH_4$ concentration and isotopic composition, DNA was extracted from biomass in pumped groundwaters and subjected to amplification and sequencing of 16S rRNA genes. 16S rRNA gene sequences of biomass collected in 2018 were searched for matches to known $CH_4$-cycling taxa, as compiled previously by Crespo-Medina et al. (2017). Sequences closely affiliated with both methanogenic and methanotrophic taxa were found to be widespread in the aquifer (Figure 5). Based on phylogenetic inference, the dominant methanogenic taxon was related to the genus *Methanobacterium*, whose members can produce $CH_4$ from $H_2$ and $CO_2$, CO, or formate (Balch et al., 1979). *Methanobacterium* comprised a high proportion (24 %) of 16S rRNA gene sequences at NSHQ14 in 2018. Relative abundances of *Methanobacterium* 16S rRNA gene reads were similarly high in 2017 (12 %) and 2016 (28 %), but lower (< 1 %) in 2015 and 2014 (Miller et al., 2016; Rempfert et al., 2017; Kraus et al., 2021). The increase in the relative abundance of 16S rRNA genes affiliated with *Methanobacterium* in samples collected in 2016 and onwards versus those collected in 2014 and 2015 coincided with a change in sampling methods from smaller, lower-flow pumps (maximum depth 20 m) prior to 2016 to larger, higher-flow

pumps (maximum depth 90 m). The obligate anaerobic nature of this methanogen genus (Boone, 2015) is consistent with its higher relative gene abundances in fluids sampled from greater depths, which presumably receive less input of atmospheric $O_2$ than do shallower fluids.

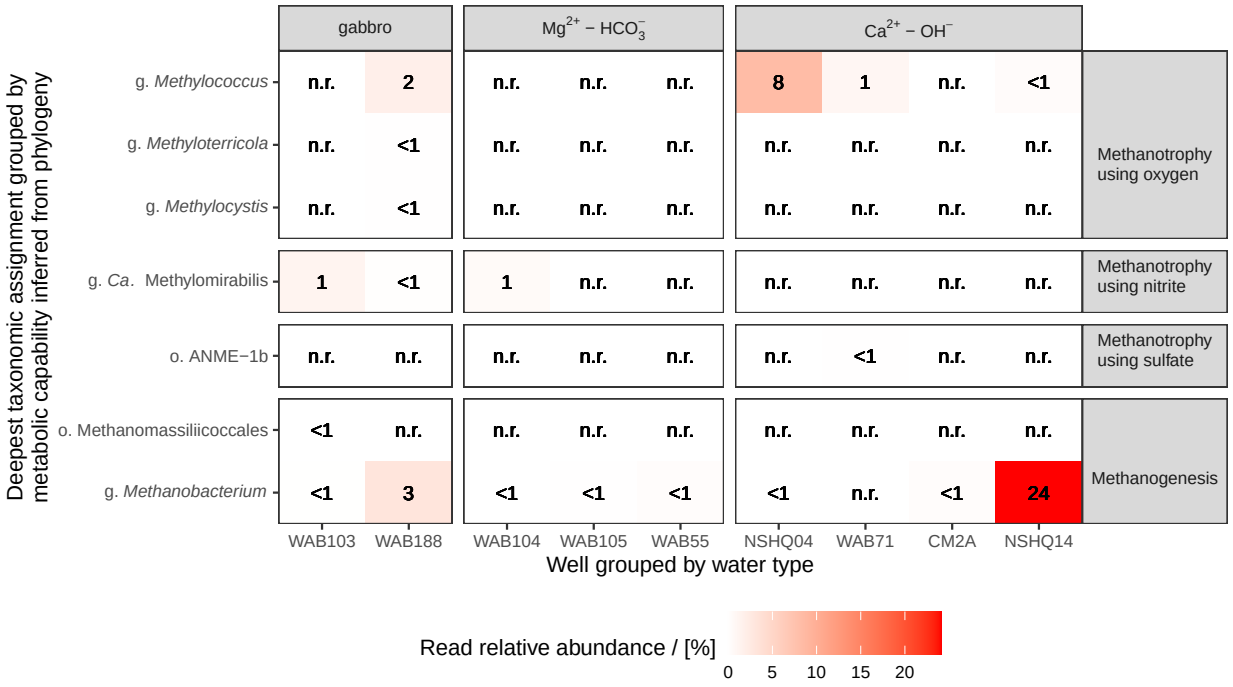


Figure 5: 16S rRNA gene read relative abundances of DNA extracted from Samail Ophiolite groundwaters sampled in 2018 affiliated with $CH_4$-cycling taxa. Read relative abundances are reported as percentages rounded to the ones place. Cases when a taxon was detected in a sample and was $< 1\,\%$ read relative abundance after rounding are labeled "$<$ 1". Cases when no reads of a taxon were detected in a sample are labeled "n.r." Data shown are from unique field samples. Previous 16S rRNA gene sequencing studies that obtained field samples in triplicate from Samail Ophiolite groundwaters through similar methods to those used here have found typical standard deviations of relative abundances less than or equal to 25 % of the mean relative abundance (Kraus et al., 2021).

Consortia capable of anaerobic oxidation of $CH_4$ coupled to $SO_4^{2-}$ reduction, including ANME, were not detected by 16S rRNA gene sequencing of samples obtained from NSHQ14 in 2018 (Figure 5), 2016, or 2014 (Miller et al., 2016; Rempfert et al., 2017), although sequences affiliated with order ANME-1b were detected in low abundance ($< 1\,\%$ of reads) in samples obtained from NSHQ14 in 2017 and 2015 (Rempfert et al., 2017; Kraus et al., 2021). This scarcity of ANME may result from metabolic inhibition by high $c_{H_2}$ in groundwaters at NSHQ14 and elsewhere in the Samail Ophiolite. It has been proposed that the thermodynamics of "reverse methanogenesis" require low $c_{H_2}$ (0.1 nM to 1 nM at Hydrate Ridge, a marine cold seep environment (Boetius et al., 2000), where $CH_4$ and $SO_4^{2-}$ concentrations can be a factor of 10 or more higher than those typically measured in ophiolitic groundwaters such as in Oman). Indeed,

593 the bioenergetics of $SO_4^{2-}$-driven oxidation of $CH_4$ are less favorable than $SO_4^{2-}$-driven oxidation of $H_2$ or
594 non-$CH_4$ organics, or other metabolisms such as methanogenesis or acetogenesis in the Samail Ophiolite
595 (Canovas III et al., 2017) and in deep continental settings where radiolytic $H_2$ accumulates (Kieft et al.,
596 2005; Moser et al., 2005; Kieft, 2016).

597 While 16S rRNA gene sequences affiliated with anaerobic $CH_4$ oxidizing microbes have only occasionally
598 been detected at NSHQ14, 16S rRNA gene sequences affiliated with the genus *Methylococcus*, which contains
599 aerobic methanotrophs (Hanson and Hanson, 1996), have been detected in all samples from NSHQ14, ranging
600 from 1 % to $< 1$ % of reads in samples obtained from 2014 to 2018 (Figure 5; Miller et al., 2016; Rempfert
601 et al., 2017; Kraus et al., 2021). Since the aerobic lifestyle of *Methylococcus* is at odds with that of the
602 obligate anaerobe, *Methanobacterium*, it seems most likely that these two taxa are spatially separated in the
603 aquifer, and that waters containing each of them were mixed during open borehole pumping. Still, the $> 10$
604 times higher abundances of *Methanobacterium*-related 16S rRNA genes relative to those of *Methylococcus*
605 at NSHQ14 in samples from 2016 to 2018 suggest that the microbial $CH_4$ cycle at this well is dominated by
606 $CH_4$ production, rather than consumption.

607 16S rRNA gene sequencing of subsurface biomass from NSHQ14 is complemented by other observations
608 that suggest that methanogens are not only prevalent, but active. Genes involved in methanogenesis are
609 actively transcribed in waters sampled from NSHQ14 (Kraus et al., 2021). Transformation of both $^{14}$C-
610 labeled $HCO_3^-$ and $^{14}$C-labeled formate to $CH_4$ have been shown to occur in water samples from NSHQ14
611 at significantly higher rates than in killed controls, with formatotrophic methanogenesis greatly outpacing
612 hydrogenotrophic methanogenesis (Fones et al., 2019, 2020). Taken together with a cell abundance of
613 $1.15 \cdot 10^5$ cells $\cdot$ mL$^{-1}$ in groundwater at NSHQ14 (Fones et al., 2019), these data suggest that aquifer regions
614 accessed by NSHQ14 host abundant active methanogenic cells (thousands per mL, assuming $\sim 24$ % of cells
615 are methanogens based on 16S rRNA gene data). These active cells could influence $CH_4$ concentration and
616 isotopic composition.

617 The genomic and cultivation data of Fones et al. (2020) indicate that formate is the dominant substrate
618 for methanogenesis at NSHQ14. Formate concentrations are 1 $\mu$mol $\cdot$ L$^{-1}$ to 2 $\mu$mol $\cdot$ L$^{-1}$ in the studied wells
619 (Rempfert et al., 2017), which are roughly two orders of magnitude lower than formate concentrations at
620 unsedimented seafloor hydrothermal vents impacted by serpentinization at warmer conditions than present in
621 the Samail Ophiolite (McDermott et al., 2015; Lang et al., 2018). These relatively low formate concentrations
622 in the ophiolite suggest that formate might be the primary limiting substrates for methanogenesis in $Ca^{2+} -$
623 $OH^-$ waters, such as at NSHQ14. Coexisting hydrogenotrophic methanogens may produce $CH_4$ through
624 direct uptake of $\sum CO_2$ in $H_2$-rich $Ca^{2+} - OH^-$ water, where kinetic inhibitions to abiotic $\sum CO_2$ reduction
625 to $CH_4$ allow for a modest energy yield for hydrogenotrophic methanogens (Section 5; Leong and Shock,
626 2020). Methanogens using $\sum CO_2$ could benefit from greater chemical disequilibrium if they inhabit zones
627 where deeply-sourced, $H_2$-rich $Ca^{2+} - OH^-$ water mixes with shallow, $Mg^{2+} - HCO_3^-$ water (Zwicker et al.,

628 2018; Leong and Shock, 2020). In addition to direct uptake of $\sum CO_2$, carbonate minerals may serve as a
629 C source for methanogenesis in carbonated peridotites (Miller et al., 2018). Another potential C source is
630 carbon monoxide (CO). CO has always been below limits of quantitation in Oman wells ($< 132\,\mathrm{nmol \cdot L^{-1}}$
631 in 2018; Table 4), but it is unclear whether this indicates minimal CO production or rapid CO turnover.

632 The microbiological data from NSHQ14 fluids are compatible with $\delta D_{CH_4}$, $\Delta^{13}CH_3D$, and $\Delta^{12}CH_2D_2$
633 values that collectively indicate a substantial addition of microbial $CH_4$ to an otherwise abiotic pool of $CH_4$.
634 Although the data presented here do not enable us to precisely determine the mole fractions and isotopic
635 compositions of the microbial and abiotic components of $CH_4$ at NSHQ14, the $\delta D_{CH_4}$ data alone suggest
636 that perhaps the majority of $CH_4$ at NSHQ14 formed through non-equilibrium processes, which include
637 microbial methanogenesis. Thus, the high $\delta^{13}C$ of $CH_4$ at NSHQ14 suggests that the microbial component
638 is more $^{13}C$-enriched than microbial $CH_4$ formed in sedimentary environments, which typically ranges from
639 $-90\,‰$ VPDB to $-50\,‰$ VPDB (Milkov and Etiope, 2018; Figure 3a). In cultures of a hydrogenotorophic
640 strain of *Methanobacterium* provided $CaCO_3\,(s)$ as a C source at pH $\sim$ 9, Miller et al. (2018) observed
641 suppressed apparent isotope effects during methanogenesis ($\alpha_{CO_2/CH_4} = 1.028$). The authors attributed
642 this to the slow kinetics of carbonate dissolution at high pH and the near-total conversion of the resultant
643 $CO_2\,(\mathrm{aq})$ to $CH_4$ by *Methanobacterium*. If the primary mode of methanogenesis at NSHQ14 is in fact
644 formate disproportionation and abiotic formate production is the rate-limiting step in the overall process
645 through which $\sum CO_2$ is converted to $CH_4$, similar isotopic bottlenecks could apply. Cellular formate uptake
646 and enzymatic conversion processes whose isotope effects remain unknown could be important drivers of
647 the isotopic composition of $CH_4$ in hyperalkaline, serpentinizing settings. In such settings, the suppression
648 of C isotope fractionation during methanogenesis is supported by observations of high $\delta^{13}C$ values (up to
649 $+14\,‰$ VPDB) of lipid biomarkers thought to be produced by methanogens at Chimaera, Turkey (Zwicker
650 et al., 2018) and at Lost City (Bradley et al., 2009). Evaluation of these hypotheses will require further
651 physiological studies of methanogens aimed at understanding substrate selection and limitation systematics
652 in hyperalkaline, low-C conditions and the isotopic implications of these factors.

653 While the data support substantial microbial $CH_4$ and abiotic, fluid inclusion-derived $CH_4$ in NSHQ14
654 fluids, we find less evidence for abiotic $CH_4$ production at the low temperatures that pervade the modern
655 weathering horizon in the ophiolite. Below $100\,^\circ\mathrm{C}$, access of gas-phase $H_2$ and $CO_2$ or CO to the catalytic
656 metals Ru or Rh is required for $CH_4$ to form at appreciable rates (Thampi et al., 1987; Jacquemin et al.,
657 2010; Etiope and Ionescu, 2015; McCollom, 2016). It has been proposed that the spatial concentration
658 of potentially-catalytic Ru-rich chromites in chromitites is important for catalysis of low-temperature $CO_2$
659 reduction to $CH_4$ in ophiolites (Etiope and Ionescu, 2015; Etiope et al., 2018). While peridotites in Oman
660 ubiquitously contain a few percent distributed chromite (Hanghøj et al., 2010), massive chromitites were
661 not reported in lithologic descriptions of cores or drill cuttings from NSHQ14 or any of the six additional
662 wells ranging from 300 m to 400 m depth that have been drilled in the same catchment by the Oman Drilling

Project (Kelemen et al., 2020). Nor are chromitites notably abundant in outcrop within this catchment. Further, although some flow paths of meteoric water through the ophiolite may result in saturation in $H_2$ and separation of a free gas phase (Canovas III et al., 2017), the depth to water is $< 20\,m$ in all wells in the catchment of NSHQ14, suggesting water-saturated conditions in the subsurface. Moreover, if free $H_2\,(g)$ were generated at high extents of reaction progress, co-existing $CO_2(g)$ would be extremely scarce due to precipitation of carbonate minerals and high pH (Etiope and Ionescu, 2015; Leong and Shock, 2020). It has been proposed that $CH_4$ in ophiolites can form through reduction of $CO_2(g)$ from non-atmospheric sources such as magma, the mantle, or sedimentary carbonate formations (Etiope and Ionescu, 2015). A magmatic/mantle $CO_2$ source is not supported at NSHQ14 because excess He above air saturation in groundwaters from this well has a dominantly radiogenic isotopic composition that is distinct from mantle-derived He (Paukert Vankeuren et al., 2019). Further, although sedimentary carbonates are present in the vicinity of NSHQ14 and elsewhere in the ophiolite (Boudier and Coleman, 1981; de Obeso and Kelemen, 2018), there is no clear mechanism to liberate $CO_2(g)$ from mineral carbonates and transfer that $CO_2(g)$ to catalytic sites of reaction on chromites where $H_2\,(g)$ is also present. Thus, the apparent lack of massive chromites and free gaseous potential reactants suggest that the subsurface surrounding NSHQ14 is not conducive to low-temperature abiotic $CH_4$ production. While substantial low-temperature $CH_4$ production in the catchment of NSHQ14 seems unlikely, NSHQ14 groundwaters could be mere carriers of $CH_4$ that was produced elsewhere in the ophiolite under gaseous conditions and that has subsequently migrated into the aquifer. Some studies of $CH_4$ origin in other peridotite bodies have favored such a hypothesis (Etiope et al., 2016; Marques et al., 2018). However, it is not clear how this hypothesis could be tested in the case of the NSHQ14, nor how it addresses the issue of $CO_2$ source.

In summary, isotopic and microbiological data lead us to conclude that the high concentrations of $CH_4$ ($10^2\,\mu mol{\cdot}L^{-1}$) in groundwaters accessed by NSHQ14 primarily result from microbial methanogenesis and the release of abiotic $CH_4$ from fluid inclusions. The known presence of $CH_4$-bearing fluid inclusions in the Samail Ophiolite and our finding of high $\delta^{13}C$ values of $CH_4$, $C_2H_6$, and $C_3H_8$ that overlap with values reported from seafloor hydrothermal vents where $CH_4$ formed at $> 270\,°C$ in fluid inclusions predominates suggest a similar source in the ophiolite. However, deficits in $^{12}CH_3D$, $^{13}CH_3D$, and $^{12}CH_2D_2$ relative to equilibrium indicate the production of additional $CH_4$ at low temperatures. The $^{13}CH_3D$ deficit in particular is more compatible with a microbial origin than a low-temperature abiotic origin. Moreover, numerous lines of microbiological evidence including genomic and cultivation data show that methanogens are abundant and active in aquifers accessed via NSHQ14. Organic geochemical and cultivation data from the literature suggest that C isotope effects of methanogenesis may be suppressed under C-limited conditions in serpentinizing settings. That genes associated with methanogens coexist with a smaller abundance of genes associated with methanotrophs (particularly aerobes) in NSHQ14 groundwaters suggests that some of the $CH_4$ has undergone microbial oxidation, which would further help explain the high $\delta^{13}C$ values of $CH_4$ at this well.

#### *4.2.3. Abundant microbial $CH_4$ produced under C-limited conditions and substantial microbial $CH_4$ oxidation in the $Ca^{2+} - OH^-$ waters of well NSHQ04*

NSHQ04 is situated in partially serpentinized harzburgite 10 m away from a faulted contact with crustal gabbros (Figure 1; Supporting Information Figure S1). Surface rock exposures surrounding NSHQ04 are dominated by serpentinized harzburgites, with lesser dunites, gabbro lenses, and pyroxenite dikes. NSHQ04 is cased to 5.8 mbgl and drilled to 304 m depth (Table 1). As of 2017, the well is obstructed at 8 m below the casing top, precluding deeper sampling (Section 3.1; Table 1).

Primary differences in fluid composition between NSHQ04 and NSHQ14 include lower pH by $\sim 1$ and higher $c_{\sum \mathrm{Ca}}$ and $c_{\sum \mathrm{Si}}$ at NSHQ04 (Tables 1 and 3; Miller et al., 2016; Rempfert et al., 2017; Paukert Vankeuren et al., 2019; Fones et al., 2019). These differences could be related to the scarcity of fresh, near-surface olivine at NSHQ04, which may result in a greater influence of pyroxene serpentinization at NSHQ04 (Miller et al., 2016). Low-temperature pyroxene serpentinization generally continues after olivine is exhausted, and leads to higher $c_{\sum \mathrm{Si}}$ and, depending on pyroxene chemical composition, can also lead to higher $c_{\sum \mathrm{Ca}}$ and lower pH (Bach et al., 2006; Leong and Shock, 2020). The relatively low pH and high $c_{\sum \mathrm{Si}}$ could also stem from mixing of $Ca^{2+} - OH^-$ waters with gabbro- or atmosphere-influenced fluids.

Compared to NSHQ14, NSHQ04 has generally had lower $c_{H_2}$ (detected in 2014, but not in 2018, 2017, 2015, or 2012; Table 4; Figure 2; Miller et al., 2016; Rempfert et al., 2017; Paukert Vankeuren et al., 2019). The relatively low $c_{H_2}$ measured in waters pumped from NSHQ04 is probably due at least in part to microbial $H_2$ oxidation. Although there are multiple enzymes with which which a diversity of microbes oxidize $H_2$ (Peters et al., 2015), aerobic $H_2$ oxidation by bacteria of the genus *Hydrogenophaga* has been identified as a particularly prevalent process in serpentinizing settings, including the Samail Ophiolite (Suzuki et al., 2014; Rempfert et al., 2017; Marques et al., 2018). Sequences affiliated with *Hydrogenophaga* accounted for 20 % of 16S rRNA gene reads in DNA extracted from biomass in waters pumped from NSHQ04 in 2018, which is similar to previous years of sampling at NSHQ04 (6 % to 18 % in 2014, 2015, and 2017; inter-annual mean of 12 %) and higher than all other studied wells (Supporting Information Figure S3; Rempfert et al., 2017; Miller et al., 2016; Kraus et al., 2021).

While $H_2$ has only been transiently detected at NSHQ04, $c_{CH_4}$ at this well has consistently been the highest among our sample sites (144 $\mu$mol·L$^{-1}$ in 2018 and 483 $\mu$mol·L$^{-1}$ in 2017. In comparison to NSHQ14, $CH_4$ at NSHQ04 is more $^{13}$C- and D-enriched (mean weighted by sample year $\delta^{13}C = +3.3$ ‰ VPDB, $s = 1.8$ ‰; $\delta D = -220$ ‰ VSMOW, $s = 11$ ‰; $n = 4$; Table 2; Figure 3a). Fluids sampled from NSHQ04 are in $CH_4 - H_2O$ H isotopic disequilibrium and intra-$CH_4$ disequilibrium (Figure 3b and d), which is also true of fluids from NSHQ14. However, $CH_4$ sampled from NSHQ04 has distinctly negative $\Delta^{12}CH_2D_2$ (−24.502 ‰) and low $\Delta^{13}CH_3D$ (mean weighted by sample year of 0.36 ‰, $s = 0.32$ ‰, $n = 3$; Table 2). As such, $CH_4$ from NSHQ04 plots squarely among methanogen culture samples in $\Delta^{13}CH_3D/\Delta^{12}CH_2D_2$ space (Figure

3d), suggesting that $CH_4$ is dominantly microbial at NSHQ04. Moreover, alkane gases dissolved in waters pumped from NSHQ04 exhibited a $C_1/(C_2+C_3)$ ratio of $5.4 \cdot 10^3$ in 2018, which is higher than other wells in this study (Table 4; Figure 3c), further supporting a major component of microbial $CH_4$ at NSHQ04.

Microbial $CH_4$ production at NSHQ04 is also indicated by microbiological data. 16S rRNA gene sequences affiliated with *Methanobacterium* have been detected in DNA extracted from biomass filtered from waters pumped from NSHQ04, albeit in low relative abundance ($< 1\,\%$ of reads in 2018; Figure 5; also detected in $< 1\,\%$ of reads in 2014, but not detected in 2015 and 2017; Rempfert et al., 2017; Miller et al., 2016; Kraus et al., 2021). The apparent low relative abundance of *Methanobacterium* at NSHQ04 could have resulted from the relatively shallow depth from which samples were collected at NSHQ04 due to well obstruction and the consequential sampling of groundwaters that may have experienced atmospheric $O_2$ infiltration. High relative read abundances of sequences affiliated with aerobes and transient $H_2$ across years of sampling NSHQ04 suggest that zones of the aquifer that are not always anoxic were accessed. These conditions may restrict methanogen abundance to greater depths than were sampled, but not constrain the upward diffusion of the product of their metabolism, $CH_4$. Nevertheless, fluids obtained from NSHQ04 have yielded robust cultures of *Methanobacterium* (Miller et al., 2018). In addition, high relative abundances of 16S rRNA gene reads of DNA extracted from biomass in waters sampled from NSHQ04 were related to an aerobic methanotroph of the genus *Methylococcus* (8 % of reads in 2018; inter-annual mean of 11 %; Figure 5; Miller et al., 2016; Rempfert et al., 2017; Kraus et al., 2021). Greater aerobic methanotrophy at NSHQ04 relative to NSHQ14 may have contributed in part to the lower $\Delta^{13}CH_3D$ and $\Delta^{12}CH_2D_2$ and higher $\delta^{13}C$ and $\delta D$ of $CH_4$ sampled from NSHQ04.

Methanotrophic activity at NSHQ04 is consistent with the observed $^{13}C$-depletion in $\sum CO_2$ at NSHQ04 ($-29.7\,‰$ VPDB $\delta^{13}C$; Table 2) relative to the other studied wells because environments of active methanotrophy often have $^{13}C$-depleted $\sum CO_2$ (Barker and Fritz, 1981; Michaelis et al., 2002). Indeed, $\delta^{13}C_{\sum CO_2}$ at NSHQ04 is compatible with aerobic oxidation of $CH_4$ of $\sim 0\,‰$ VPDB $\delta^{13}C$ (Barker and Fritz, 1981; Feisthauer et al., 2011). Alternatively, $^{13}C$-depletion in $\sum CO_2$ could be explained by kinetic isotope fractionation during hydroxylation of atmospheric $CO_2$ upon contact with $Ca^{2+} - OH^-$ water, which has been interpreted as the cause of $\delta^{13}C$ as low as $-27.21\,‰$ VPDB in Ca-rich carbonates from hyperalkaline seeps in the Samail Ophiolite (Clark et al., 1992; Kelemen et al., 2011; Falk et al., 2016). Considering the relatively shallow sampling depth at NSHQ04 in 2018 (Table 1), it is plausible that the sampled groundwaters continuously interact with atmospheric $CO_2$. Although the relative influences of methanotrophy and atmospheric $CO_2$ hydroxylation cannot be determined based on the available data, both processes could affect $\delta^{13}C_{\sum CO_2}$ at NSHQ04.

In summary, low $\Delta^{13}CH_3D$ and $\Delta^{12}CH_2D_2$, high $C_1/(C_2+C_3)$, the presence of *Methanobacterium* that were readily cultured, and high 16S rRNA gene relative abundances of *Methylococcus* lead us to conclude that microbial production and consumption of $CH_4$ are the dominant factors controlling $CH_4$ concentration

and isotopic composition at NSHQ04.

#### *4.2.4. $H_2$-limited microbial methanogenesis with classic C isotope effect expressed at well WAB188*

WAB188 is situated 2 km down-gradient from NSHQ04 and is set in gabbro on the opposite side of a fault from NSHQ04 (Figure 1; Supporting Information Figure S1; Table 1). Fluids pumped from WAB188 have had variable pH (8.72 to 5.75) and oxidation-reduction potential ($f_{O_2}$ of $10^{-61}$ bar to $10^{-34}$ bar and *Eh* of −220 mV to +214 mV) across four years of sampling (Table 1; Rempfert et al., 2017; Fones et al., 2019). WAB188 has consistently had major ion compositions similar to the gabbro-hosted well WAB103, except that WAB188 has had higher $c_{\sum Ca}$ (Table 3; Rempfert et al., 2017; Fones et al., 2019). $H_2$ has occasionally been detected in fluids pumped from WAB188 ($c_{H_2} = 0.992\,\mu mol \cdot L^{-1}$ in 2017), and $CH_4$ has consistently been detected at moderate concentrations ($c_{CH_4} = 1.83\,\mu mol \cdot L^{-1}$ in 2017 and $0.917\,\mu mol \cdot L^{-1}$ in 2018) (Table 4; Rempfert et al., 2017; Fones et al., 2019). The high $c_{\sum Ca}$ and moderate but variable pH, *Eh*, and $c_{H_2}$ in fluids sampled from WAB188 suggest that fluid chemical composition at WAB188 is dominantly controlled by water-rock reaction with gabbro (McCollom, 1999; Hoehler, 2004), but may also be affected by inputs of fresh rainwater and/or $H_2$-bearing $Ca^{2+} - OH^-$ water flowing from the peridotite aquifer into the gabbro aquifer across a fault at depth. Flows of water from higher-head, lower-permeability peridotite aquifers into gabbro aquifers in the Samail Ophiolite have been proposed on the basis of physical hydrologic data (Dewandel et al., 2005). Instead or in addition, serpentinization of olivine and pyroxene entirely within gabbro might have produced $H_2$ observed in water samples from WAB188.

Microbial methanogenesis at WAB188 is indicated by high relative abundances of 16S rRNA gene reads affiliated with methanogens in pumped groundwaters. Sequences affiliated with *Methanobacterium* accounted for 3 % of 16S rRNA gene reads of DNA extracted from subsurface fluids sampled from WAB188 in 2018, which was second only to NSHQ14 among our sampling sites, and consistent with prior years of sampling at WAB188 (mean 2015 to 2018 of 4 %; Figure 5; Rempfert et al., 2017; Kraus et al., 2021). There was also evidence for methanotrophy. 2 % of 16S rRNA gene reads from WAB188 were affiliated with *Methylococcus* in 2018, which was second only to NSHQ04 among our sampling sites, and consistent with prior years of sampling (Figure 5; Rempfert et al., 2017; Kraus et al., 2021). Further, 16S rRNA gene sequences affiliated with genus *Candidatus* Methylomirabilis, which includes species that mediate anaerobic methane oxidation coupled to nitrite reduction (Ettwig et al., 2010; Luesken et al., 2012; Welte et al., 2016), were detected in samples from WAB188 in 2018 albeit at low relative gene abundance (< 1 %). As a whole, the 16S rRNA gene sequencing data from WAB188 fluids are consistent with microbial production of $CH_4$ and, secondarily, methanotrophy using $O_2$ and/or $NO_2^-$. The 16S rRNA data are bolstered by genomic and cultivation data that demonstrate that *Methanobacterium* at WAB188 can produce $CH_4$ from $CO_2$ and/or formate (Fones et al., 2020) and that genes involved in methanogenesis are transcribed in groundwater samples obtained from WAB188 (Kraus et al., 2021).

While subsurface fluids sampled at WAB188, NSHQ14, and NSHQ04 all bear evidence of methanogenic activity, the conditions under which methanogenesis proceeds at WAB188 are fundamentally distinct. In contrast to the $Ca^{2+} - OH^-$ fluids from NSHQ14 and NSHQ04, the circumneutral fluids from WAB188 have $\sim 10^2$ to $\sim 10^3$ times higher $c_{\sum CO_2}$ (inter-annual mean of $2910\,\mu mol \cdot L^{-1}$, $s = 620\,\mu mol \cdot L^{-1}$, $n = 3$; Table 3) and $\sim 75\,‰$ lower $\delta^{13}C_{CH_4}$ (inter-annual mean $\delta^{13}C = -73\,‰$ VPDB, $s = 13\,‰$, $n = 3$; Table 2; Figure S5). Since WAB188 fluids contain relatively $^{13}C$-depleted $CH_4$ that is not associated with substantial concentrations of $C_2 - C_6$ alkanes (Table 4), a standard interpretation (Bernard et al., 1977; Milkov and Etiope, 2018) would be that the source of $CH_4$ at WAB188 is dominantly microbial. Such an interpretation is largely based on data from sedimentary settings, where $H_2$ is typically more scarce than $CO_2$. In this regard, conditions in sedimentary settings are analogous to those at WAB188. Evidence that considerable methanogenesis proceeds through a hydrogenotrophic pathway under $H_2$-limited conditions at WAB188 include microbiological data confirming the capacity of *Methanobacterium* to perform hydrogenotrophic methanogenesis at WAB188 and thermodynamic calculations showing that hydrogenotrophic methanogenesis (with $H_2$ as limiting substrate) was more energetically favorable than formatotrophic methanogenesis for a fluid with $c_{\sum CO_2}$ and $c_{H_2}$ similar to WAB188 in 2017 (Section 4.2.1; Table 5). Further, the apparent $\alpha_{CO_2/CH_4}$ at WAB188 (based on measured $\delta^{13}C_{\sum CO_2}$ of $-13.52\,‰$ VPDB; Table 3) is compatible with that of *Methanobacterium* cultures grown hydrogenotrophically with excess $HCO_3^-$ (aq), which was greater than the $\alpha_{CO_2/CH_4}$ observed for parallel cultures under $CO_2$-poor conditions (Miller et al., 2018). In sum, the conditions at WAB188 contrast starkly with those that prevail in $Ca^{2+} - OH^-$ fluids, where C substrates for methanogenesis are often more scarce than $H_2$. These differences may be reflected in the inverse relationship between $c_{\sum CO_2}$ and $\delta^{13}C_{CH_4}$ across fluids from wells WAB188, NSHQ14, and NSHQ04 (Figure S5), which is consistent with an effect of C availability on the apparent C isotope effect of microbial methanogenesis.

## 5. Conclusions

Through integration of isotopic, microbiological, and hydrogeochemical data, we conclude that substantial microbial $CH_4$ is produced under varying degrees of C or $H_2$ limitation in subsurface waters of the Samail Ophiolite and mixes with abiotic $CH_4$ released from fluid inclusions (Figure 6). Across subsurface fluids ranging in pH from circumneutral to 11.39, microbial $CH_4$ production is evidenced by 16S rRNA gene sequencing and other microbiological data indicating that methanogens are widespread and active in groundwaters in the ophiolite. We propose that $CH_4$ produced by these microbes constitutes a substantial portion of the total $CH_4$ pool, which is consistent with our finding of $^{13}CH_3D$ and $^{12}CH_2D_2$ relative abundances significantly less than equilibrium. Using a simple thermodynamic model, we find that formatotrophic methanogenesis may become more energetically favorable than hydrogenotrophic methanogenesis as $Mg^{2+} - HCO_3^-$ waters transition to $Ca^{2+} - OH^-$ waters where $CO_2$(aq) is extremely scarce, despite

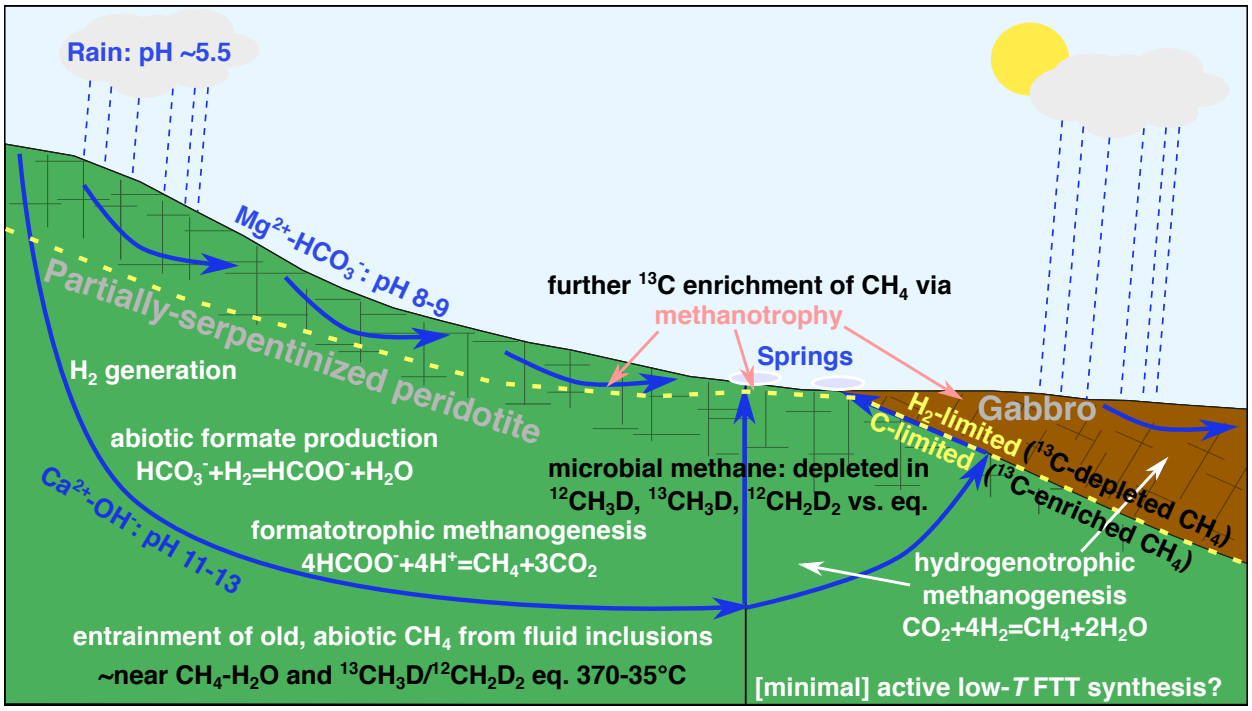


Figure 6: Conceptual model of $CH_4$ dynamics in Samail Ophiolite. Cross section after Neal and Stanger (1985), Dewandel et al. (2005), and Rempfert et al. (2017). Groundwater flow is depicted with blue arrows. Cross-hatching illustrates fissured zone of aquifer, extending to $\sim 50$ m depth. A deep tectonic fracture hosting upward groundwater flow is shown as a black line. Yellow dashed line indicates proposed transition between conditions where methanogenesis is limited by $H_2$ versus C availability. Isotopic systematics are written in black text. *Abbreviations:* eq., equilibrium; $T$, temperature; FTT, Fischer-Tropsch-type.

relatively low formate concentrations of $\sim 1\,\mu\text{mol}\cdot\text{L}^{-1}$ across fluid types (Rempfert et al., 2017). This lends geochemical support to recent microbiological findings that independently indicate that the activity of formatotrophic methanogens increases relative to hydrogenotrophic methanogens as groundwater pH increases in the ophiolite (Fones et al., 2020).

In addition, an abiotic, fluid inclusion-derived source of $CH_4$, $C_2H_6$, and $C_3H_8$ is inferred from the widespread occurrence of $CH_4$ in fluid inclusions in peridotites, including those in Oman, and is supported by the relatively $^{13}$C-enriched compositions of $CH_4$, $C_2H_6$, and $C_3H_8$ measured in gases exsolved from peridotite-hosted groundwaters in this study. The measured $\delta^{13}C$ values overlap with those of $CH_4$, $C_2H_6$ and $C_3H_8$ from seafloor hydrothermal vents where fluid inclusions are the dominant source of these alkanes, suggesting similar $CH_4$ sources across these environments. In contrast, abiotic, low-temperature reduction of $CO_2$ to $CH_4$ appears less likely to contribute substantially to the $CH_4$ pool in the study area due to a scarcity of conditions favorable to catalysis, namely, access of gas-phase $H_2$ and $CO_2$/CO to Ru-bearing chromites.

Further, we note an inverse relationship between $c_{\sum CO_2}$ and $\delta^{13}C_{CH_4}$ across groundwaters bearing

microbiological evidence of methanogenic activity. This finding supports the hypothesis that the apparent C isotope fractionation between the C substrate used by methanogens and the $CH_4$ they produce is suppressed when the C substrate is limiting. Thus, our finding that $\delta^{13}C_{CH_4}$ varies by 90 ‰ in the Samail Ophiolite suggests that, in some settings, $\delta^{13}C_{CH_4}$ may be a powerful indicator of transitions from $H_2$-limited to C-limited conditions for microbial methanogenesis, rather than a discriminant between microbial versus abiotic $CH_4$. The 16S rRNA gene sequencing data also indicate the presence of microbes capable of $CH_4$ oxidation, particularly using $O_2$ as an oxidant. This oxidation may also contribute in part to the $^{13}C$-enriched composition of $CH_4$ in the ophiolite, which is considered unusual for $CH_4$ with a substantial microbial component.

This study supports the premise that $H_2$ produced from water/rock reaction can fuel microbial life, even under challenging conditions of high pH and low oxidant availability. By identifying where and how microbial methanogenesis can reasonably be expected to occur in $H_2$-rich, subsurface environments, this work complements theoretical models in guiding the search for rock-hosted life, including extraterrestrial life. For example, our findings substantiate predictions that microbial methanogenesis could occur in the reduced, alkaline ocean of Saturn's moon, Enceladus (McKay et al., 2008; Glein et al., 2015; Waite et al., 2017) and in the Martian subsurface (Kral et al., 2014).

## 6. Acknowledgements

This research was directly supported by the Rock-Powered Life NASA Astrobiology Institute (NNA15BB02A). This research also used samples and/or data provided by the Oman Drilling Project. The Oman Drilling Project (OmanDP) has been possible through co-mingled funds from the International Continental Scientific Drilling Project (ICDP), the Sloan Foundation – Deep Carbon Observatory (Grant 2014-3-01, Kelemen PI), the National Science Foundation (NSF-EAR-1516300, Kelemen PI), the NASA Astrobiology Institute (NNA15BB02A), the German Research Foundation (DFG), the Japanese Society for the Promotion of Science (JSPS), the European Research Council, the Swiss National Science Foundation, JAMSTEC, the TAMU-JR Science operator, and contributions from the Sultanate of Oman Ministry of Regional Municipalities and Water Resources, the Oman Public Authority of Mining, Sultan Qaboos University, CRNS-Univ. Montpellier II, Columbia University, and the University of Southampton. Work at LBNL was supported by the U.S. Department of Energy, Office of Science, Office of Basic Energy Sciences, Chemical Sciences, Geosciences, and Biosciences Division, under Award Number DE-AC02-05CH11231.

We thank the Ministry of Regional Municipalities and Water Resources in the Sultanate of Oman (particularly Said Al Habsi, Rashid Al Abri, Salim Al Khanbashi, and Haider Ahmed Mohammed Alajmi) for allowing access to wells and logistical support, Zaher Al Sulaimani and Mazin Al Sulaimani from the Oman Water Centre and AZD Engineering for their technical and logistical support, Jude Coggon for coordinating

Oman Drilling Project activities, Benoît Ildefonse for sharing geologic map data, Eric Ellison and Kaitlin Rempfert for their assistance in the field and laboratory, Elizabeth Fones for sharing biomass samples, Emily Kraus for critical discussion of Oman $CH_4$ cycle processes, and Noah Fierer, Jen Reeves, Corinne Walsh, Matthew Gebert, and Angela Oliverio for assisting with DNA sequencing and interpretation.

Data (in Excel format) and source code (in R Markdown format) used to produce the figures, data tables and analyses for this paper (as well as additional data on analytical uncertainties and trace element concentrations) are available online at `https://github.com/danote/Oman_CH4_stable_isotopes`. Additional DNA sequence data processing codes are available at `https://github.com/danote/Samail_16S_compilation`. The sequences are accessible on the NCBI Short Read Archive under accession PRJNA655565.

## 7. References

Abrajano, T., Sturchio, N., Kennedy, B., Lyon, G., Muehlenbachs, K., Bohlke, J.. Geochemistry of reduced gas related to serpentinization of the Zambales ophiolite, Philippines. Appl Geochem 1990;5(5):625 – 630. URL: http://www.sciencedirect.com/science/article/pii/088329279090060I. doi:10.1016/0883-2927(90)90060-I; water-Rock Interactions Special Memorial Issue Ivan Barnes (1931–1989).

Alsharhan, A.S.. PETROLEUM GEOLOGY OF THE UNITED ARAB EMIRATES. J Pet Geol 1989;12(3):253–288. URL: https://onlinelibrary.wiley.com/doi/abs/10.1111/j.1747-5457.1989.tb00197.x. doi:10.1111/j.1747-5457.1989.tb00197.x. arXiv:https://onlinelibrary.wiley.com/doi/pdf/10.1111/j.1747-5457.1989.tb00197.x.

Alt, J.C., Garrido, C.J., Shanks, W., Turchyn, A., Padrón-Navarta, J.A., Sánchez-Vizcaíno, V.L., Pugnaire, M.T.G., Marchesi, C.. Recycling of water, carbon, and sulfur during subduction of serpentinites: A stable isotope study of Cerro del Almirez, Spain. Earth Planet Sci Lett 2012a;327-328:50 – 60. URL: http://www.sciencedirect.com/science/article/pii/S0012821X12000568. doi:10.1016/j.epsl.2012.01.029.

Alt, J.C., Schwarzenbach, E.M., Früh-Green, G.L., Shanks, W.C., Bernasconi, S.M., Garrido, C.J., Crispini, L., Gaggero, L., Padrón-Navarta, J.A., Marchesi, C.. The role of serpentinites in cycling of carbon and sulfur: Seafloor serpentinization and subduction metamorphism. Lithos 2013;178:40 – 54. URL: http://www.sciencedirect.com/science/article/pii/S0024493712004975. doi:10.1016/j.lithos.2012.12.006; serpentinites from mid-oceanic ridges to subduction.

Alt, J.C., Shanks, W., Crispini, L., Gaggero, L., Schwarzenbach, E.M., Früh-Green, G.L., Bernasconi, S.M.. Uptake of carbon and sulfur during seafloor serpentinization and the effects of subduction metamorphism in Ligurian peridotites. Chem Geol 2012b;322-323:268 – 277. URL: http://www.sciencedirect.com/science/article/pii/S0009254112003154. doi:10.1016/j.chemgeo.2012.07.009.

Ash, J.L., Egger, M.. Exchange catalysis during anaerobic methanotrophy revealed by $^{12}CH_2D_2$ and $^{13}CH_3D$ in methane. Geochem Perspect Lett 2019;10:26–30. URL: https://www.geochemicalperspectivesletters.org/article1910. doi:10.7185/geochemlet.1910.

Assayag, N., Rivé, K., Ader, M., Jézéquel, D., Agrinier, P.. Improved method for isotopic and quantitative analysis of dissolved inorganic carbon in natural water samples. Rapid Commun Mass Spectrom 2006;20(15):2243–2251. doi:10.1002/rcm.2585.

Bach, W., Paulick, H., Garrido, C.J., Ildefonse, B., Meurer, W.P., Humphris, S.E.. Unraveling the sequence of serpentinization reactions: petrography, mineral chemistry, and petrophysics of serpentinites from MAR 15 °N (ODP Leg 209, Site 1274). Geophys Res Lett 2006;33(13). URL: https://agupubs.onlinelibrary.wiley.com/doi/abs/10.1029/2006GL025681. doi:10.1029/2006GL025681. arXiv:https://agupubs.onlinelibrary.wiley.com/doi/pdf/10.1029/2006GL025681.

Balch, W.E., Fox, G.E., Magrum, L.J., Woese, C.R., Wolfe, R.S.. Methanogens: reevaluation of a unique biological group. Microbiol Rev 1979;43(2):260. URL: https://www.ncbi.nlm.nih.gov/pmc/articles/PMC281474.

Barker, J.F., Fritz, P.. Carbon isotope fractionation during microbial methane oxidation. Nature 1981;293(5830):289–291. doi:10.1038/293289a0.

Barnes, I., LaMarche, j.V., Himmelberg, G.. Geochemical evidence of present-day serpentinization. Science 1967;156(3776):830–832. doi:10.1126/science.156.3776.830.

Barnes, I., O'Neil, J., Trescases, J.. Present day serpentinization in New Caledonia, Oman and Yugoslavia. Geochim Cosmochim Acta 1978;42(1):144 – 145. URL: http://www.sciencedirect.com/science/article/pii/0016703778902259. doi:10.1016/0016-7037(78)90225-9.

Barnes, I., O'Neil, J.R.. The relationship between fluids in some fresh alpine-type ultramafics and possible modern serpentinization, western United States. Geol Soc Am Bull 1969;80(10):1947–1960. doi:10.1130/0016-7606(1969)80[1947:TRBFIS]2.0.CO;2.

Bernard, B., Brooks, J.M., Sackett, W.M., et al. A geochemical model for characterization of hydrocarbon gas sources in marine sediments. In: Offshore Technology Conference. Offshore Technology Conference; 1977. p. 435–438. doi:10.4043/2934-MS.

Boetius, A., Ravenschlag, K., Schubert, C.J., Rickert, D., Widdel, F., Gieseke, A., Amann, R., Jørgensen, B.B., Witte, U., Pfannkuche, O.. A marine microbial consortium apparently mediating anaerobic oxidation of methane. Nature 2000;407(6804):623–626. URL: https://doi.org/10.1038/35036572. doi:10.1038/35036572.

Boone, D.R.. Methanobacterium; American Cancer Society. p. 1–8. URL: https://onlinelibrary.wiley.com/doi/abs/10.1002/9781118960608.gbm00495. doi:10.1002/9781118960608.gbm00495. arXiv:https://onlinelibrary.wiley.com/doi/pdf/10.1002/9781118960608.gbm00495.

Bottinga, Y.. Calculated fractionation factors for carbon and hydrogen isotope exchange in the system calcite-carbon dioxide-graphite-methane-hydrogen-water vapor. Geochim Cosmochim Acta 1969;33(1):49 – 64. URL: http://www.sciencedirect.com/science/article/pii/0016703769900921. doi:10.1016/0016-7037(69)90092-1.

Boudier, F., Baronnet, A., Mainprice, D.. Serpentine Mineral Replacements of Natural Olivine and their Seismic Implications: Oceanic Lizardite versus Subduction-Related Antigorite. J Petrol 2009;51(1-2):495–512. doi:10.1093/petrology/egp049.

Boudier, F., Coleman, R.G.. Cross section through the peridotite in the Samail Ophiolite, southeastern Oman Mountains. J Geophys Res: Solid Earth 1981;86(B4):2573–2592. URL: https://agupubs.onlinelibrary.wiley.com/doi/abs/10.1029/JB086iB04p02573. doi:10.1029/JB086iB04p02573. arXiv:https://agupubs.onlinelibrary.wiley.com/doi/pdf/10.1029/JB086iB04p02573.

Boulart, C., Chavagnac, V., Monnin, C., Delacour, A., Ceuleneer, G., Hoareau, G.. Differences in gas venting from ultramafic-hosted warm springs: the example of Oman and Voltri ophiolites. Ofioliti 2013;38(2):142–156. doi:10.4454/ofioliti.v38i2.423.

Bradley, A.S., Hayes, J.M., Summons, R.E.. Extraordinary $^{13}$C enrichment of diether lipids at the Lost City Hydrothermal Field indicates a carbon-limited ecosystem. Geochim Cosmochim Acta 2009;73(1):102–118. doi:10.1016/j.gca.2008.10.005.

Brazelton, W.J., Thornton, C.N., Hyer, A., Twing, K.I., Longino, A.A., Lang, S.Q., Lilley, M.D., Früh-Green, G.L., Schrenk, M.O.. Metagenomic identification of active methanogens and methanotrophs in serpentinite springs of the Voltri Massif, Italy. PeerJ 2017;5:e2945. doi:10.7717/peerj.2945.

Bruni, J., Canepa, M., Chiodini, G., Cioni, R., Cipolli, F., Longinelli, A., Marini, L., Ottonello, G., Zuccolini, M.V.. Irreversible water–rock mass transfer accompanying the generation of the neutral, Mg–HCO3 and high-pH, Ca–OH spring waters of the Genova province, Italy. Appl Geochem 2002;17(4):455–474. doi:10.1016/S0883-2927(01)00113-5.

Burnham, A.K.. A simple kinetic model of petroleum formation and cracking. Technical Report UCID-21665; Lawrence Livermore National Lab., CA (USA); 1989. URL: https://www.osti.gov/biblio/6189092.

963 Callahan, B.J., McMurdie, P.J., Rosen, M.J., Han, A.W., Johnson, A.J.A., Holmes, S.P.. DADA2: High-resolution sample
964 inference from Illumina amplicon data. Nat Methods 2016;13(7):581. doi:10.1038/nmeth.3869.
965 Canovas III, P.A., Hoehler, T., Shock, E.L.. Geochemical bioenergetics during low-temperature serpentinization: An example
966 from the Samail ophiolite, Sultanate of Oman. J Geophys Res: Biogeosci 2017;122(7):1821–1847. doi:10.1002/2017JG003825.
967 Charlou, J., Donval, J., Douville, E., Jean-Baptiste, P., Radford-Knoery, J., Fouquet, Y., Dapoigny, A., Stievenard, M..
968 Compared geochemical signatures and the evolution of Menez Gwen (37°50′N) and Lucky Strike (37°17′N) hydrothermal
969 fluids, south of the Azores Triple Junction on the Mid-Atlantic Ridge. Chem Geol 2000;171(1):49 – 75. URL: http:
970 //www.sciencedirect.com/science/article/pii/S0009254100002448. doi:10.1016/S0009-2541(00)00244-8.
971 Charlou, J., Donval, J., Fouquet, Y., Jean-Baptiste, P., Holm, N.. Geochemistry of high $H_2$ and $CH_4$ vent fluids
972 issuing from ultramafic rocks at the Rainbow hydrothermal field (36° 14′ N, MAR). Chem Geol 2002;191(4):345–359.
973 doi:10.1016/S0009-2541(02)00134-1.
974 Charlou, J.L., Donval, J.P., Konn, C., Ondréas, H., Fouquet, Y., Jean-Baptiste, P., Fourré, E..
975 High production and fluxes of $H_2$ and $CH_4$ and evidence of abiotic hydrocarbon synthesis by serpentinization
976 in ultramafic-hosted hydrothermal systems on the Mid-Atlantic Ridge; American Geophysical Union (AGU). p.
977 265–296. URL: https://agupubs.onlinelibrary.wiley.com/doi/abs/10.1029/2008GM000752. doi:10.1029/2008GM000752.
978 arXiv:https://agupubs.onlinelibrary.wiley.com/doi/pdf/10.1029/2008GM000752.
979 Charlou, J.L., Fouquet, Y., Donval, J.P., Auzende, J.M., Jean-Baptiste, P., Stievenard, M., Michel, S.. Min-
980 eral and gas chemistry of hydrothermal fluids on an ultrafast spreading ridge: East Pacific Rise, 17 ° to 19 °S (Naudur
981 cruise, 1993) phase separation processes controlled by volcanic and tectonic activity. J Geophys Res: Solid Earth
982 1996;101(B7):15899–15919. URL: https://agupubs.onlinelibrary.wiley.com/doi/abs/10.1029/96JB00880. doi:10.1029/
983 96JB00880. arXiv:https://agupubs.onlinelibrary.wiley.com/doi/pdf/10.1029/96JB00880.
984 Charlton, S.R., Parkhurst, D.L.. Modules based on the geochemical model PHREEQC for use in scripting and programming
985 languages. Comput Geosci 2011;37(1653-1663). doi:10.1016/j.cageo.2011.02.005.
986 Chavagnac, V., Ceuleneer, G., Monnin, C., Lansac, B., Hoareau, G., Boulart, C.. Mineralogical assemblages forming at
987 hyperalkaline warm springs hosted on ultramafic rocks: A case study of Oman and Ligurian ophiolites. Geochem, Geophys,
988 Geosyst 2013a;14(7):2474–2495. URL: https://agupubs.onlinelibrary.wiley.com/doi/abs/10.1002/ggge.20146. doi:10.
989 1002/ggge.20146. arXiv:https://agupubs.onlinelibrary.wiley.com/doi/pdf/10.1002/ggge.20146.
990 Chavagnac, V., Monnin, C., Ceuleneer, G., Boulart, C., Hoareau, G.. Characterization of hyperalkaline fluids produced by
991 low-temperature serpentinization of mantle peridotites in the Oman and Ligurian ophiolites. Geochem, Geophys, Geosyst
992 2013b;14(7):2496–2522. doi:10.1002/ggge.20147.
993 Cipolli, F., Gambardella, B., Marini, L., Ottonello, G., Zuccolini, M.V.. Geochemistry of high-pH waters from serpentinites
994 of the Gruppo di Voltri (Genova, Italy) and reaction path modeling of $CO_2$ sequestration in serpentinite aquifers. Appl
995 Geochem 2004;19(5):787 – 802. URL: http://www.sciencedirect.com/science/article/pii/S0883292703002105. doi:10.
996 1016/j.apgeochem.2003.10.007.
997 Clark, I.D., Fontes, J.C., Fritz, P.. Stable isotope disequilibria in travertine from high pH waters: Laboratory investigations
998 and field observations from Oman. Geochim Cosmochim Acta 1992;56(5):2041 – 2050. URL: http://www.sciencedirect.
999 com/science/article/pii/001670379290328G. doi:10.1016/0016-7037(92)90328-G.
1000 Coleman, R.G., Hopson, C.A.. Introduction to the Oman Ophiolite Special Issue. J Geophys Res: Solid Earth
1001 1981;86(B4):2495–2496. URL: https://agupubs.onlinelibrary.wiley.com/doi/abs/10.1029/JB086iB04p02495. doi:10.
1002 1029/JB086iB04p02495. arXiv:https://agupubs.onlinelibrary.wiley.com/doi/pdf/10.1029/JB086iB04p02495.
1003 Collier, M.L.. Spatial-Statistical Properties of Geochemical Variability as Constraints on Magma Transport and Evolution
1004 Processes at Ocean Ridges. Ph.D. thesis; Columbia University; 2012. doi:10.7916/D82V2P43.
1005 Crespo-Medina, M., Twing, K.I., Sánchez-Murillo, R., Brazelton, W.J., McCollom, T.M., Schrenk, M.O.. Methane

Dynamics in a Tropical Serpentinizing Environment: The Santa Elena Ophiolite, Costa Rica. Front Microb 2017;8. URL: http://dx.doi.org/10.3389/fmicb.2017.00916. doi:10.3389/fmicb.2017.00916.

Cumming, E.A., Rietze, A., Morrissey, L.S., Cook, M.C., Rhim, J.H., Ono, S., Morrill, P.L.. Potential sources of dissolved methane at the Tablelands, Gros Morne National Park, NL, CAN: A terrestrial site of serpentinization. Chem Geol 2019;514:42 – 53. URL: http://www.sciencedirect.com/science/article/pii/S0009254119301299. doi:10.1016/j.chemgeo.2019.03.019.

de Obeso, J.C., Kelemen, P.B.. Fluid rock interactions on residual mantle peridotites overlain by shallow oceanic limestones: Insights from Wadi Fins, Sultanate of Oman. Chem Geol 2018;498:139 – 149. URL: http://www.sciencedirect.com/science/article/pii/S0009254118304625. doi:10.1016/j.chemgeo.2018.09.022.

Deines, P.. The carbon isotope geochemistry of mantle xenoliths. Earth-Sci Rev 2002;58(3):247 – 278. URL: http://www.sciencedirect.com/science/article/pii/S0012825202000648. doi:10.1016/S0012-8252(02)00064-8.

Delacour, A., Früh-Green, G.L., Bernasconi, S.M., Schaeffer, P., Kelley, D.S.. Carbon geochemistry of serpentinites in the Lost City Hydrothermal System (30 °N, MAR). Geochim Cosmochim Acta 2008;72(15):3681 – 3702. URL: http://www.sciencedirect.com/science/article/pii/S0016703708002585. doi:10.1016/j.gca.2008.04.039.

Dewandel, B., Boudier, F., Kern, H., Warsi, W., Mainprice, D.. Seismic wave velocity and anisotropy of serpentinized peridotite in the Oman ophiolite. Tectonophysics 2003;370(1):77 – 94. URL: http://www.sciencedirect.com/science/article/pii/S0040195103001781. doi:10.1016/S0040-1951(03)00178-1; physical Properties of Rocks and other Geomaterials, a Special Volume to honour Professor H. Kern.

Dewandel, B., Lachassagne, P., Boudier, F., Al-Hattali, S., Ladouche, B., Pinault, J.L., Al-Suleimani, Z.. A conceptual hydrogeological model of ophiolite hard-rock aquifers in Oman based on a multiscale and a multidisciplinary approach. Hydrogeol J 2005;13(5-6):708–726. doi:10.1007/s10040-005-0449-2.

Etiope, G.. Methane origin in the Samail ophiolite: Comment on "Modern water/rock reactions in Oman hyperalkaline peridotite aquifers and implications for microbial habitability" [Geochim. Cosmochim. Acta 179 (2016) 217–241]. Geochim Cosmochim Acta 2017;197:467 – 470. URL: http://www.sciencedirect.com/science/article/pii/S0016703716304379. doi:10.1016/j.gca.2016.08.001.

Etiope, G., Ifandi, E., Nazzari, M., Procesi, M., Tsikouras, B., Ventura, G., Steele, A., Tardini, R., Szatmari, P.. Widespread abiotic methane in chromitites. Sci Rep 2018;8(1). URL: http://dx.doi.org/10.1038/s41598-018-27082-0. doi:10.1038/s41598-018-27082-0.

Etiope, G., Ionescu, A.. Low-temperature catalytic $CO_2$ hydrogenation with geological quantities of ruthenium: a possible abiotic $CH_4$ source in chromitite-rich serpentinized rocks. Geofluids 2015;15(3):438–452. doi:10.1111/gfl.12106.

Etiope, G., Judas, J., Whiticar, M.. Occurrence of abiotic methane in the eastern United Arab Emirates ophiolite aquifer. Arabian J Geosci 2015;8(12):11345–11348. doi:10.1007/s12517-015-1975-4.

Etiope, G., Vadillo, I., Whiticar, M., Marques, J., Carreira, P., Tiago, I., Benavente, J., Jiménez, P., Urresti, B.. Abiotic methane seepage in the Ronda peridotite massif, southern Spain. Appl Geochem 2016;66:101–113. doi:doi.org/10.1016/j.apgeochem.2015.12.001.

Etiope, G., Whiticar, M.. Abiotic methane in continental ultramafic rock systems: Towards a genetic model. Appl Geochem 2019;102:139 – 152. URL: http://www.sciencedirect.com/science/article/pii/S0883292719300204. doi:10.1016/j.apgeochem.2019.01.012.

Ettwig, K.F., Butler, M.K., Le Paslier, D., Pelletier, E., Mangenot, S., Kuypers, M.M.M., Schreiber, F., Dutilh, B.E., Zedelius, J., de Beer, D., Gloerich, J., Wessels, H.J.C.T., van Alen, T., Luesken, F., Wu, M.L., van de Pas-Schoonen, K.T., Op den Camp, H.J.M., Janssen-Megens, E.M., Francoijs, K.J., Stunnenberg, H., Weissenbach, J., Jetten, M.S.M., Strous, M.. Nitrite-driven anaerobic methane oxidation by oxygenic bacteria. Nature 2010;464(7288):543. doi:10.1038/nature08883.

Evans, B.W.. Metamorphism of alpine peridotite and serpentinite. Annu Rev Earth Planet Sci 1977;5(1):397–447. URL: https://doi.org/10.1146/annurev.ea.05.050177.002145. doi:10.1146/annurev.ea.05.050177.002145. arXiv:https://doi.org/10.1146/annurev.ea.05.050177.002145.

Falk, E., Guo, W., Paukert, A., Matter, J., Mervine, E., Kelemen, P.. Controls on the stable isotope compositions of travertine from hyperalkaline springs in Oman: Insights from clumped isotope measurements. Geochim Cosmochim Acta 2016;192:1 – 28. URL: http://www.sciencedirect.com/science/article/pii/S0016703716303568. doi:10.1016/j.gca.2016.06.026.

Feisthauer, S., Vogt, C., Modrzynski, J., Szlenkier, M., Krüger, M., Siegert, M., Richnow, H.H.. Different types of methane monooxygenases produce similar carbon and hydrogen isotope fractionation patterns during methane oxidation. Geochim Cosmochim Acta 2011;75(5):1173 – 1184. URL: http://www.sciencedirect.com/science/article/pii/S0016703710006691. doi:10.1016/j.gca.2010.12.006.

Fiebig, J., Stefánsson, A., Ricci, A., Tassi, F., Viveiros, F., Silva, C., Lopez, T.M., Schreiber, C., Hofmann, S., Mountain, B.W.. Abiogenesis not required to explain the origin of volcanic-hydrothermal hydrocarbons. Geochem Perspect Lett 2019;11:23–27. URL: http://www.geochemicalperspectivesletters.org/article1920. doi:10.7185/geochemlet.1920.

Fones, E.M., Colman, D.R., Kraus, E.A., Nothaft, D.B., Poudel, S., Rempfert, K.R., Spear, J.R., Templeton, A.S., Boyd, E.S.. Physiological adaptations to serpentinization in the Samail Ophiolite, Oman. ISME J 2019;:1doi:10.1038/s41396-019-0391-2.

Fones, E.M., Colman, D.R., Kraus, E.A., Stepanauskas, R., Templeton, A.S., Spear, J.R., Boyd, E.S.. Diversification of methanogens into hyperalkaline serpentinizing environments through adaptations to minimize oxidant limitation. ISME J 2020;URL: https://doi.org/10.1038/s41396-020-00838-1. doi:10.1038/s41396-020-00838-1.

Fritz, P., Clark, I., Fontes, J.C., Whiticar, M., Faber, E.. Deuterium and $^{13}C$ evidence for low temperature production of hydrogen and methane in a highly alkaline groundwater environment in Oman. In: International symposium on water-rock interaction. AA Balkema Rotterdam; volume 1; 1992. p. 793–796.

Frost, B.R.. On the Stability of Sulfides, Oxides, and Native Metals in Serpentinite. J Petrol 1985;26(1):31–63. doi:10.1093/petrology/26.1.31.

Giunta, T., Young, E.D., Warr, O., Kohl, I., Ash, J.L., Martini, A., Mundle, S.O., Rumble, D., Pérez-Rodríguez, I., Wasley, M., LaRowe, D.E., Gilbert, A., Lollar, B.S.. Methane sources and sinks in continental sedimentary systems: New insights from paired clumped isotopologues $^{1}3CH_3D$ and $^{1}2CH_2D^{2}$. Geochim Cosmochim Acta 2019;245:327 – 351. URL: http://www.sciencedirect.com/science/article/pii/S0016703718306161. doi:10.1016/j.gca.2018.10.030.

Glein, C.R., Baross, J.A., Waite Jr, J.H.. The pH of Enceladus' ocean. Geochim Cosmochim Acta 2015;162:202–219. doi:10.1016/j.gca.2015.04.017.

Glein, C.R., Zolotov, M.Y.. Hydrogen, Hydrocarbons, and Habitability Across the Solar System. Elements 2020;16(1):47–52. URL: https://doi.org/10.2138/gselements.16.1.47. doi:10.2138/gselements.16.1.47. arXiv:https://pubs.geoscienceworld.org/elements/article-pdf/16/1/47/4960732/gselements-16-1-47.pdf.

Glennie, K., Boeuf, M., Clarke, M.H., Moody-Stuart, M., Pilaar, W., Reinhardt, B.. Late Cretaceous nappes in Oman Mountains and their geologic evolution. AAPG Bull 1973;57(1):5–27. doi:10.1306/819A4240-16C5-11D7-8645000102C1865D.

Godard, M., Jousselin, D., Bodinier, J.L.. Relationships between geochemistry and structure beneath a palaeo-spreading centre: a study of the mantle section in the Oman ophiolite. Earth Planet Sci Lett 2000;180(1):133 – 148. URL: http://www.sciencedirect.com/science/article/pii/S0012821X00001497. doi:10.1016/S0012-821X(00)00149-7.

Grozeva, N.G., Klein, F., Seewald, J.S., Sylva, S.P.. Chemical and isotopic analyses of hydrocarbon-bearing fluid inclusions in olivine-rich rocks. Philos Trans R Soc, A 2020;378(2165, SI). doi:10.1098/rsta.2018.0431.

Gruen, D.S., Wang, D.T., Könneke, M., Topçuoğlu, B.D., Stewart, L.C., Goldhammer, T., Holden, J.F., Hinrichs, K.U., Ono, S.. Experimental investigation on the controls of clumped isotopologue and hydrogen isotope ratios in microbial

methane. Geochim Cosmochim Acta 2018;237:339 – 356. URL: http://www.sciencedirect.com/science/article/pii/S0016703718303442. doi:10.1016/j.gca.2018.06.029.

Guilmette, C., Smit, M.A., van Hinsbergen, D.J.J., Gürer, D., Corfu, F., Charette, B., Maffione, M., Rabeau, O., Savard, D.. Forced subduction initiation recorded in the sole and crust of the Semail Ophiolite of Oman. Nat Geosci 2018;11(9):688–695. URL: https://doi.org/10.1038/s41561-018-0209-2. doi:10.1038/s41561-018-0209-2.

Hanghøj, K., Kelemen, P.B., Hassler, D., Godard, M.. Composition and Genesis of Depleted Mantle Peridotites from the Wadi Tayin Massif, Oman Ophiolite; Major and Trace Element Geochemistry, and Os Isotope and PGE Systematics. J Petrol 2010;51(1-2):201–227. doi:10.1093/petrology/egp077.

Hanson, R.S., Hanson, T.E.. Methanotrophic bacteria. Microbiol Mol Biol Rev 1996;60(2):439–471. URL: https://mmbr.asm.org/content/60/2/439. arXiv:https://mmbr.asm.org/content/60/2/439.full.pdf.

Henry, E.A., Devereux, R., Maki, J.S., Gilmour, C.C., Woese, C.R., Mandelco, L., Schauder, R., Remsen, C.C., Mitchell, R.. Characterization of a new thermophilic sulfate-reducing bacterium. Arch Microbiol 1994;161(1):62–69. URL: https://doi.org/10.1007/BF00248894. doi:10.1007/BF00248894.

Hoehler, T.M.. Biological energy requirements as quantitative boundary conditions for life in the subsurface. Geobiology 2004;2(4):205–215. URL: https://onlinelibrary.wiley.com/doi/abs/10.1111/j.1472-4677.2004.00033.x. doi:10.1111/j.1472-4677.2004.00033.x. arXiv:https://onlinelibrary.wiley.com/doi/pdf/10.1111/j.1472-4677.2004.00033.x.

Horibe, Y., Craig, H.. DH fractionation in the system methane-hydrogen-water. Geochim Cosmochim Acta 1995;59(24):5209–5217. doi:10.1016/0016-7037(95)00391-6.

Hunt, J.M.. Petroleum geochemistry and geology. New York: W.H. Freeman, 1996.

Jacquemin, M., Beuls, A., Ruiz, P.. Catalytic production of methane from $CO_2$ and $H_2$ at low temperature: Insight on the reaction mechanism. Catal Today 2010;157(1-4):462–466. doi:10.1016/j.cattod.2010.06.016.

Johnson, J.W., Oelkers, E.H., Helgeson, H.C.. SUPCRT92: A software package for calculating the standard molal thermodynamic properties of minerals, gases, aqueous species, and reactions from 1 to 5000 bar and 0 to 1000°C. Comput Geosci 1992;18(7):899–947. URL: https://www.sciencedirect.com/science/article/pii/009830049290029Q. doi:10.1016/0098-3004(92)90029-Q.

Kampbell, D., Wilson, J., McInnes, D.. DETERMINING DISSOLVED HYDROGEN, METHANE, AND VINYL CHLORIDE CONCENTRATIONS IN AQUEOUS SOLUTION ON A NANOMOLAR SCALE WITH THE BUBBLE STRIP METHOD. In: Proceedings of the 1998 Conference on Hazardous Waste Research. 1998. p. 176–190.

Kelemen, P., Al Rajhi, A., Godard, M., Ildefonse, B., Köpke, J., MacLeod, C., Manning, C., Michibayashi, K., Nasir, S., Shock, E., Takazawa, E., Teagle, D.. Scientific drilling and related research in the samail ophiolite, sultanate of Oman. Scientific Drilling 2013 (2013), Nr 15 2013;2013(15):64–71. URL: https://www.repo.uni-hannover.de/handle/123456789/1086.

Kelemen, P., Matter, J., Teagle, D., Coggon, J., the Oman Drilling Project Science Team, . Proceedings of the oman drilling project. In: Proceedings of the Oman Drilling Project. College Station, TX: International Ocean Discovery Program; 2020. p. All pages. doi:10.14379/OmanDP.proc.2020.

Kelemen, P.B., Matter, J.. In situ carbonation of peridotite for $CO_2$ storage. Proc Natl Acad Sci U S A 2008;105(45):17295–17300. doi:10.1073/pnas.0805794105.

Kelemen, P.B., Matter, J., Streit, E.E., Rudge, J.F., Curry, W.B., Blusztajn, J.. Rates and mechanisms of mineral carbonation in peridotite: natural processes and recipes for enhanced, in situ $CO_2$ capture and storage. Annu Rev Earth Planet Sci 2011;39:545–576. doi:10.1146/annurev-earth-092010-152509.

Kelley, D.S.. Methane-rich fluids in the oceanic crust. J Geophys Res: Solid Earth 1996;101(B2):2943–2962. doi:10.1029/95JB02252.

Kelley, D.S., Früh-Green, G.L.. Abiogenic methane in deep-seated mid-ocean ridge environments: Insights from stable isotope

analyses. J Geophys Res: Solid Earth 1999;104(B5):10439–10460. doi:10.1029/1999JB900058.

Kieft, T.L.. Microbiology of the Deep Continental Biosphere; Cham: Springer International Publishing. p. 225–249. URL: https://doi.org/10.1007/978-3-319-28071-4_6. doi:10.1007/978-3-319-28071-4_6.

Kieft, T.L., McCuddy, S.M., Onstott, T.C., Davidson, M., Lin, L.H., Mislowack, B., Pratt, L., Boice, E., Lollar, B.S., Lippmann-Pipke, J., Pfiffner, S.M., Phelps, T.J., Gihring, T., Moser, D., van Heerden, A.. Geochemically Generated, Energy-Rich Substrates and Indigenous Microorganisms in Deep, Ancient Groundwater. Geomicrobiol J 2005;22(6):325–335. URL: https://doi.org/10.1080/01490450500184876. doi:10.1080/01490450500184876. arXiv:10.1080/01490450500184876.

Klein, F., Bach, W.. Fe–Ni–Co–O–S Phase Relations in Peridotite–Seawater Interactions. J Petrol 2009;50(1):37–59. URL: https://doi.org/10.1093/petrology/egn071. doi:10.1093/petrology/egn071. arXiv:http://oup.prod.sis.lan/petrology/article-pdf/50/1/37/16669457/egn071.pdf.

Klein, F., Bach, W., Jöns, N., McCollom, T., Moskowitz, B., Berquó, T.. Iron partitioning and hydrogen generation during serpentinization of abyssal peridotites from 15 °N on the Mid-Atlantic Ridge. Geochim Cosmochim Acta 2009;73(22):6868 – 6893. URL: http://www.sciencedirect.com/science/article/pii/S0016703709005353. doi:10.1016/j.gca.2009.08.021.

Klein, F., Grozeva, N.G., Seewald, J.S.. Abiotic methane synthesis and serpentinization in olivine-hosted fluid inclusions. Proc Natl Acad Sci U S A 2019;116(36):17666–17672. URL: https://www.pnas.org/content/116/36/17666. doi:10.1073/pnas.1907871116. arXiv:https://www.pnas.org/content/116/36/17666.full.pdf.

Knittel, K., Boetius, A.. Anaerobic Oxidation of Methane: Progress with an Unknown Process. Annu Rev Microbiol 2009;63(1):311–334. URL: https://doi.org/10.1146/annurev.micro.61.080706.093130. doi:10.1146/annurev.micro.61.080706.093130. arXiv:https://doi.org/10.1146/annurev.micro.61.080706.093130; pMID: 19575572.

Kopf, S., Davidheiser-Kroll, B., Kocken, I.. Isoreader: An R package to read stable isotope data files for reproducible research. J Open Source Software 2021;6(61):2878. URL: https://doi.org/10.21105/joss.02878. doi:10.21105/joss.02878.

Kral, T.A., Birch, W., Lavender, L.E., Virden, B.T.. Potential use of highly insoluble carbonates as carbon sources by methanogens in the subsurface of Mars. Planet Space Sci 2014;101:181 – 185. URL: http://www.sciencedirect.com/science/article/pii/S0032063314002049. doi:10.1016/j.pss.2014.07.008.

Kraus, E.A., Nothaft, D., Stamps, B.W., Rempfert, K.R., Ellison, E.T., Matter, J.M., Templeton, A.S., Boyd, E.S., Spear, J.R.. Molecular Evidence for an Active Microbial Methane Cycle in Subsurface Serpentinite-Hosted Groundwaters in the Samail Ophiolite, Oman. Appl Environ Microbiol 2021;87(2). URL: https://aem.asm.org/content/87/2/e02068-20. doi:10.1128/AEM.02068-20. arXiv:https://aem.asm.org/content/87/2/e02068-20.full.pdf.

Kumagai, H., Nakamura, K., Toki, T., Morishita, T., Okino, K., Ishibashi, J.i., Tsunogai, U., Kawaguchi, S., Gano, T., Shibuya, T., Sawaguchi, T., Neo, N., Joshima, M., Sato, T., Takai, K.. Geological background of the Kairei and Edmond hydrothermal fields along the Central Indian Ridge : Implications for the distinct chemistry between their vent fluids. Geofluids 2008;8(4):239–251. URL: https://ci.nii.ac.jp/naid/120006389526/en/. doi:10.1111/j.1468-8123.2008.00223.x.

Labidi, J., Young, E., Giunta, T., Kohl, I., Seewald, J., Tang, H., Lilley, M., Früh-Green, G.. Methane thermometry in deep-sea hydrothermal systems: Evidence for re-ordering of doubly-substituted isotopologues during fluid cooling. Geochim Cosmochim Acta 2020;288:248 – 261. URL: http://www.sciencedirect.com/science/article/pii/S0016703720305068. doi:10.1016/j.gca.2020.08.013.

Lang, S.Q., Früh-Green, G.L., Bernasconi, S.M., Brazelton, W.J., Schrenk, M.O., McGonigle, J.M.. Deeply-sourced formate fuels sulfate reducers but not methanogens at Lost City hydrothermal field. Sci Rep 2018;8(1):755. doi:10.1038/s41598-017-19002-5.

Laso-Pérez, R., Hahn, C., van Vliet, D.M., Tegetmeyer, H.E., Schubotz, F., Smit, N.T., Pape, T., Sahling, H., Bohrmann, G., Boetius, A., Knittel, K., Wegener, G.. Anaerobic Degradation of Non-Methane Alkanes by "Candidatus Methanoliparia"

in Hydrocarbon Seeps of the Gulf of Mexico. mBio 2019;10(4). URL: https://mbio.asm.org/content/10/4/e01814-19. doi:10.1128/mBio.01814-19. arXiv:https://mbio.asm.org/content/10/4/e01814-19.full.pdf.

Leong, J.A.M., Shock, E.L.. Thermodynamic constraints on the geochemistry of low-temperature, continental, serpentinization-generated fluids. Am J Sci 2020;320(3):185–235. doi:10.2475/03.2020.01.

Lippard, S., Shelton, A., Gass, I.. The Ophiolite of Northern Oman. volume 11. Geological Society of London, 1986. URL: https://mem.lyellcollection.org/content/11/1/39. doi:10.1144/GSL.MEM.1986.011.01.03. arXiv:https://mem.lyellcollection.org/content/11/1/39.full.pdf.

Lowell, R., Kolandaivelu, K., Rona, P.. Hydrothermal Activity. In: Reference Module in Earth Systems and Environmental Sciences. Elsevier; 2014. URL: http://www.sciencedirect.com/science/article/pii/B9780124095489091326. doi:10.1016/B978-0-12-409548-9.09132-6.

Luesken, F.A., Wu, M.L., Op den Camp, H.J.M., Keltjens, J.T., Stunnenberg, H., Francoijs, K.J., Strous, M., Jetten, M.S.M.. Effect of oxygen on the anaerobic methanotroph 'Candidatus Methylomirabilis oxyfera': kinetic and transcriptional analysis. Environ Microbiol 2012;14(4):1024–1034. URL: https://onlinelibrary.wiley.com/doi/abs/10.1111/j.1462-2920.2011.02682.x. doi:10.1111/j.1462-2920.2011.02682.x. arXiv:https://onlinelibrary.wiley.com/doi/pdf/10.1111/j.1462-2920.2011.02682.x.

MacDougall, D., Crummett, W.B., et al. Guidelines for data acquisition and data quality evaluation in environmental chemistry. Anal Chem 1980;52(14):2242–2249.

Marques, J., Etiope, G., Neves, M., Carreira, P., Rocha, C., Vance, S., Christensen, L., Miller, A., Suzuki, S.. Linking serpentinization, hyperalkaline mineral waters and abiotic methane production in continental peridotites: an integrated hydrogeological-bio-geochemical model from the Cabeço de Vide $CH_4$-rich aquifer (Portugal). Appl Geochem 2018;96:287 – 301. URL: http://www.sciencedirect.com/science/article/pii/S0883292718301987. doi:10.1016/j.apgeochem.2018.07.011.

Martini, A.M., Walter, L.M., Ku, T.C.W., Budai, J.M., McIntosh, J.C., Schoell, M.. Microbial production and modification of gases in sedimentary basins: A geochemical case study from a Devonian shale gas play, Michigan basin. AAPG Bull 2003;87(8):1355–1375. URL: https://doi.org/10.1306/031903200184. doi:10.1306/031903200184. arXiv:https://pubs.geoscienceworld.org/aapgbull/article-pdf/87/8/1355/3363261/1355.pdf.

Matter, J.M., Pezard, P.A., Henry, G., Brun, L., Célérier, B., Lods, G., Robert, P., Benchikh, A.M., Al Shukaili, M., Al Qassabi, A.. Oman Drilling Project Phase I Borehole Geophysical Survey. AGU Fall Meeting Abstracts 2017;.

Matter, J.M., Waber, H., Loew, S., Matter, A.. Recharge areas and geochemical evolution of groundwater in an alluvial aquifer system in the Sultanate of Oman. Hydrogeol J 2006;14(1-2):203–224. doi:10.1007/s10040-004-0425-2.

McCollom, T.M.. Methanogenesis as a potential source of chemical energy for primary biomass production by autotrophic organisms in hydrothermal systems on Europa. Journal of Geophysical Research: Planets 1999;104(E12):30729–30742. doi:10.1029/1999JE001126.

McCollom, T.M.. Abiotic methane formation during experimental serpentinization of olivine. Proc Natl Acad Sci U S A 2016;113(49):13965–13970. doi:10.1073/pnas.1611843113.

McCollom, T.M., Bach, W.. Thermodynamic constraints on hydrogen generation during serpentinization of ultramafic rocks. Geochim Cosmochim Acta 2009;73(3):856–875. doi:10.1016/j.gca.2008.10.032.

McCollom, T.M., Seewald, J.S.. Experimental constraints on the hydrothermal reactivity of organic acids and acid anions: I. Formic acid and formate. Geochim Cosmochim Acta 2003;67(19):3625 – 3644. URL: http://www.sciencedirect.com/science/article/pii/S0016703703001364. doi:10.1016/S0016-7037(03)00136-4.

McDermott, J.M., Seewald, J.S., German, C.R., Sylva, S.P.. Pathways for abiotic organic synthesis at submarine hydrothermal fields. Proc Natl Acad Sci U S A 2015;112(25):7668–7672. doi:10.1073/pnas.1506295112.

McKay, C.P., Porco, C.C., Altheide, T., Davis, W.L., Kral, T.A.. The Possible Origin and Persistence of Life on Enceladus

and Detection of Biomarkers in the Plume. Astrobiology 2008;8(5):909–919. URL: https://doi.org/10.1089/ast.2008.0265. doi:10.1089/ast.2008.0265. arXiv:https://doi.org/10.1089/ast.2008.0265; pMID: 18950287.

Ménez, B.. Abiotic Hydrogen and Methane: Fuels for Life. Elements 2020;16(1):39–46. URL: https://doi.org/10.2138/gselements.16.1.39. doi:10.2138/gselements.16.1.39. arXiv:https://pubs.geoscienceworld.org/elements/article-pdf/16/1/39/4960722/gselements-16-1-39.pdf.

Merlivat, L., Pineau, F., Javoy, M.. Hydrothermal vent waters at 13 °N on the East Pacific Rise: isotopic composition and gas concentration. Earth Planet Sci Lett 1987;84(1):100 – 108. URL: http://www.sciencedirect.com/science/article/pii/0012821X87901804. doi:10.1016/0012-821X(87)90180-4.

Mervine, E.M., Humphris, S.E., Sims, K.W., Kelemen, P.B., Jenkins, W.J.. Carbonation rates of peridotite in the Samail Ophiolite, Sultanate of Oman, constrained through $^{14}$C dating and stable isotopes. Geochim Cosmochim Acta 2014;126:371 – 397. URL: http://www.sciencedirect.com/science/article/pii/S0016703713006467. doi:10.1016/j.gca.2013.11.007.

Michaelis, W., Seifert, R., Nauhaus, K., Treude, T., Thiel, V., Blumenberg, M., Knittel, K., Gieseke, A., Peterknecht, K., Pape, T., Boetius, A., Amann, R., Jørgensen, B.B., Widdel, F., Peckmann, J., Pimenov, N.V., Gulin, M.B.. Microbial Reefs in the Black Sea Fueled by Anaerobic Oxidation of Methane. Science 2002;297(5583):1013–1015. URL: https://science.sciencemag.org/content/297/5583/1013. doi:10.1126/science.1072502. arXiv:https://science.sciencemag.org/content/297/5583/1013.full.pdf.

Milkov, A.V., Etiope, G.. Revised genetic diagrams for natural gases based on a global dataset of >20,000 samples. Org Geochem 2018;125:109–120. doi:10.1016/j.orggeochem.2018.09.002.

Miller, H.M., Chaudhry, N., Conrad, M.E., Bill, M., Kopf, S.H., Templeton, A.S.. Large carbon isotope variability during methanogenesis under alkaline conditions. Geochim Cosmochim Acta 2018;237:18 – 31. URL: http://www.sciencedirect.com/science/article/pii/S0016703718303223. doi:10.1016/j.gca.2018.06.007.

Miller, H.M., Matter, J.M., Kelemen, P., Ellison, E.T., Conrad, M., Fierer, N., Ruchala, T., Tominaga, M., Templeton, A.S.. Reply to "Methane origin in the Samail ophiolite: Comment on 'Modern water/rock reactions in Oman hyperalkaline peridotite aquifers and implications for microbial habitability"' [Geochim. Cosmochim. Acta 179 (2016) 217–241]. Geochim Cosmochim Acta 2017a;197:471 – 473. URL: http://www.sciencedirect.com/science/article/pii/S0016703716306482. doi:10.1016/j.gca.2016.11.011.

Miller, H.M., Matter, J.M., Kelemen, P., Ellison, E.T., Conrad, M.E., Fierer, N., Ruchala, T., Tominaga, M., Templeton, A.S.. Modern water/rock reactions in Oman hyperalkaline peridotite aquifers and implications for microbial habitability. Geochim Cosmochim Acta 2016;179:217 – 241. URL: http://www.sciencedirect.com/science/article/pii/S0016703716300205. doi:10.1016/j.gca.2016.01.033.

Miller, H.M., Mayhew, L.E., Ellison, E.T., Kelemen, P., Kubo, M., Templeton, A.S.. Low temperature hydrogen production during experimental hydration of partially-serpentinized dunite. Geochim Cosmochim Acta 2017b;209:161 – 183. URL: http://www.sciencedirect.com/science/article/pii/S0016703717302454. doi:10.1016/j.gca.2017.04.022.

Miura, M., Arai, S., Mizukami, T.. Raman spectroscopy of hydrous inclusions in olivine and orthopyroxene in ophiolitic harzburgite: Implications for elementary processes in serpentinization. J Mineral Petrol Sci 2011;advpub:1103030170–1103030170. doi:10.2465/jmps.101021d.

Moser, D.P., Gihring, T.M., Brockman, F.J., Fredrickson, J.K., Balkwill, D.L., Dollhopf, M.E., Lollar, B.S., Pratt, L.M., Boice, E., Southam, G., Wanger, G., Baker, B.J., Pfiffner, S.M., Lin, L.H., Onstott, T.C.. Desulfotomaculum and Methanobacterium spp. Dominate a 4- to 5-Kilometer-Deep Fault. Appl Environ Microbiol 2005;71(12):8773–8783. URL: https://aem.asm.org/content/71/12/8773. doi:10.1128/AEM.71.12.8773-8783.2005. arXiv:https://aem.asm.org/content/71/12/8773.full.pdf.

Murad, A.A., Krishnamurthy, R.. Factors controlling groundwater quality in Eastern United Arab Emirates: a chemical and isotopic approach. J Hydro 2004;286(1):227 – 235. URL: http://www.sciencedirect.com/science/article/pii/

S0022169403003949. doi:10.1016/j.jhydrol.2003.09.020.

Neal, C., Stanger, G.. Hydrogen generation from mantle source rocks in Oman. Earth Planet Sci Lett 1983;66:315 – 320. URL: http://www.sciencedirect.com/science/article/pii/0012821X83901449. doi:10.1016/0012-821X(83)90144-9.

Neal, C., Stanger, G.. Past and present serpentinisation of ultramafic rocks; an example from the Semail Ophiolite Nappe of Northern Oman. In: The Chemistry of Weathering. Springer; 1985. p. 249–275. doi:10.1007/978-94-009-5333-8_15.

Nicolas, A.. Structures of Ophiolites and Dynamics of Oceanic Lithosphere | SpringerLink. Springer, Dordrecht, 1989. doi:10.1007/978-94-009-2374-4.

Nicolas, A., Boudier, F., Ildefonse, B., Ball, E.. Accretion of Oman and United Arab Emirates ophiolite–discussion of a new structural map. Marine Geophysical Researches 2000;21(3-4):147–180. doi:10.1023/A:1026769727917.

Noël, J., Godard, M., Oliot, E., Martinez, I., Williams, M., Boudier, F., Rodriguez, O., Chaduteau, C., Escario, S., Gouze, P.. Evidence of polygenetic carbon trapping in the Oman Ophiolite: Petro-structural, geochemical, and carbon and oxygen isotope study of the Wadi Dima harzburgite-hosted carbonates (Wadi Tayin massif, Sultanate of Oman). Lithos 2018;323:218 – 237. URL: http://www.sciencedirect.com/science/article/pii/S0024493718302998. doi:10.1016/j.lithos.2018.08.020; aBYSS.

Nolan, S.C., Skelton, P.W., Clissold, B.P., Smewing, J.D.. Maastrichtian to early Tertiary stratigraphy and palaeogeography of the Central and Northern Oman Mountains. Geological Society, London, Special Publications 1990;49(1):495–519. URL: https://sp.lyellcollection.org/content/49/1/495. doi:10.1144/GSL.SP.1992.049.01.31. arXiv:https://sp.lyellcollection.org/content/49/1/495.full.pdf.

Nothaft, D., Templeton, A.S., Boyd, E., Matter, J., Stute, M., Paukert Vankeuren, A.N.. Aqueous geochemical and microbial variation across discrete depth intervals in a peridotite aquifer assessed using a packer system in the samail ophiolite, oman. Earth and Space Science Open Archive 2021;:34URL: https://doi.org/10.1002/essoar.10506402.2. doi:10.1002/essoar.10506402.2.

Ono, S., Wang, D.T., Gruen, D.S., Sherwood Lollar, B., Zahniser, M.S., McManus, B.J., Nelson, D.D.. Measurement of a Doubly Substituted Methane Isotopologue, $^{13}CH_3D$, by Tunable Infrared Laser Direct Absorption Spectroscopy. Anal Chem 2014;86(13):6487–6494. URL: https://doi.org/10.1021/ac5010579. doi:10.1021/ac5010579. arXiv:https://doi.org/10.1021/ac5010579; pMID: 24895840.

Parkhurst, D.L., Appelo, C.A.J.. Description of input and examples for PHREEQC version 3–A computer program for speciation, batch-reaction, one-dimensional transport, and inverse geochemical calculations. U.S. Geological Survey; 6th ed.; 2013. .

Parsons International & Co., L.. Report on Findings of Exploration Program of Deep Groundwater in Northern Sharqiyah. Technical Report; Ministry of Regional Municipalities, Environment and Water Resources; PO Box 162, Postal Code 117, Wadi Al Kabir, Sultanate of Oman; 2005.

Paukert, A.. Mineral Carbonation in Mantle Peridotite of the Samail Ophiolite, Oman: Implications for permanent geological carbon dioxide capture and storage. Ph.D. thesis; Columbia University; 2014. doi:10.7916/D85M63WZ.

Paukert, A.N., Matter, J.M., Kelemen, P.B., Shock, E.L., Havig, J.R.. Reaction path modeling of enhanced in situ $CO_2$ mineralization for carbon sequestration in the peridotite of the Samail Ophiolite, Sultanate of Oman. Chem Geol 2012;330:86–100. doi:10.1016/j.chemgeo.2012.08.013.

Paukert Vankeuren, A.N., Matter, J.M., Stute, M., Kelemen, P.B.. Multitracer determination of apparent groundwater ages in peridotite aquifers within the Samail ophiolite, Sultanate of Oman. Earth Planet Sci Lett 2019;516:37–48. doi:10.1016/j.epsl.2019.03.007.

Peters, J.W., Schut, G.J., Boyd, E.S., Mulder, D.W., Shepard, E.M., Broderick, J.B., King, P.W., Adams, M.W.. [FeFe]- and [NiFe]-hydrogenase diversity, mechanism, and maturation. Biochim Biophys Acta, Mol Cell Res 2015;1853(6):1350 – 1369. URL: http://www.sciencedirect.com/science/article/pii/S0167488914004194. doi:10.1016/j.bbamcr.2014.11.

021; sI: Fe/S proteins.

Proskurowski, G., Lilley, M.D., Seewald, J.S., Früh-Green, G.L., Olson, E.J., Lupton, J.E., Sylva, S.P., Kelley, D.S.. Abiogenic hydrocarbon production at Lost City hydrothermal field. Science 2008;319(5863):604–607. doi:10.1126/science.1151194.

Quast, C., Pruesse, E., Gerken, J., Peplies, J., Yarza, P., Yilmaz, P., Schweer, T., Glöckner, F.O.. The SILVA ribosomal RNA gene database project: improved data processing and web-based tools. Nucleic Acids Res 2012;41(D1):D590–D596. doi:10.1093/nar/gks1219.

R Core Team, . R: A Language and Environment for Statistical Computing. 2019. URL: https://www.R-project.org/.

Rabu, D., Nehlig, P., Roger, J.. Stratigraphy and structure of the Oman Mountains. Documents- B R G M 1993;.

Rempfert, K.R., Miller, H.M., Bompard, N., Nothaft, D., Matter, J.M., Kelemen, P., Fierer, N., Templeton, A.S.. Geological and geochemical controls on subsurface microbial life in the Samail Ophiolite, Oman. Front Microb 2017;8(56):1–21. doi:10.3389/fmicb.2017.00056.

Rioux, M., Garber, J., Bauer, A., Bowring, S., Searle, M., Kelemen, P., Hacker, B.. Synchronous formation of the metamorphic sole and igneous crust of the Semail ophiolite: New constraints on the tectonic evolution during ophiolite formation from high-precision U–Pb zircon geochronology. Earth Planet Sci Lett 2016;451:185 – 195. URL: http://www.sciencedirect.com/science/article/pii/S0012821X16303387. doi:10.1016/j.epsl.2016.06.051.

Rollinson, H.. Chromite in the mantle section of the Oman ophiolite: A new genetic model. Island Arc 2005;14(4):542–550. URL: https://onlinelibrary.wiley.com/doi/abs/10.1111/j.1440-1738.2005.00482.x. doi:10.1111/j.1440-1738.2005.00482.x. arXiv:https://onlinelibrary.wiley.com/doi/pdf/10.1111/j.1440-1738.2005.00482.x.

Rooney, M.A., Claypool, G.E., Moses Chung, H.. Modeling thermogenic gas generation using carbon isotope ratios of natural gas hydrocarbons. Chem Geol 1995;126(3):219–232. URL: https://www.sciencedirect.com/science/article/pii/0009254195001190. doi:10.1016/0009-2541(95)00119-0; processes of Natural Gas Formation.

Sachan, H.K., Mukherjee, B.K., Bodnar, R.J.. Preservation of methane generated during serpentinization of upper mantle rocks: Evidence from fluid inclusions in the Nidar ophiolite, Indus Suture Zone, Ladakh (India). Earth Planet Sci Lett 2007;257(1):47 – 59. URL: http://www.sciencedirect.com/science/article/pii/S0012821X07000969. doi:10.1016/j.epsl.2007.02.023.

Sander, R.. Compilation of Henry's law constants (version 4.0) for water as solvent. Atmos Chem Phys 2015;15(8). doi:10.5194/ACP-15-4399-2015.

Schidlowski, M.. Carbon isotopes as biogeochemical recorders of life over 3.8 Ga of Earth history: evolution of a concept. Precambrian Res 2001;106(1):117 – 134. URL: http://www.sciencedirect.com/science/article/pii/S0301926800001285. doi:10.1016/S0301-9268(00)00128-5.

Schink, B.. Energetics of syntrophic cooperation in methanogenic degradation. Microbiol Mol Biol Rev 1997;61(2):262–280. URL: https://mmbr.asm.org/content/61/2/262. arXiv:https://mmbr.asm.org/content/61/2/262.full.pdf.

Schink, B., Stams, A.J.M.. Syntrophism among Prokaryotes. In: Dworkin, M and Falkow, S and Rosenberg, E and Schleifer, KH and Stackebrandt, E, , editor. PROKARYOTES: A HANDBOOK ON THE BIOLOGY OF BACTERIA, VOL 2, THIRD EDITION: ECOPHYSIOLOGY AND BIOCHEMISTRY. 233 SPRING STREET, NEW YORK, NY 10013, UNITED STATES: SPRINGER; 2006. p. 309–335. doi:{10.1007/0-387-30742-7_11}.

Sekiguchi, Y., Muramatsu, M., Imachi, H., Narihiro, T., Ohashi, A., Harada, H., Hanada, S., Kamagata, Y.. Thermodesulfovibrio aggregans sp. nov. and Thermodesulfovibrio thiophilus sp. nov., anaerobic, thermophilic, sulfate-reducing bacteria isolated from thermophilic methanogenic sludge, and emended description of the genus Thermodesulfovibrio. Int J Syst Evol Microbiol 2008;58(11):2541–2548. URL: https://www.microbiologyresearch.org/content/journal/ijsem/10.1099/ijs.0.2008/000893-0. doi:10.1099/ijs.0.2008/000893-0.

Shennan, J.L.. Utilisation of C2–C4 gaseous hydrocarbons and isoprene by microorganisms. J Appl Chem Biotech-

nol 2006;81(3):237–256. URL: https://onlinelibrary.wiley.com/doi/abs/10.1002/jctb.1388. doi:10.1002/jctb.1388. arXiv:https://onlinelibrary.wiley.com/doi/pdf/10.1002/jctb.1388.

Sherwood Lollar, B., Lacrampe-Couloume, G., Voglesonger, K., Onstott, T., Pratt, L., Slater, G.. Isotopic signatures of $CH_4$ and higher hydrocarbon gases from Precambrian Shield sites: A model for abiogenic polymerization of hydrocarbons. Geochim Cosmochim Acta 2008;72(19):4778 – 4795. URL: http://www.sciencedirect.com/science/article/pii/S0016703708004250. doi:10.1016/j.gca.2008.07.004.

Sherwood Lollar, B., Westgate, T.D., Ward, J.A., Slater, G.F., Lacrampe-Couloume, G.. Abiogenic formation of alkanes in the Earth's crust as a minor source for global hydrocarbon reservoirs. Nature 2002;416(6880):522–524. doi:10.1038/416522a.

Shock, E.L.. Chemical Environments of Submarine Hydrothermal Systems; Springer, Dordrecht. p. 67–107. doi:10.1007/978-94-011-2741-7_5.

Singh, R., Guzman, M.S., Bose, A.. Anaerobic Oxidation of Ethane, Propane, and Butane by Marine Microbes: A Mini Review. Front Microb 2017;8:2056. URL: https://www.frontiersin.org/article/10.3389/fmicb.2017.02056. doi:10.3389/fmicb.2017.02056.

Skelton, P.W., Nolan, S.C., Scott, R.W.. The Maastrichtian transgression onto the northwestern flank of the Proto-Oman Mountains: sequences of rudist-bearing beach to open shelf facies. Geological Society, London, Special Publications 1990;49(1):521–547. URL: https://sp.lyellcollection.org/content/49/1/521. doi:10.1144/GSL.SP.1992.049.01.32. arXiv:https://sp.lyellcollection.org/content/49/1/521.full.pdf.

Soret, M., Bonnet, G., Larson, K., Agard, P., Cottle, J., Dubacq, B., Button, M.. Slow subduction initiation forces fast ophiolite formation Soret. In: International Conference on Ophiolites and the Oceanic Lithosphere: Results of the Oman Drilling Project and Related Research. Sultan Qaboos University, Muscat, Sultanate of Oman; 2020. p. 232.

Stanger, G.. The hydrogeology of the Oman Mountains. Ph.D. thesis; Open University; 1986.

Stolper, D., Martini, A., Clog, M., Douglas, P., Shusta, S., Valentine, D., Sessions, A., Eiler, J.. Distinguishing and understanding thermogenic and biogenic sources of methane using multiply substituted isotopologues. Geochim Cosmochim Acta 2015;161:219 – 247. URL: http://www.sciencedirect.com/science/article/pii/S0016703715002082. doi:10.1016/j.gca.2015.04.015.

Stolper, D.A., Lawson, M., Formolo, M.J., Davis, C.L., Douglas, P.M.J., Eiler, J.M.. The utility of methane clumped isotopes to constrain the origins of methane in natural gas accumulations. Geological Society, London, Special Publications 2018;468(1):23–52. URL: https://sp.lyellcollection.org/content/468/1/23. doi:10.1144/SP468.3. arXiv:https://sp.lyellcollection.org/content/468/1/23.full.pdf.

Streit, E., Kelemen, P., Eiler, J.. Coexisting serpentine and quartz from carbonate-bearing serpentinized peridotite in the Samail Ophiolite, Oman. Contrib Mineral Petrol 2012;164(5):821–837. URL: https://doi.org/10.1007/s00410-012-0775-z. doi:10.1007/s00410-012-0775-z.

Suzuki, S., Kuenen, J.G., Schipper, K., van der Velde, S., Ishii, S., Wu, A., Sorokin, D.Y., Tenney, A., Meng, X., Morrill, P.L., Kamagata, Y., Muyzer, G., Nealson, K.H.. Physiological and genomic features of highly alkaliphilic hydrogen-utilizing Betaproteobacteria from a continental serpentinizing site. Nat Commun 2014;5:3900. doi:10.1038/ncomms4900.

Terken, J.M.J.. The Natih Petroleum System of North Oman. GeoArabia 1999;4(2):157–180. URL: https://pubs.geoscienceworld.org/geoarabia/article/4/2/157/566618.

Terzer, S., Wassenaar, L.I., Araguás-Araguás, L.J., Aggarwal, P.K.. Global isoscapes for $\delta^{18}$O and $\delta^{2}$H in precipitation: improved prediction using regionalized climatic regression models. Hydrol Earth Syst Sci 2013;17(11):4713–4728. URL: https://www.hydrol-earth-syst-sci.net/17/4713/2013/. doi:10.5194/hess-17-4713-2013.

Thampi, K.R., Kiwi, J., Graetzel, M.. Methanation and photo-methanation of carbon dioxide at room temperature and atmospheric pressure. Nature 1987;327(6122):506.

Timmers, P.H., Welte, C.U., Koehorst, J.J., Plugge, C.M., Jetten, M.S., Stams, A.J.. Reverse methanogenesis and

respiration in methanotrophic archaea. Archaea 2017;2017. doi:10.1155/2017/1654237.

USGS, . Digital Elevation - Global Multi-resolution Terrain Elevation Data 2010 (GMTED2010). 2010. doi:/10.5066/F7J38R2N.

Vacquand, C., Deville, E., Beaumont, V., Guyot, F., Sissmann, O., Pillot, D., Arcilla, C., Prinzhofer, A.. Reduced gas seepages in ophiolitic complexes: evidences for multiple origins of the $H_2$-$CH_4$-$N_2$ gas mixtures. Geochim Cosmochim Acta 2018;223:437–461. doi:10.1016/j.gca.2017.12.018.

Waite, J.H., Glein, C.R., Perryman, R.S., Teolis, B.D., Magee, B.A., Miller, G., Grimes, J., Perry, M.E., Miller, K.E., Bouquet, A., Lunine, J.I., Brockwell, T., Bolton, S.J.. Cassini finds molecular hydrogen in the Enceladus plume: Evidence for hydrothermal processes. Science 2017;356(6334):155–159. URL: https://science.sciencemag.org/content/356/6334/155. doi:10.1126/science.aai8703. arXiv:https://science.sciencemag.org/content/356/6334/155.full.pdf.

Wang, D.T., Gruen, D.S., Lollar, B.S., Hinrichs, K.U., Stewart, L.C., Holden, J.F., Hristov, A.N., Pohlman, J.W., Morrill, P.L., Könneke, M., et al. Nonequilibrium clumped isotope signals in microbial methane. Science 2015;348(6233):428–431. doi:10.1126/science.aaa4326.

Wang, D.T., Reeves, E.P., McDermott, J.M., Seewald, J.S., Ono, S.. Clumped isotopologue constraints on the origin of methane at seafloor hot springs. Geochim Cosmochim Acta 2018;223:141–158. doi:10.1016/j.gca.2017.11.030.

Wang, D.T., Welander, P.V., Ono, S.. Fractionation of the methane isotopologues $^{13}CH_4$, $^{12}CH_3D$, and $^{13}CH_3D$ during aerobic oxidation of methane by Methylococcus capsulatus (Bath). Geochim Cosmochim Acta 2016;192:186–202. doi:10.1016/j.gca.2016.07.031.

Wang, Q., Garrity, G.M., Tiedje, J.M., Cole, J.R.. Naïve Bayesian Classifier for Rapid Assignment of rRNA Sequences into the New Bacterial Taxonomy. Appl Environ Microbiol 2007;73(16):5261–5267. URL: https://aem.asm.org/content/73/16/5261. doi:10.1128/AEM.00062-07. arXiv:https://aem.asm.org/content/73/16/5261.full.pdf.

Welhan, J.A., Craig, H.. Methane, Hydrogen and Helium in Hydrothermal Fluids at 21 °N on the East Pacific Rise; Boston, MA: Springer US. p. 391–409. URL: https://doi.org/10.1007/978-1-4899-0402-7_17. doi:10.1007/978-1-4899-0402-7_17.

Welte, C.U., Rasigraf, O., Vaksmaa, A., Versantvoort, W., Arshad, A., Op den Camp, H.J., Jetten, M.S., Lüke, C., Reimann, J.. Nitrate- and nitrite-dependent anaerobic oxidation of methane. Environ Microbiol Rep 2016;8(6):941–955. URL: https://onlinelibrary.wiley.com/doi/abs/10.1111/1758-2229.12487. doi:10.1111/1758-2229.12487. arXiv:https://onlinelibrary.wiley.com/doi/pdf/10.1111/1758-2229.12487.

Weyhenmeyer, C.E., Burns, S.J., Waber, H.N., Macumber, P.G., Matter, A.. Isotope study of moisture sources, recharge areas, and groundwater flow paths within the eastern Batinah coastal plain, Sultanate of Oman. Water Resources Research 2002;38(10). doi:10.1029/2000WR000149.

Whiticar, M.J.. Carbon and hydrogen isotope systematics of bacterial formation and oxidation of methane. Chem Geol 1999;161(1):291 – 314. URL: http://www.sciencedirect.com/science/article/pii/S0009254199000923. doi:10.1016/S0009-2541(99)00092-3.

Young, E., Kohl, I., Lollar, B.S., Etiope, G., Rumble Iii, D., Li, S., Haghnegahdar, M., Schauble, E., McCain, K., Foustoukos, D., et al. The relative abundances of resolved $^{12}CH_2D_2$ and $^{13}CH_3D$ and mechanisms controlling isotopic bond ordering in abiotic and biotic methane gases. Geochim Cosmochim Acta 2017;203:235–264. doi:10.1016/j.gca.2016.12.041.

Young, E.D.. A Two-Dimensional Perspective on $CH_4$ Isotope Clumping : Distinguishing Process from Source; Cambridge University Press. p. 388–414. URL: https://www.cambridge.org/us/academic/subjects/earth-and-environmental-science/geochemistry-and-environmental-chemistry/deep-carbon-past-present?format=HB&isbn=9781108477499#resources. doi:10.1017/9781108677950.

Young, E.D., Rumble, D., Freedman, P., Mills, M.. A large-radius high-mass-resolution multiple-collector isotope ratio mass spectrometer for analysis of rare isotopologues of $O_2$, $N_2$, $CH_4$ and other gases. Int J Mass Spectrom 2016;401:1 – 10. URL: http://www.sciencedirect.com/science/article/pii/S138738061600035X. doi:10.1016/j.ijms.2016.01.006.

Zimmer, K., Zhang, Y., Lu, P., Chen, Y., Zhang, G., Dalkilic, M., Zhu, C.. SUPCRTBL: A revised and extended thermodynamic dataset and software package of SUPCRT92. Comput Geosci 2016;90:97–111. URL: https://www.sciencedirect.com/science/article/pii/S0098300416300371. doi:10.1016/j.cageo.2016.02.013.

Zwicker, J., Birgel, D., Bach, W., Richoz, S., Smrzka, D., Grasemann, B., Gier, S., Schleper, C., Rittmann, S.M., Koşun, E., et al. Evidence for archaeal methanogenesis within veins at the onshore serpentinite-hosted Chimaera seeps, Turkey. Chem Geol 2018;483:567–580. doi:10.1016/j.chemgeo.2018.03.027.

Table 1: Well data and field measurements.

| Well | UTM coordinates (WGS-84) | | Geologic description | Well depth / [mbgl] | Screen interval / [mbct] | Water level / [mbct] | Pump depth / [mbct] | Conductivity / $[\mu S \cdot cm^{-1}]$ | Temperature / [°C] | pH | *Eh*/ [mV] | $f_{O_2}$ / [bar][b] |
|---|---|---|---|---|---|---|---|---|---|---|---|---|
| | easting | northing | | | | | | | | | | |
| WAB103 | 648 577 | 2 530 362 | Gabbro | 101 | 90 – 98 | 15 | 70. | 1410 | 34.9 | 8.51 | 167[a] | $2.99 \cdot 10^{-36}$ |
| WAB188 | 671 123 | 2 529 798 | Gabbro, near contact with harzburgite | 78 | 34.5 – 51 | 9.5 | 50. | 1120 | 35.6 | 8.16 | 214[a] | $2.01 \cdot 10^{-34}$ |
| WAB104 | 643 099 | 2 541 124 | Harzburgite | 120.4 | 100.8 – 104 | 40. | 85 | 548 | 33.7 | 8.79 | 133 | $1.23 \cdot 10^{-37}$ |
| WAB105 | 644 678 | 2 536 524 | Harzburgite | 120.5 | 110 – 117 | 16.5 | 60. | 498 | 33.7 | 8.66 | 162 | $2.99 \cdot 10^{-36}$ |
| WAB55 | 634 777 | 2 506 101 | Harzburgite with abundant carbonate veins, near contact with gabbro | 102 | 8 – 97 | 7.5[a] | 50.[a] | 1183[a] | 36.2[a] | 9.62[a] | 269[a] | $7.17 \cdot 10^{-25}$ |
| WAB56 | 634 851 | 2 501 617 | Harzburgite | 106 | 7 – 27 | 7.62[a] | 30.[a] | 930.[a] | 35.6[a] | 10.61[a] | 20.2[a] | $2.81 \cdot 10^{-37}$ |
| NSHQ04 | 670 971 | 2 531 699 | Harzburgite, near fault with gabbro | 304 | open > 5.8 | 4.7 | 8 | 3350 | 33.4 | 10.51[a] | −174 | $5.14 \cdot 10^{-51}$ |
| WAB71 | 670 322 | 2 533 981 | Dunite, near fault with harzburgite | 136.5 | 128 – 131 | 8.3 | 70. | 1970 | 34.9 | 11.22 | −229 | $2.52 \cdot 10^{-51}$ |
| CM2A | 636 988 | 2 534 284 | Mostly dunite with occasional gabbro and harzburgite | 400. | open > 23.7 | 13.4 | 75 | 2860 | 33.6 | 11.32 | n.d. | n.d. |
| NSHQ14 | 675 495 | 2 529 716 | Harzburgite | 304 | open > 5.8 | 9.2 | 85 | 2670 | 36.7 | 11.39 | −253[a] | $1.19 \cdot 10^{-51}$ |

Measurements refer to sampling February-March, 2018, unless noted. Well elevations are given in Supporting Information Figure S1. *Abbreviations:* n.d., not determined; mbgl, meters below ground level; mbct, meters below casing top. Casings extend ∼ 1 m above ground level.

[a]Not determined during 2018 sampling, so most recent prior data is reported (2015 to 2017; Rempfert et al., 2017; Fones et al., 2019).

[b]Calculated from temperature, pH, and *Eh*. Where one or more of these parameters were obtained during different sampling years, $f_{O_2}$ should be considered a representative estimate.

Table 2: Isotopic compositions of $CH_4$, $C_2H_6$, and $C_3H_8$.

| Well | Sample year | Pump depth / [mbct] | laboratory | $\delta^{13}C_{CH_4}$ | $\delta D_{CH_4}$ | $\Delta^{13}CH_3D$ | $\Delta^{12}CH_2D_2$ | $\delta^{13}C_{C_2H_6}$ | $\delta^{13}C_{C_3H_8}$ |
|---|---|---|---|---|---|---|---|---|---|
| WAB188 | 2018 | 50. | CUB | −86.7 | n.d. | n.d. | n.d. | n.d. | n.d. |
| | 2017 | 78 | CUB | −60.8 | n.d. | n.d. | n.d. | n.d. | n.d. |
| | 2015 | 20. | LBNL | −71.3 | n.d. | n.d. | n.d. | n.d. | n.d. |
| WAB56 | 2015 | 12 | LBNL | −83.2 | n.d. | n.d. | n.d. | n.d. | n.d. |
| NSHQ04 | 2018 | 8 | CUB | 4.7 | −229 | n.d. | n.d. | n.d. | n.d. |
| | | | UCLA | 4.177 | −227.396 | $0.229 \pm 0.288$ | $-24.502 \pm 0.944$ | n.d. | n.d. |
| | 2017 | 5.8 | CUB | 6.8 | −225 | n.d. | n.d. | n.d. | n.d. |
| | | | MIT | 3.59 | −229.67 | $0.12 \pm 0.17$ | n.d. | n.d. | n.d. |
| | 2015 | 22 | LBNL | 0.8 | −209 | n.d. | n.d. | n.d. | n.d. |
| | | | MIT | 1.60 | −230.00 | $0.72 \pm 0.29$ | n.d. | n.d. | n.d. |
| | 2014 | 18 | LBNL | 2.4 | −205 | n.d. | n.d. | n.d. | n.d. |
| WAB71 | 2018 | 70. | CUB | 3.6 | −307 | n.d. | n.d. | n.d. | n.d. |
| | 2017 | 50. | CUB | 3.9 | −313 | n.d. | n.d. | n.d. | n.d. |
| | 2016 | 50. | LBNL | 3.0 | n.d. | n.d. | n.d. | n.d. | n.d. |
| | 2015 | 18 | LBNL | 2.9 | n.d. | n.d. | n.d. | n.d. | n.d. |
| CM2A | 2018 | 75 | CUB | −4.3 | −206 | n.d. | n.d. | n.d. | n.d. |
| | | | MIT | −3.83 | −190.32 | $2.87 \pm 0.57$ | n.d. | n.d. | n.d. |
| | | | UCLA | −4.710 | −197.73 | $2.638 \pm 0.284$ | $-1.267 \pm 0.886$ | n.d. | n.d. |
| NSHQ14 | 2018 | 85 | CUB | −2.3 | −314 | n.d. | n.d. | n.d. | n.d. |
| | | | MIT | −5.02 | −311.73 | $0.77 \pm 0.44$ | n.d. | n.d. | n.d. |
| | | | UCLA | −3.352 | −293.58 | $2.074 \pm 0.298$ | $-0.204 \pm 1.358$ | n.d. | n.d. |
| | 2017 | 85 | CUB | 0.2 | −271 | n.d. | n.d. | −6.0 | +3.3 |
| | | | MIT | −0.08 | −268.82 | $0.69 \pm 0.23$ | n.d. | n.d. | n.d. |
| | 2016 | 70. | LBNL | 1.8 | −273 | n.d. | n.d. | n.d. | n.d. |
| | | | MIT | −6.89 | −308.52 | $0.69 \pm 0.17$ | n.d. | n.d. | n.d. |
| | 2015 | 20. | LBNL | 3.7 | n.d. | n.d. | n.d. | n.d. | n.d. |
| | 2014 | 260. | LBNL | 3.0 | −232 | n.d. | n.d. | n.d. | n.d. |

All isotopic values reported in ‰ units. $\delta^{13}C$ and $\delta D$ reported in the VPDB and VSMOW reference frames, respectively. Data from 2014 previously reported by Miller et al. (2016). *Abbreviations:* n.d., not determined; mbct, meters below casing top.

Table 3: Chemical and isotopic composition of water samples.

| Well | $\delta D_{H_2O}$ | $\delta^{18}O_{H_2O}$ | $\sum CO_2$ | $\delta^{13}C_{\sum CO_2}$ | $\sum$ Na | $\sum$ Ca | $\sum$ Mg | $\sum$ Fe | $\sum$ Si | $NO_3^-$ | $SO_4^{2-}$ | $Cl^-$ | $Br^-$ |
|---|---|---|---|---|---|---|---|---|---|---|---|---|---|
| *gabbro-hosted groundwaters* | | | | | | | | | | | | | |
| WAB103 | −0.5 | 0.34 | $2.67 \cdot 10^3$ | −13.54 | $1.18 \cdot 10^3$ | $2.58 \cdot 10^2$ | $1.87 \cdot 10^3$ | 7.35 | $4.63 \cdot 10^2$ | $4.72 \cdot 10^2$ | $1.57 \cdot 10^3$ | $6.25 \cdot 10^3$ | $1.39 \cdot 10^2$ |
| WAB188 | −2.1 | −0.71 | $3.48 \cdot 10^3$ | −13.52 | $4.06 \cdot 10^3$ | $1.41 \cdot 10^3$ | $1.82 \cdot 10^3$ | $2.90 \cdot 10^1$ | $4.77 \cdot 10^2$ | $3.21 \cdot 10^2$ | $1.41 \cdot 10^3$ | $4.22 \cdot 10^3$ | $6.78 \cdot 10^1$ |
| *$Mg^{2+} - HCO_3^-$ groundwaters* | | | | | | | | | | | | | |
| WAB104 | −0.5 | −0.53 | $3.62 \cdot 10^3$ | −13.88 | $7.53 \cdot 10^2$ | $1.96 \cdot 10^2$ | $2.30 \cdot 10^3$ | 3.88 | $4.15 \cdot 10^2$ | $3.14 \cdot 10^2$ | $3.80 \cdot 10^2$ | $7.76 \cdot 10^2$ | 3.55 |
| WAB105 | 0.4 | 0.50 | $3.32 \cdot 10^3$ | −10.88 | $1.18 \cdot 10^3$ | $2.58 \cdot 10^2$ | $1.87 \cdot 10^3$ | 4.83 | $2.83 \cdot 10^2$ | $3.02 \cdot 10^2$ | $2.92 \cdot 10^2$ | $8.54 \cdot 10^2$ | 8.60 |
| WAB55 | 2.2 | 0.26 | $2.40 \cdot 10^3$ | −12.63 | $4.44 \cdot 10^3$ | $5.06 \cdot 10^1$ | $3.34 \cdot 10^3$ | 2.52 | $3.58 \cdot 10^1$ | $3.02 \cdot 10^2$ | $8.03 \cdot 10^2$ | $6.54 \cdot 10^3$ | $1.12 \cdot 10^2$ |
| *$Ca^{2+} - OH^-$ groundwaters* | | | | | | | | | | | | | |
| WAB56 | n.d. | n.d. | $1.3 \cdot 10^{2a}$ | n.d. | $3.56 \cdot 10^{3a}$ | $5.43 \cdot 10^{2a}$ | $1.00^a$ | n.d. | $2.22 \cdot 10^2$ | $3.00^a$ | $6.00^a$ | $1.33 \cdot 10^{1a}$ | $1.79 \cdot 10^{-1a}$ |
| NSHQ04 | $-15^a$ | $-3.0^a$ | $1.8 \cdot 10^1$ | −29.7 | $1.04 \cdot 10^{4a}$ | $7.79 \cdot 10^{3a}$ | $1.80 \cdot 10^{1a}$ | $8.20 \cdot 10^{-1a}$ | $3.60 \cdot 10^{1a}$ | $3.00^a$ | $6.83 \cdot 10^{2a}$ | $1.82 \cdot 10^{4a}$ | $1.25^a$ |
| WAB71 | −3.0 | −0.40 | $< 1.2 \cdot 10^1$ | n.d. | $6.25 \cdot 10^3$ | $4.14 \cdot 10^3$ | $< 2.06 \cdot 10^{-1}$ | $8.48 \cdot 10^1$ | $2.35 \cdot 10^1$ | $1.84 \cdot 10^2$ | $6.08 \cdot 10^1$ | $1.17 \cdot 10^4$ | $1.50 \cdot 10^2$ |
| CM2A | 1.7 | 0.67 | $< 1.2 \cdot 10^1$ | n.d. | $2.07 \cdot 10^4$ | $1.75 \cdot 10^3$ | 9.49 | $4.03 \cdot 10^1$ | $2.81 \cdot 10^1$ | $1.64 \cdot 10^2$ | $5.56 \cdot 10^2$ | $1.85 \cdot 10^4$ | $2.48 \cdot 10^2$ |
| NSHQ14 | 0.2 | 0.43 | $< 1.2 \cdot 10^1$ | n.d. | $1.03 \cdot 10^4$ | $3.60 \cdot 10^3$ | 6.23 | $8.48 \cdot 10^1$ | $1.03 \cdot 10^1$ | $3.60 \cdot 10^2$ | $1.57 \cdot 10^2$ | $1.36 \cdot 10^4$ | $1.67 \cdot 10^2$ |

Concentrations reported in $\mu mol \cdot L^{-1}$. $\sum$ indicates the sum of all dissolved species of the element. All $\delta$ values reported in ‰ units. $\delta^{18}O$ and $\delta D$ reported relative to VSMOW. $\delta^{13}C$ reported relative to VPDB. Samples obtained in February-March 2018, unless noted. *Abbreviations:* n.d., not determined.

[a]Not determined during 2018 sampling, so most recent prior data is reported (2015 to 2017; Rempfert et al., 2017; Fones et al., 2019).

Table 4: Aqueous gas concentrations, reported in $\mu\text{mol} \cdot \text{L}^{-1}$.

| Well | Sample year | $H_2$ | CO | $CH_4$ | $C_2H_6$ | $C_3H_8$ | $i$-$C_4H_{10}$ | $n$-$C_4H_{10}$ | $i$-$C_5H_{12}$ | $n$-$C_5H_{12}$ | $C_6H_{14}$[a] |
|---|---|---|---|---|---|---|---|---|---|---|---|
| WAB103 | 2018 | $< 5.98 \cdot 10^{-1}$ | $< 1.32 \cdot 10^{-1}$ | $1.45 \cdot 10^{-1}$ | $< 9.88 \cdot 10^{-4}$ | $< 7.60 \cdot 10^{-4}$ | $< 4.61 \cdot 10^{-4}$ | $6.05 \cdot 10^{-3}$ | $< 3.43 \cdot 10^{-4}$ | $8.73 \cdot 10^{-4}$ | $< 2.81 \cdot 10^{-4}$ |
| WAB188 | 2018 | $< 5.98 \cdot 10^{-1}$ | $< 1.32 \cdot 10^{-1}$ | $9.17 \cdot 10^{-1}$ | $< 9.88 \cdot 10^{-4}$ | $< 7.60 \cdot 10^{-4}$ | $< 4.61 \cdot 10^{-4}$ | $< 5.78 \cdot 10^{-4}$ | $< 3.43 \cdot 10^{-4}$ | $< 3.81 \cdot 10^{-4}$ | $< 2.81 \cdot 10^{-4}$ |
| | 2017 | $9.92 \cdot 10^{-1}$ | $< 2.79 \cdot 10^{-1}$ | 1.83 | $< 1.01 \cdot 10^{-3}$ | $< 7.79 \cdot 10^{-4}$ | $< 4.72 \cdot 10^{-4}$ | $< 6.01 \cdot 10^{-4}$ | $< 3.50 \cdot 10^{-4}$ | $< 3.91 \cdot 10^{-4}$ | $< 2.88 \cdot 10^{-4}$ |
| WAB104 | 2018 | $< 5.98 \cdot 10^{-1}$ | $< 1.32 \cdot 10^{-1}$ | $< 1.53 \cdot 10^{-2}$ | $< 9.88 \cdot 10^{-4}$ | $< 7.60 \cdot 10^{-4}$ | $4.82 \cdot 10^{-4}$ | $< 5.78 \cdot 10^{-4}$ | $7.56 \cdot 10^{-4}$ | $< 3.81 \cdot 10^{-4}$ | $< 2.81 \cdot 10^{-4}$ |
| | 2017 | $< 4.80 \cdot 10^{-2}$ | $< 2.79 \cdot 10^{-1}$ | $2.30 \cdot 10^{-2}$ | $< 1.01 \cdot 10^{-3}$ | $< 7.79 \cdot 10^{-4}$ | $< 4.72 \cdot 10^{-4}$ | $< 6.01 \cdot 10^{-4}$ | $< 3.50 \cdot 10^{-4}$ | $< 3.91 \cdot 10^{-4}$ | $< 2.88 \cdot 10^{-4}$ |
| WAB105 | 2018 | $< 5.98 \cdot 10^{-1}$ | $< 1.32 \cdot 10^{-1}$ | $< 1.53 \cdot 10^{-2}$ | $< 9.88 \cdot 10^{-4}$ | $< 7.60 \cdot 10^{-4}$ | $3.70 \cdot 10^{-2}$ | $< 5.78 \cdot 10^{-4}$ | $< 3.43 \cdot 10^{-4}$ | $< 3.81 \cdot 10^{-4}$ | $< 2.81 \cdot 10^{-4}$ |
| | 2017 | $< 4.80 \cdot 10^{-2}$ | $< 2.79 \cdot 10^{-1}$ | $2.01 \cdot 10^{-2}$ | $< 1.01 \cdot 10^{-3}$ | $< 7.79 \cdot 10^{-4}$ | $< 4.72 \cdot 10^{-4}$ | $< 6.01 \cdot 10^{-4}$ | $< 3.50 \cdot 10^{-4}$ | $< 3.91 \cdot 10^{-4}$ | $< 2.88 \cdot 10^{-4}$ |
| WAB55 | 2018 | $< 5.98 \cdot 10^{-1}$ | $< 1.32 \cdot 10^{-1}$ | $1.15 \cdot 10^{-1}$ | $1.55 \cdot 10^{-3}$ | $< 7.60 \cdot 10^{-4}$ | $2.25 \cdot 10^{-3}$ | $7.91 \cdot 10^{-4}$ | $1.60 \cdot 10^{-3}$ | $< 3.81 \cdot 10^{-4}$ | $5.52 \cdot 10^{-3}$ |
| | 2017 | $< 4.80 \cdot 10^{-2}$ | $< 2.79 \cdot 10^{-1}$ | $1.06 \cdot 10^{-1}$ | $< 1.01 \cdot 10^{-3}$ | $< 7.79 \cdot 10^{-4}$ | $< 4.72 \cdot 10^{-4}$ | $< 6.01 \cdot 10^{-4}$ | $< 3.50 \cdot 10^{-4}$ | $< 3.91 \cdot 10^{-4}$ | $< 2.88 \cdot 10^{-4}$ |
| WAB56 | 2017 | $2.40 \cdot 10^{-1}$ | $< 2.79 \cdot 10^{-1}$ | $1.60 \cdot 10^{-1}$ | $< 1.01 \cdot 10^{-3}$ | $< 7.79 \cdot 10^{-4}$ | $< 4.72 \cdot 10^{-4}$ | $< 6.01 \cdot 10^{-4}$ | $< 3.50 \cdot 10^{-4}$ | $< 3.91 \cdot 10^{-4}$ | $< 2.88 \cdot 10^{-4}$ |
| NSHQ04 | 2018 | $< 5.98 \cdot 10^{-1}$ | $< 1.32 \cdot 10^{-1}$ | $1.44 \cdot 10^{2}$ | $2.45 \cdot 10^{-2}$ | $2.22 \cdot 10^{-3}$ | $< 4.61 \cdot 10^{-4}$ | $< 5.78 \cdot 10^{-4}$ | $< 3.43 \cdot 10^{-4}$ | $< 3.81 \cdot 10^{-4}$ | $< 2.81 \cdot 10^{-4}$ |
| | 2017 | $< 4.80 \cdot 10^{-2}$ | $< 2.79 \cdot 10^{-1}$ | $4.83 \cdot 10^{2}$ | $< 1.01 \cdot 10^{-3}$ [b] | $1.03 \cdot 10^{-3}$ | $< 4.72 \cdot 10^{-4}$ | $< 6.01 \cdot 10^{-4}$ | $< 3.50 \cdot 10^{-4}$ | $< 3.91 \cdot 10^{-4}$ | $< 2.88 \cdot 10^{-4}$ |
| WAB71 | 2018 | $< 5.98 \cdot 10^{-1}$ | $< 1.32 \cdot 10^{-1}$ | 7.76 | $1.00 \cdot 10^{-3}$ | $< 7.60 \cdot 10^{-4}$ | $< 4.61 \cdot 10^{-4}$ | $< 5.78 \cdot 10^{-4}$ | $< 3.43 \cdot 10^{-4}$ | $< 3.81 \cdot 10^{-4}$ | $< 2.81 \cdot 10^{-4}$ |
| | 2017 | $5.92 \cdot 10^{-1}$ | $< 2.79 \cdot 10^{-1}$ | $1.48 \cdot 10^{1}$ | $< 1.01 \cdot 10^{-3}$ | $< 7.79 \cdot 10^{-4}$ | $< 4.72 \cdot 10^{-4}$ | $1.94 \cdot 10^{-2}$ | $< 3.50 \cdot 10^{-4}$ | $4.79 \cdot 10^{-4}$ | $< 2.88 \cdot 10^{-4}$ |
| CM2A | 2018 | 3.38 | $< 1.32 \cdot 10^{-1}$ | $1.52 \cdot 10^{2}$ | $4.11 \cdot 10^{-2}$ | $1.75 \cdot 10^{-3}$ | $< 4.61 \cdot 10^{-4}$ | $6.48 \cdot 10^{-3}$ | $< 3.43 \cdot 10^{-4}$ | $< 3.81 \cdot 10^{-4}$ | $< 2.81 \cdot 10^{-4}$ |
| NSHQ14 | 2018 | $1.31 \cdot 10^{2}$ | $< 1.32 \cdot 10^{-1}$ | $7.12 \cdot 10^{1}$ | $7.32 \cdot 10^{-2}$ | $7.64 \cdot 10^{-3}$ | $2.26 \cdot 10^{-3}$ | $2.88 \cdot 10^{-3}$ | $1.27 \cdot 10^{-3}$ | $2.23 \cdot 10^{-3}$ | $1.12 \cdot 10^{-3}$ |
| | 2017 | $2.53 \cdot 10^{2}$ | $< 2.79 \cdot 10^{-1}$ | $1.06 \cdot 10^{2}$ | $7.98 \cdot 10^{-2}$ | $9.00 \cdot 10^{-3}$ | $1.53 \cdot 10^{-3}$ | $4.77 \cdot 10^{-3}$ | $< 3.50 \cdot 10^{-4}$ | $< 3.91 \cdot 10^{-4}$ | $9.70 \cdot 10^{-4}$ |

[a]Hexane isomers not chromatographically resolved.

[b]High $C_1/(C_2 + C_3)$ at NSHQ04 resulted in $CH_4$ tailing into and preventing quantitation of the $C_2H_6$ peak in 2017. Chromatographic improvements were made between analyses of 2017 and 2018 samples.

Table 5: Gibbs free energies of potential $CH_4$-forming reactions and log activities of relevant species. *Abbreviations*: HT, hydrogenotrophic (Equation 2); AC, acetoclastic (Equation 3); FD, formate disproportionation (Equation 4).

| | log (activity) | | | | | | $\Delta G_r$ / $\left[\text{kJ} \cdot \text{mol}^{-1}\right]$ | | |
|---|---|---|---|---|---|---|---|---|---|
| water type | $H^+$ | $CO_2$(aq) | $HCOO^-$ | $CH_3COO^-$ | $CH_4$(aq) | $H_2$(aq) | HT | AC | FD |
| $Ca^{2+} - OH^-$ | −11.1 | −11.6 | −6.1 | −6.1 | −4.0 | −9.0 | 64 | −115 | −90 |
| | | | | | | −6.0 | −6 | −115 | −90 |
| | | | | | | −3.0 | −77 | −115 | −90 |
| $Mg^{2+} - HCO_3^-$ | −8.7 | −4.9 | −6.0 | −6.0 | −7.0 | −9.0 | 8 | −107 | −47 |
| | | | | | | −6.0 | −63 | −107 | −47 |